J

Aramco
Journal
of ## Technology

J

Aramco
Journal
of Technology

Contents

Geochemical Techniques to Detect Sources of Fluids in Highly Pressured Casing-Casing Annuli (CCA)

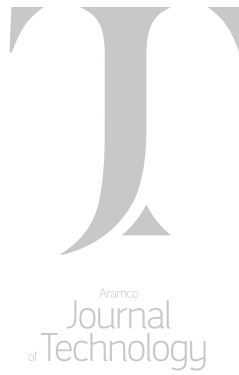*Dr. Peter Birkle and Hamdi A. Alramadan*

Abstract /

The buildup of high casing-casing annulus (CCA) pressure compromises the well integrity and can lead to serious incidents if left untreated. Potential sources of water causing the elevated CCA pressure are either trapped water in the cement column or water from a constant feeding source. This study utilizes inorganic geochemical techniques to determine the provenance of CCA produced water as a trigger for high pressure in newly drilled wells. Affinities in the hydrochemical (major, minor, and trace elements) and stable isotopic (δ^2H, $\delta^{18}O$) composition are monitored to identify single fluid types, multicomponent mixing, and secondary fluid alteration processes.

As a proof-of-concept, geochemical fingerprints of CCA produced water from three wells were correlated with potential source candidates, i.e., utilized drilling fluids (mud filtrate (MF), supply water (SW)) from the target well site, Early - Late Cretaceous aquifers and Late Jurassic - Late Triassic formation waters (FWs) from adjacent wells and fields. Geochemical affinities of CCA water with groundwater from an Early Cretaceous aquifer postulate the presence of one single horizon for active water inflow. Nonreactive elements (sodium (Na) and chloride (Cl)) and environmental isotopes (δ^2H, $\delta^{18}O$) were found to be most suited tools for fluid identification.

The $^2H/^1H$ and $^{18}O/^{16}O$ ratios of SW and MF are close to global meteoric water composition, whereas FWs are enriched in ^{18}O. Elevated sulfate (SO_4) and potassium concentrations and extreme alkaline conditions for CCA water indicates the occurrence of minor secondary alteration processes, such as the contact of inflowing groundwater with cement or fluid mixing with minor portions of potassium chloride additives.

The presented technology in this study enables the detection of high CCA pressure and fluid leakage sources, thereby allowing workover engineers to plan for potential remedial actions prior to moving the rig to the affected well; thereby significantly reducing operational costs. Appropriate remedial solutions can be prompted for safe well abandonment as well as to resume operation at the earliest time.

Introduction

The casing-casing annulus (CCA) seal is essential to prevent invasion of downhole reservoir fluids that can potentially compromise the integrity of the wellbore. Cement is applied to seal the annulus between two casing strings as part of the completion process in drilled wells. This seal is required to permanently shut off water penetration into the well and enhance the integrity of the wellbore.

CCA leaks can be detrimental to the well integrity and the reservoir health. Well deterioration can be imposed due to casing exposure to corrosive reservoir or aquifer fluids, and therefore, safety issues are encountered, especially in cases where leaking channels lead high-pressure fluids to the surface. On the other hand, the loss of reserves may be incurred due to cross flow between reservoirs through the leaking channels in the CCA. In addition, the CCA induced reservoir cross flow may contaminate clean shallow aquifers. Therefore, early detection and remediation of downhole CCA leaks is essential to ensure sustainable operational excellence while maintaining the highest safety and environmental standards.

If encountered, high CCA pressures must be remediated to protect the wellbore and ensure an incident-free work environment. A high-pressure CCA cannot be cured if the fluid source is not detected. Complex wellhead design, inadequate cement behind the casing, the threat of shallow gas presence, and multiple downhole tubular leaks are some of the common perils in sustaining the production[1]. Potential sources of water causing the elevated CCA pressure are either trapped water in the cement column or water from a constant feeding source. The inflow of formation fluid into the annulus is mainly caused by poor cement bond in the outer casing strings.

Geochemical solutions for the management of well integrity are generally focused on the assessment of the compositional analysis of crude oil and gas. The signature of hydrocarbon peaks by gas chromatography geochemical fingerprinting is utilized to trace the migration of reservoir fluids into the wellbore through any potential leak path behind the casing annulus[1].

The application of inorganic geochemical methods in the oil and gas industry is mainly focused to solve flow assurance problems, which are triggered by inorganic scale deposit under subsurface conditions or at surface installations. Additionally, multi-isotope analysis of formation water (FW) can provide direct evidence for the presence of connected or compartmentalized reservoirs and fluid migration, as performed for Cretaceous and Jurassic carbonate reservoirs in the Gulf of Mexico[2] or for the Northern Appalachian basins[3].

The present study introduces the utilization of combined inorganic methods as a practical tool to determine the provenance of CCA produced water as a trigger for high CCA pressure in newly drilled wells. In detail, the geochemical composition of CCA produced water from three wells will be correlated with potential source candidates, such as drilling fluids (mud filtrate (MF), supply water (SW)) from the target well site, or Early - Late Cretaceous aquifers and Late Jurassic - Late Triassic FWs from adjacent wells and fields.

The detection of MFs or SW in CCA produced water would indicate the presence of trapped water in the cement column, whereas geochemical affinities with groundwater or FW suggest the dynamic water inflow from a constant feeding source.

CCA Leak Triggers

CCA leaks are caused by the failure of the cement between casing strings, pipe joints, and packers, or any directly exposed completion component. Consequently, most of the casing leaks are caused by poor cement jobs that result in open pathways allowing reservoir fluids to flow through. A unique cement design is required for every well due to the variations in well trajectory, casing design, and formations drilled through.

When drilling through highly permeable formations before reaching the well's target reservoir, certain important additives are required to prevent premature cement fluid loss into these formations. Controlling filtrate loss in cement slurries is vital to the integrity of the cement column and is of equal importance as controlling the cement thickening time or the compressive-strength development[4].

Premature cement dehydration impairs the cement quality and promotes the creation of fluid conducting channels within the cement column. Moreover, excessive use of cement fluid loss additives causes cement to shrink and alters the seal across the formation face or the casing wall. Therefore, fluid loss additives must be optimized to proper levels depending on the formation permeability, and it is normally measured in terms of cubic centimeters of fluid lost per 30 minutes while circulating the cement.

Cement between two casing strings can be contaminated by the mud cake residue, which can affect the seal of the cement column. The injected spacer between the mud and the cement column normally removes mud cake. The spacer volume must be optimized while considering the rheological properties to ensure mud removal efficiency and to ensure intact cement in the CCA. Also, ensuring the achievement of a turbulent flow or maximum flow rate while injecting the spacer proved to effectively remove the mud cake with the use of optimum spacer volumes[5].

Figure 1 illustrates some of the conditions that lead to an impaired cement column where insufficient fluid loss additives cause the cement to dehydrate and shrink prematurely and cause cracks and channels within the cement column across the permeable formation. Moreover, incomplete mud cake removal leads to separation between the cement column and casing or rock surface, which compromises the seal from formation fluids.

Leak Detection Methodologies

The best approach to alleviate severe casing leak issues is to routinely run suitable surveys, especially in high volume producing fields. Typically, temperature and annuli pressure surveys are run periodically to ensure normal profiles in every well. Any suspicious abnormalities calls for an immediate action to further investigate the source of leak within the annulus and avoid any potential consequences that can be detrimental to the well's integrity or the environment.

The very first task is normally to identify the type of leaking fluid through surface annuli samples analyzed in the laboratory. In cases with suspected corroded casing strings, one method to detect the casing leak source is to utilize high-resolution electromagnetic induction, which is capable of analyzing three layers of casing strings. This is solely dependent on the extent and severity of the casing corrosion log results, and the method is effective with confirmed deteriorated casing strings to locate the source of the leak, while helping to optimize the casing metallurgy design to prolong the casing life in future planned wells in the area[6].

Fig. 1 *An illustration of the cement-mud column displacement indicating potential conditions where cement integrity can be compromised.*
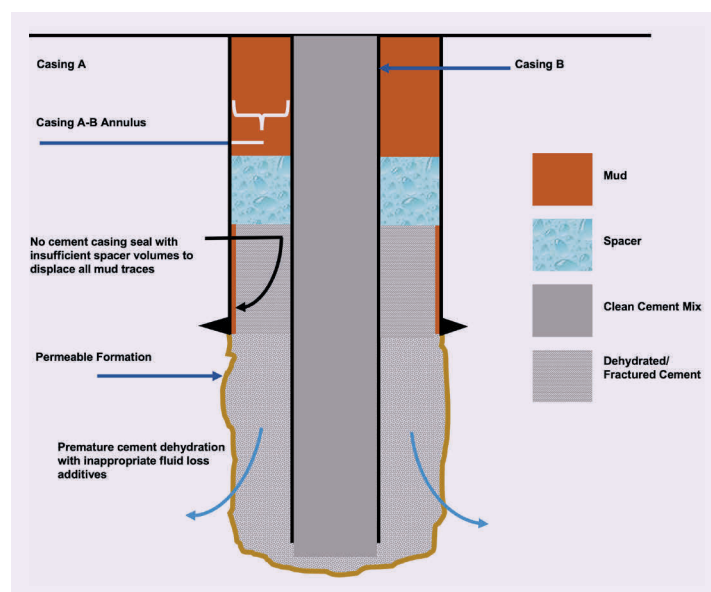
In other cases where carbon dioxide (CO_2) rich fluids and micro-annuli cracks exist, CO_2 can interact with the cement column and form a gel-like calcite component referred to as "silica gel." The leakage rate and silica gel growth behavior can be simulated while coupling the main physical phenomenon related to flow, elasticity, and chemistry. This simulation allows for the determination of proper remedial actions to such leak scenarios[7].

Furthermore, production logging can be combined with pulsed neutron logging and analyzed for formation cross flow scenarios where a deteriorated separating formation seal is suspected[8]. Various other techniques to detect leaks in CCA include ultrasonic tools, water flow logs, and temperature logs that are used in the industry.

Remediation Techniques

Curing CCA leaks is immensely challenging and many proposed solutions seem to cure the symptoms of the issue while keeping the root cause alive. Potential effective solutions to remediate CCA leaks must be studied in detail to ensure accomplishing a complete seal in all conductive channels within the annulus. Various remedial solutions were invented to target and seal the leaking source, and resolve the elevated CCA pressure issues.

Some solutions include pumping especially designed resins through the wellhead annuli ports that set and solidify at the leaking source with appropriate temperatures achieved[9]. Others are pH-triggered polymer gels that are sensitive and viscosify when in contact with alkaline cement to create a highly swollen substance that can block fluid flow with substantial yield stress[10]. Moreover, the straightforward remedial action approach is mechanical where the identified leaking interval is perforated, and a properly designed cement is squeezed to seal off the CCA at the source.

Subsequently, squeezing cement into an annulus where only fine microchannels exist has a low probability for success and requires other feasible remediation options.

Potential Sources for CCA Water

High CCA pressure in newly drilled wells causes the loss of well integrity during drilling. Produced CCA water at the well site can either be related to: (1) the presence of trapped water within the CCA cement column, or (2) a constant CCA feeding by aquifer inflow, caused by casing leaks. In the first case, the geochemistry of CCA water should be identical or similar to involved fluids for the drilling or cementing job, which is composed of MF and/or SW, Fig. 2.

Identical concentrations for nonreactive elements (Na and Cl) and stable isotope ratios (δ^2H, $\delta^{18}O$) in both CCA water and drilling/cementing fluids, are conclusive to define a trapped water origin for recovered CCA fluids. The targeting of the source for CCA water is complicated through the abundance of different FW, "FW Type 1" and "FW Type 2," Figs. 2 to 4, and MF types, "MF Type 1" and "MF Type 2,"

Fig. 2 *A conceptual model of using the concentration of Na and Cl as conservative elements to define the provenance of CCA water. In the case of water entrapment in the cement column (brown circles), the CCA water composition is similar to WBM filtrate (MF Type 1 and MF Type 2) or SW. Similar geochemical fingerprints for CCA water and local formation water (FW Type 1 and FW Type 2) reflect the inflow of aquifer or FW (yellow circles).*
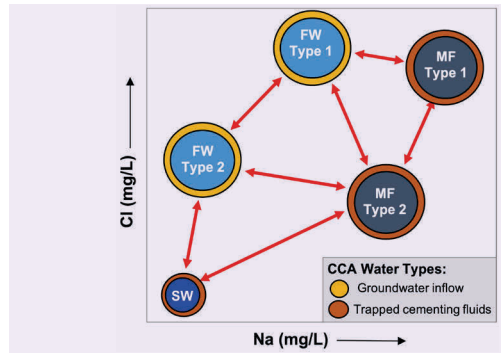
Fig. 3 *The mixing of different fluid types, i.e., between formation water (FW Type 1) and mud filtrate (MF Type 2), in the borehole camouflages the primary fluid composition.*
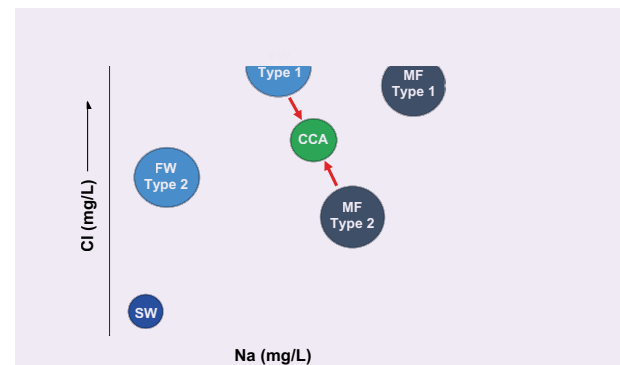
Fig. 4 *A secondary water-rock or water-water interaction processes cause changes in the concentration of reactive elements, i.e., the contact of SO_4 enriched shallow mud filtrate (MF Type 2) with Ba enriched formation water (FW Type 1) triggers the precipitation of sulfate minerals with a decrease of both aqueous species in CCA*.*
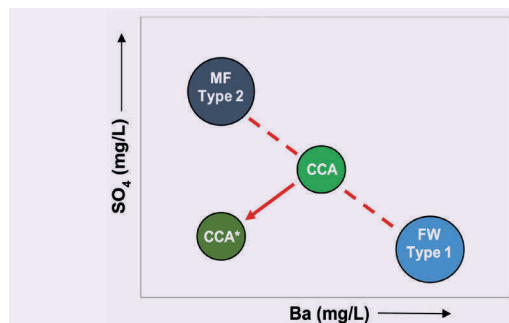
Figs. 2 to 4, both of them characterized by a broad range in geochemical composition.

In the second case, the inflow of FW into the borehole is reflected by geochemical affinities of CCA water with FW from a specific reservoir interval (yellow circles in Fig. 2). Even further, the precise interval of water inflow can be specified by knowing the geochemical characteristics of FW from interval 1, FW Type 1 and from interval 2, FW Type 2. An analogue correlation between water types can be performed with stable isotope ratios.

Additionally, the mixing of different fluid types, Fig. 3, and secondary alteration of the fluid by water-rock or water-water interaction, Fig. 4, can alter the primary composition of enclosed CCA water. In the case of having the input of several fluid sources to feed the CCA column, Na and Cl concentration of CCA water will be intermediate between two endmembers as part of a mixing line, Fig. 3.

In Fig. 3, CCA water represents a mixed product between the MF of Type 2 and FW of Type 1. In the case of additional secondary water-rock and/or water-water interaction processes, changes in the concentration of reactive elements, such as HCO_3, SO_4, and K, represent indicators to diagnose the alteration of the primary CCA water composition, Fig. 4.

Examples would be the precipitation of SO_4 by thermogenic conditions in deep reservoirs. The contact of SO_4 enriched shallow MF, (MF Type 2, Fig. 4) with barium (Ba) enriched FW (FW Type 1, Fig. 4) triggers the precipitation of sulfate minerals, i.e., barite, under reduced subsurface conditions. The primary CCA water composition would shift to a modified CCA water type (CCA*, Fig. 4).

Methodology

Sampling and Geochemical Analysis

Produced water samples were recovered from three affected wells (CCA-1, CCA-2, and CCA-3) as part of two sampling campaigns from October 2019 to December 2019 and in May 2020 as representative cases for CCA pressurized wells. A specific handling and conservation procedure, including the use of high-density polyethylene sample bottles, avoidance of air in the bottleneck, immediate sample filtration, and reduced delivery time from field to lab, was applied to assure sample quality.

The water samples were filtered through a 0.45 µm membrane and subsequently analyzed on their hydrochemical composition in major elements (Na^+, Ca^{2+}, K^+, Mg^{2+}, Cl^-, HCO_3^-, CO_3^{2-}, SO_4^{2-}), minor elements (Ba^+, Br^-, Fe^{+2}, Sr^{2+}) and trace elements (B^{3+}, I^-, Li^+, Si^{2-}) at the Chemistry Analysis Unit (R&DC). Cations were analyzed by flame atomic absorption spectrometry (Na^+, K^+, Ca^{2+}, Mg^2) or EDTA titration (Ca^{2+}, Mg^{2+}). Major anions were analyzed by using an ion chromatograph, or alternatively, acid (HCO_3^- and CO_3^-), $AgNO_3$ (Cl^-), and $BaCl_2$ (SO_4^{2-}) titration methods. Total dissolved solids (TDS) were determined by calculating the sum of cation and anion balance. The Geochemistry Unit

of EXPEC ARC analyzed five samples on their stable isotopic composition (δ^2H, $\delta^{18}O$) on a Picarro L2130-i Isotopic Water Analyzer.

Selected samples from the field and from the geochemical database went through a quality check to assure their representativeness and usability for provenance studies. Because of the requirements of electroneutrality, cations and anions are present at equal concentrations in water and comprise most of the dissolved solids in groundwater. The main criteria are to assure an electrical neutrality for the water samples, which requires an error below 5% for the ion balance between cations and anions, Eqn. 1.

$$\%E = 100 * \frac{\sum Cations - \sum Anions}{\sum Cations + \sum Anions} \qquad \boxed{1}$$

The ionic composition of water is used to classify it into ionic types based on the dominant dissolved cation and anion, expressed in milliequivalents per liter (meq/L). A meq is a measurement of the molar concentration of the ion, normalized by the ionic charge of the ion. The water type of each sample was determined by calculating the percentage contribution of each element from the total ion concentrations, whereby exclusively elements with a contribution above 10% to 12.5%, were considered. The geochemistry of the MF, SW, and different FW types from the study area were collected and utilized as potential endmembers of the CCA water.

A historical geochemical data set of two reference samples of water-based mud (WBM) filtrate (MF-1, MF-2), one groundwater sample from an Early Tertiary (Paleocene) aquifer from four supply wells (SW-1), and 12 FW samples from Early - Late Cretaceous (Formation A), Early Cretaceous (Formation B, C), Late Jurassic (Formation D), and Late Triassic (Formation E) from adjacent wells and fields was utilized as a reference database to correlate with recent geochemical data from the CCA produced water. The mentioned water types represent potential endmembers and candidates for fluid sources at CCA wells.

Environmental Isotopes

During the last few decades, several isotopic techniques have been adapted from groundwater resources management toward their application in the petroleum industry, and have greatly expanded our knowledge of the isotopic composition of natural fluids[11,12]. Oxygen-18 ($\delta^{18}O$) and Deuterium (δ^2H) are the most commonly used isotope techniques to characterize the type of produced fluid, plus to trace potential flow migration from recharge areas toward the present groundwater system.

Together with ^{13}C, oxygen and hydrogen isotopes provide measures to reconstruct heterogeneities in porosity and permeability, caused by the formation of secondary minerals through hydrothermal processes. Stable isotopes of natural meteoric waters are generally aligned with the Global Meteoric Water Line (GMWL). Craig (1961)[15] developed Eqn. 2:

$$\delta D = 8.0 \cdot \delta 18 O + 10 \qquad \boxed{2}$$

where $\delta^{18}O$ and $\delta^{2}H$ (also known as δD) are the ratio of heavy to light isotopes, e.g., $^{18}O/^{16}O$ and $^{2}H/^{1}H$.

A positive O-18 isotopic shift implies enhanced hydrothermal water-rock interaction process by the relative accumulation of heavier O-18 isotopes in the fluid phase in comparison to the rock phase. Due to the individual isotopic fingerprint of specific fluid types in their environmental setting, both isotopes are utilized to trace the provenance of surface water and subterranean fluids, plus to reconstruct coupled fluid-fluid or fluid-rock interactions.

Results

Hydrochemical Characterization of CCA Water

The wells CCA-1, CCA-2, and CCA-3 were sampled twice during the period from October to December 2019, and in May 2020, respectively, to recover and analyze six CCA water samples on their hydrochemical and isotopic composition. Samples with the extension "A" were sampled during the first campaign, and samples with the ending "B" at the second campaign. The concentration of TDS varies between 19,000 mg/L and 34,200 mg/L, Annex 1. The TDS concentration decreases slightly for all three wells between both sampling campaigns, from 30,000 mg/L to 22,400 mg/L for Well CCA-1, from 34,200 mg/L to 28,900 mg/L for Well CCA-2, and from 25,600 to 19,000 mg/L for Well CCA-3. This trend indicates a continuous mixing or alteration process of inflowing fluids between October 2019 and May 2020. Na, Cl, SO_4, and K represent the most abundant elements with a concentration range between 4,000 mg/L and 12,000 mg/L, each, followed by OH and CO_3 and Ca as minor elements, and Sr and Mg as trace elements (below 20 mg/L). In general, the geochemical composition of the CCA samples from both sampling periods is very stable with fluctuations of less than 10%.

The water type of each sample was determined by calculating the percentage contribution of each element as part of the total ion concentrations. Considering elements with a contribution above 10%, and to 12.5% of the total molar concentration, the CCA samples are classified as Na-K-Cl (CCA-2A), Na-K-Cl-SO_4 (CCA-1A, CCA-2B, CCA-3A), Na-K-SO_4-OH-Cl (CCA-1B), and Na-K-OH-SO_4-Cl (CCA-3B) water types, which reflect major varieties in the concentration of SO_4 and Cl, Annex 1. Figure 5 illustrates the dominance of Cl, Na, SO_4, and K ions in all CCA samples, but also slight compositional variations, especially for the Na, HCO_3+CO_3+OH, K, and SO_4 concentrations. The CCA-1A and CCA-2A samples are mostly enriched in Na and Cl, respectively, while CCA-3B as the lowest saline sample presents the highest CO_3 and OH concentrations.

Comparison with Reference Fluids

In case the CCA water was identified as dynamic fluid from a natural aquifer or from a reservoir-related FW system, its geochemical properties have to be linked to local or regional groundwater systems. Therefore, 12 representative FW samples from five stratigraphic units (A to E) of Late Cretaceous to Late Triassic age were analyzed and compared with CCA fluids, Annex 1. The geochemical composition of FW in the study area is very heterogeneous, with low concentrations — 8,100 mg/L to 29,400 mg/L — of TDS for brackish-type FW from the Early to Late Cretaceous units of A, B, and C. Toward depth, Late Jurassic FW from Formation D is extremely hypersaline with TDS concentrations between 189,900 mg/L (E-4) and 248,500 mg/L (D-1). Most hypersaline brines were encountered in the Late Triassic (Formation E) with maximum salinities of 310,200 mg/L.

Fig. 5 *A Spider diagram with the visual characterization of six CCA water samples, based on their major and minor elemental abundance.*
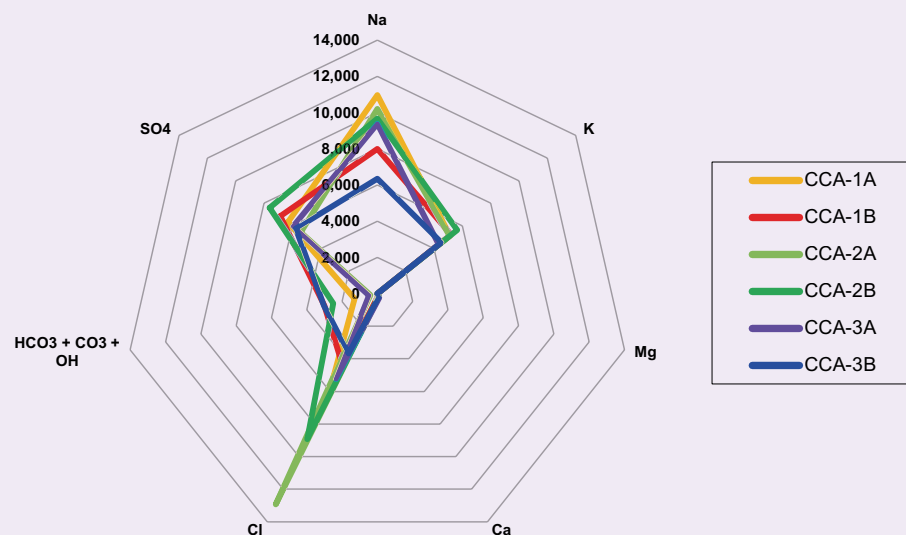
All of the mentioned FW samples are classified as Na-Cl, Na-Ca-Cl, or Ca-Na-Cl type. The visual comparison of geochemical characteristics between CCA water and FW reveals most common features with low saline, Cretaceous FW from Formation A (Albian-Cenomanian) and Formation B (Aptian), Fig. 6.

Two representative MF samples show a wide range in their salinity from 65,300 mg/L (MF-2) to 199,800 mg/L (MF-3). Both samples are dominated by Na and Cl as aqueous species, whereas CCA water is more abundant in CO_3, OH, SO_4, and K, Fig. 7. Low saline water from a Late Tertiary aquifer, used as SW for drilling, (SW-1), has the lowest salinity of all analyzed samples — TDS = 1,130 mg/L — and is depleted for all elements in comparison to CCA water.

Isotopic Characterization

Figure 8 shows the isotopic data from different water sources that was compiled and used as endmembers to trace to the source of the CCA water. Low saline Tertiary groundwater and local meteoric water are generally characterized by relative depleted and negative isotopic values ($\delta^{18}O$ below -8.0‰, and δ^2H below -40.0‰), which is related to their recharge at cooler climate conditions on the Arabian Peninsula during the last global glacial period at the end of Pleistocene period.

SW, which was utilized for cement preparation, is similarly depleted in stable isotopes, as shown for the ratios of -8.5‰ for $\delta^{18}O$, and -45.4‰ for δ^2H. Similar negative values of $\delta^{18}O$ (-10.0‰) and δ^2H (-56.2‰) for MF reflects shallow groundwater as the primary fluid

Fig. 6 *A Spider diagram with a visual comparison of the geochemical composition of CCA water with aquifer water samples from three stratigraphic units (A to C) and formation water from two stratigraphic units (D to E).*
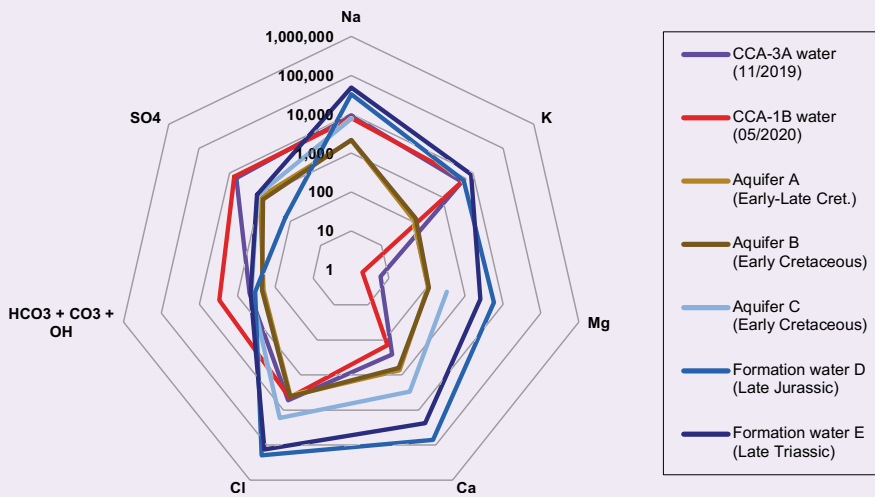
Fig. 7 *A Spider diagram with a visual comparison of the geochemical composition of CCA water with two types of MF and SW from a Late Tertiary aquifer.*
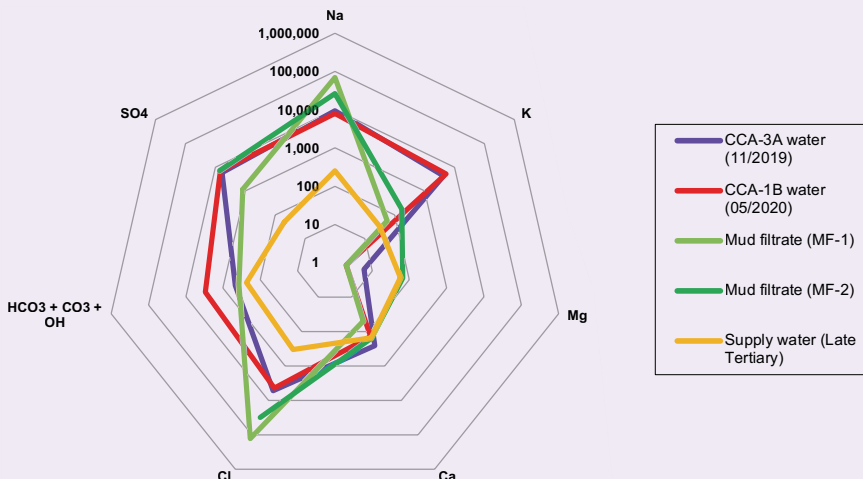
type used for the preparation of MF. The isotopic composition of all mentioned shallow surface samples is aligned with the Eastern Meteoric Water Line (EMWL), which is slightly shifted from the trend of the GMWL.

Early Cretaceous aquifer samples from different units are very similar in their isotopic composition to CCA water, and are slightly depleted in comparison to global seawater and Arabian Gulf seawater. FW from Late Jurassic units (D-1) shows a general positive shift of O-18 isotope values, caused by water-rock interaction processes. A secondary water-rock alteration process similarly affects hypersaline brine from Late Triassic (E-1), but the depletion in Deuterium indicates a different primary fluid origin compared to the Late Jurassic brines.

Annex 1

Sample No.	Water Type	Formation	Epoch	Date (mm/dd/yy)	TDS (mg/L)	pH	Na (mg/L)	K (mg/L)	Mg (mg/L)
CCA-1A	CCA Water - Well CCA-1	—	—	10/01/19	30,000	13.1	11,000	5,130	3
CCA-1B	CCA Water - Well CCA-1	—	—	05/04/20	22,400	12.7	7,990	5,210	2
CCA-2A	CCA Water - Well CCA-2	—	—	12/26/19	34,200	12.8	10,200	5,110	—
CCA-2B	CCA Water - Well CCA-2	—	—	05/04/20	28,900	12.8	9,670	5,640	< 1
CCA-3A	CCA Water - Well CCA-3	—	—	12/24/19	25,600	13.1	9,380	4,330	6
CCA-3B	CCA Water - Well CCA-3	—	—	05/04/20	19,000	12.9	6,345	4,520	2
MF-1	Mud Filtrate	—	—	05/04/20	199,800	10.8	69,500	56	2
MF-2	Mud Filtrate	—	—	08/27/13	65,300	8.3	26,400	173	66
SW-1	Supply Water	—	Tertiary	05/04/20	1,130	7.7	252	32	57
A-1	Formation Water	A	E.-L. Cretaceous	—	8,145	7.1	2,130	113	106
B-1	Formation Water	B	Early Cretaceous	—	18,700	7.1	6,640	—	148
B-2	Formation Water	B	Early Cretaceous	09/08/86	12,600	6.9	4,350	—	90
B-3	Formation Water	B	Early Cretaceous	05/29/17	8,070	7.1	2,190	132	112
C-1	Formation Water	C	Early Cretaceous	12/07/80	29,400	7.4	7,620	—	332
D-1	Formation Water	D	Late Jurassic	05/29/19	235,100	5.2	35,400	4,430	3,840
D-2	Formation Water	D	Late Jurassic	12/25/09	248,500	6.7	73,700	3,390	2,220
D-3	Formation Water	D	Late Jurassic	07/15/09	189,900	5.9	51,300	13,200	1,630
D-4	Formation Water	D	Late Jurassic	06/09/09	217,900	6.2	48,600	8,620	2,540
D-5	Formation Water	D	Late Jurassic	06/09/09	231,200	6.0	40,900	2,810	3,840
D-6	Formation Water	D	Late Jurassic	06/09/09	215,400	6.3	42,500	5,900	2,880
E-1	Formation Water	E	Late Triassic	05/23/08	310,200	5.1	32,700	4,910	5,780

Conclusions

1. Geochemical fingerprinting of CCA water and its correlation with reference samples of anthropogenic (drilling fluids) and natural (aquifer horizons, FW) origin provides a quantitative tool to determine the provenance of CCA produced water.

2. For the presented field case, compositional affinities are closest between CCA water and groundwater from a lithological unit from the Early Cretaceous epoch. This suggests that an Early Cretaceous aquifer is most likely to represent the source of dynamic water inflow into the borehole for the described three CCA cases.

3. Distinct hydrochemical and isotopic characteristics between the CCA water, WBM filtrate, and

Ca	Sr	Cl	HCO$_3$	CO$_3$	OH	SO$_4$	δ^{18}O	δ^2H	Ion Balance	Water Type
(mg/L)	(mg/L)	(mg/L)	(mg/L)	(mg/L)	(mg/L)	(mg/L)	(‰ vs. VPDB)	(‰ vs. VPDB)	(%)	
113	—	6,210	0	1,290	—	6,310	—	—	27.4	Na-K-Cl-SO4
142	5	4,400	0	743	2,240	6,850	-1.42	-21.75	7.1	Na-K-SO4-OH-Cl
173	—	12,900	0	398		5,410	—	—	8.6	Na-K-Cl
206	14	8,930	0	656	1,830	7,600	-0.73	-11.49	3.2	Na-K-Cl-SO4
259	—	5,250	0	473		5,950	—	—	29.8	Na-K-Cl-SO4
211	6	3,680	0	685	2,330	5,760	-2.01	-24.46	2.5	Na-K-OH-SO4-Cl
50	4	128,700	0	336	39	1,200	-9.94	-55.12	-9.6	Na-Cl
158	—	31,360	—	—	—	7,150	—	—	6.1	Na-Cl
152	2	334	235	0	0	< 50	-8.83	-46.2	25.5	Na-Ca-Mg-Cl
721	—	3,960	198	4	0	996	—	—	1.6	Na-Ca-Cl
444	—	10,800	268	0	0	743	—	—	-0.4	Na-Cl
290	—	6,690	280	0	0	870	—	—	-0.1	Na-Cl
637	14	4,120	223	0	0	789	—	—	1.3	Na-Ca-Cl
2,960	—	16,800	427	0	0	1,190	—	—	0.0	Na-Ca-Cl
42,200	—	147,400	—	0	0	1,850	—	—	-1.5	Ca-Na-Cl
18,600	—	150,200	218	0	0	288	4.40	-0.4	1.8	Na-Cl
10,800	—	111,700	604	0	0	709	2.33	-5.4	1.1	Na-Cl
23,400	—	133,100	447	0	0	1,240	6.54	2.9	-1.0	Na-Ca-Cl
36,100	—	146,900	384	0	0	253	9.81	2.6	-2.3	Ca-Na-Cl
26,100	—	136,600	401	0	0	931	7.52	0.0	-4.6	Na-Ca-Cl
70,800	—	195,500	339	0	0	146	7.06	-12.1	0.3	Ca-Na-Cl

Fig. 8 *A stable isotope composition of three CCA samples, in comparison to WBM filtrate, SW, Tertiary groundwater, Early Cretaceous aquifers, and formation water from Late Jurassic and Late Triassic. Also shown is the linear trend of the GMWL, the EMWL, and the composition of local meteoric water and global seawater.*
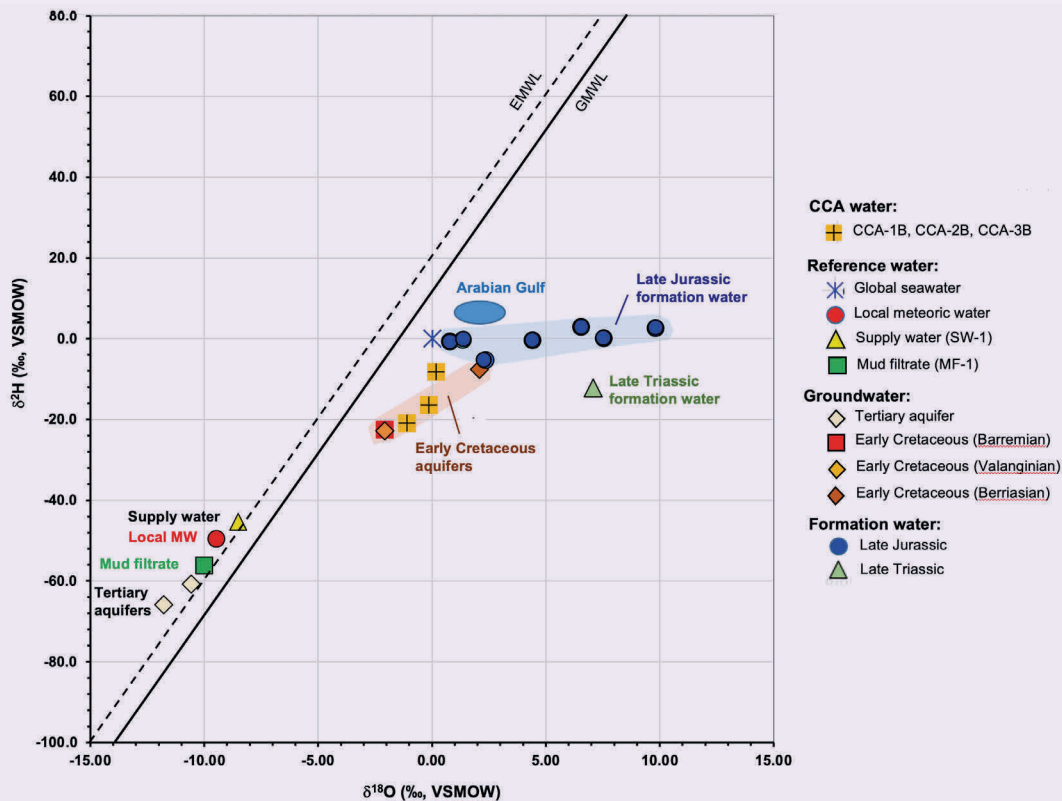
raw water, used for drilling and cementing of the described CCA wells, respectively, confirms that produced CCA water is not released from a trapped water source.

4. The homogeneous composition of CCA water between December 2019 and May 2020 — valid for all three wells — indicates the constant inflow of one single fluid source from a defined interval.

5. The deviation of pH, SO_4, and K concentration of CCA water from the Early Cretaceous aquifer water composition indicates the occurrence of minor secondary alteration processes, such the contact of inflowing groundwater with cement or by mixing with minor portions of a potassium chloride additive.

6. The application of extended multi-isotopic analysis (^2H, ^6Li, ^{10}B, ^{13}C, ^{14}C, ^{18}O, $^{87}Sr/^{86}Sr$) of all reference fluid types is recommended as an advanced geochemical tool to assess the origin of CCA produced water in newly drilled wells.

Acknowledgments

References

1. Zulkipli, S.N. and Harun, N.: "Application of Geochemical Forensic as the New Eye in Well Diagnostic," SPE paper 197984, presented at the SPE Kuwait Oil and Gas Show and Conference, Mishref, Kuwait, October 13-16, 2019.

2. Birkle, P., Martínez García, B., Milland Padrón, C.M. and Eglington, B.M.: "Origin and Evolution of Formation Water at the Jujo-Tecominoacán Oil Reservoir, Gulf of Mexico. Part 2: Isotopic and Field Production Evidence for Fluid Connectivity," *Applied Geochemistry*, Vol. 24, Issue 4, April 2009, pp. 555-573.

3. Osborn, S.G., McIntosh, J.C., Hanor, J.S. and Biddulph, D.: "Iodine-129, $^{87}Sr/^{86}Sr$, and Trace Elemental Geochemistry of Northern Appalachian Basin Brines: Evidence for Basinal-Scale Fluid Migration and Clay Mineral Diagenesis," *American Journal of Science*, Vol. 312, Issue 3, March 2012, pp. 263-287.

4. Cook, C. and Cunningham, W.C.: "Filtrate Control — A Key in Successful Cementing Practices," *Journal of Petroleum Technology*, Vol. 29, Issue 8, August 1977, pp. 951-956.

5. Haut, R.C. and Crook, R.J.: "Laboratory Investigation of Lightweight, Low-Viscosity Cementing Spacer Fluids," *Journal of Petroleum Technology*, Vol. 34, Issue 8, August 1982, pp. 1828-1834.

6. Al-Khamis, M.N., Al-Yateem, K. and Kima, E.A.: "Proactive Casing Leak Detection Methodologies: A Case History," IPTC paper 17516, presented at the International Petroleum Technology Conference, Doha, Qatar, January 19-22, 2014.

7. Deremble, L., Loizzo, M., Huet, B., Lecampion, B., et al.: "Assessment of Leakage Pathways along a Cemented Annulus," SPE paper 139693, presented at the SPE International Conference on CO$_2$ Capture, Storage, and Utilization, New Orleans, Louisiana, November 10-12, 2010.

8. Al-Mulhim, A., Al-Thwaiqib, I., Bogari, A., Bawazir, M., et al.: "Integrated Production Logging Approach for Successful Leak Detection between Two Formations: A Case Study," SPE paper 174835, presented at the SPE Annual Technical Conference and Exhibition, Houston, Texas, September 28-30, 2015.

9. Al-Ansari, A.A., Al-Refai, I.M., Al-Beshri, M.H., Pino, R.M., et al.: "Thermal Activated Resin to Avoid Pressure Build-up in Casing-Casing Annulus (CCA)," SPE paper 175425, presented at the SPE Offshore Europe Conference and Exhibition, Aberdeen, Scotland, U.K., September 8-11, 2015.

10. Tavassoli, S., Shafiei, M., Minnig, C., Gisiger, J., et al.: "Pilot Case Study of Wellbore Leakage Mitigation Using pH-Triggered Polymer Gelant," SPE paper 194251, presented at the SPE/ICoTA Well Intervention Conference and Exhibition, The Woodlands, Texas, March 26-27, 2019.

11. Birkle, P., Lozada Aguilar, M.A., Soriano Mercado, E. and Torres Villaseñor, J.J.: "Isotopic Exchange between Thermal Fluids and Carbonates at Offshore Campeche Oil Fields, Gulf of Mexico," chapter in Birkle, P. and Torres-Alvarado, I.S. (eds.) *Water-Rock Interaction*, Vol. 13, 2010, pp. 59-62.

12. Fantle, M.S. and Bullen, T.D.: "Essentials of Iron, Chromium and Calcium Isotope Analysis of Natural Materials by Thermal Ionization Mass Spectrometry," *Chemical Geology*, Vol. 258, Issues 1-2, 2009, pp. 50-64.

13. Craig, H.: "Isotopic Variations in Meteoric Waters," *Science*, Vol. 133, Issue 3465, May 1961, pp. 1702-1703.

About the Authors

Dr. Peter Birkle

Ph.D. in Geochemistry and Hydrogeology, Freiberg University of Mining and Technology

Dr. Peter Birkle is a Geological Consultant with the Geology Technology Division of Saudi Aramco's Exploration and Petroleum Engineering Center – Advanced Research Center (EXPEC ARC). His research focuses on the development and deployment of an artificial intelligence (AI)-based Oil Field Water Expert System (OWES). The main goal is to enhance exploration performance and operational productivity by preventing/reducing excess water, improving well control and resistivity prediction, and tracking fluid migration and reservoir compartmentalization.

Prior to joining Saudi Aramco in 2011, Peter worked as a scientist for the Secretary of Energy and PEMEX (Mexico) in the development of geothermal and oil fields, respectively, in several countries of Latin America.

He is active member of the Society of Petroleum Engineering (SPE), American Association of Petroleum Geologists (AAPG), and the Mexican Academy of Sciences (AMC). In 2004, he received the National Science Award in Engineering and Technology from AMC and the Saudi Aramco Excellence Award in 2017.

Peter has published more than 80 papers in peer-reviewed journals and conferences, three books and 12 book chapters (h-index = 22; i10-index = 34). He has been the associate editor for *Applied Geochemistry* and *Revista Mexicana de Ciencias Geológicas*.

In 1988, Peter received his B.S. degree and in 1993, his M.S. degree, both in Geology from the University of Tübingen, Tübingen, Germany. In 1998, Peter received his Ph.D. degree in Geochemistry and Hydrogeology from the Freiberg University of Mining and Technology, Saxony, Germany.

Hamdi A. Alramadan

M.S. in Petroleum Engineering, University of Texas at Austin

Hamdi A. Alramadan is a Petroleum Engineer working in Saudi Aramco's Southern Area Reservoir Management Department. He has over 10 years of experience in reservoir development, reservoir health maintenance, and reservoir recovery maximization and modeling. Hamdi's research interests include the effects of surface treated nanoparticles on wettability and oil-brine interfacial tension along with applications to enhance oil recovery.

In 2011, he received his B.S. degree in Petroleum Engineering from the Colorado School of Mines, Golden, CO. In 2016, Hamdi received his M.S. degree in Petroleum Engineering from the University of Texas at Austin, Austin, TX.

An Innovative Acid Diversion Using in Situ Foam Generation: Experimental and Successful Field Application

Ayman R. Al-Nakhli, Abdualilah I. Albaiz, Mohammed Yami, Mohannad A. Gizany and Wajdi Buheazah

Abstract /

In carbonate reservoirs, effective acid stimulation is essential to overcome reservoir damage and mainline high oil production. Recently, most oil wells have been drilled horizontally to maximize production. Acid stimulation of horizontal wells with long intervals requires a very effective acid diversion system. If the diversion system is not efficient enough, most of the acid will leakoff near the casing shoe — in an open hole well — which will result in a fast water breakthrough and diminish production.

This study describes a breakthrough treatment for acidizing long horizontal wells in carbonate formations. The novel technology is based on in situ foam generation to divert the acid. Gas diversion, as a foam, is a perfect diversion mechanism as gas creates pressure resistance, which forces the acid stages to be diverted to new ones. The diversion will not require the acid to be spent, compared to the viscoelastic diverting system. No gel is left behind post-treatment, which will eliminate any damage potential. The system is not impacted with the presence of corrosion products, where a diverting system will not function without effective pickling and tubular cleanup.

Lab results showed that the new in situ foam generation system was very effective on both dolomite and calcite cores. The system creates high back pressure when foam is generated, which significantly diverts the acid stages to stimulate other intervals. The new system minimizes acid leakoff and penetration. Upon completing the job, the foam collapse did not leave behind any damaging material. Field application of the in situ foam generating system showed a high success rate and outperformed other diversion mechanisms. The wells' gain was up to 18 times that of the original injectivity.

Introduction

Matrix acidizing is one of the most used methods for oil well stimulation, where hydrochloric (HCl) acid — 15% to 20% — is injected into the well and reacts with the formation rocks. This reaction forms connected channels, and wormholes that can bypass the formation damage and increase the permeability, which can increase the production rates[1-3]. According to Abdrazakov et al. (2019)[4], use of matrix acidizing has two goals: (1) maximizing the penetration into the reservoir, and (2) increasing the wellbore coverage.

In heterogeneous formations with a permeability contrast, the acid is spent mostly in the high permeable zones, which can leave the lower permeable zones untreated or poorly treated, affecting the success of the stimulation[5, 6]. To get better results from the acidizing treatment, acid diverters are used where these can force the acid to stimulate a specific area and have a better acid distribution over the well. Diverters can be categorized as mechanical diverters and chemical diverters. Mechanical diverters used as ball sealers and isolation packers cannot be used in open hole wells[7]. Chemical diverters are molecules injected with the acid, and these play a role in diverting it as in situ gelled acid, emulsified acid, or foamed acid that can plug the generated wormholes and divert the acid[8].

In situ gel is one of the methods where viscoelastic surfactants (VES) and crosslinkers increase the viscosity of the acid. There are different classifications of VES, and these include cationic, anionic, and amphoteric surfactants[1, 9, 10]. These surfactants can increase the viscosity of the acid in different mechanisms where part of them are crosslinked with metallic multivalent cations as Fe (III) aluminum and zirconium (IV). The issue with these in situ gels is that they can form formation damage as the polymer is retained in the fractures or by precipitation of the crosslinker with iron in the formation[5, 11]. These polymers require different breakers where parts of them break with the hydrocarbon production or formation water, which can change salt concentrations, and other parts require an external breaker[9].

Sarmah et al. (2019)[1] discussed a cationic surfactant that is crosslinked when the pH increases, and when it reaches to specific pH they break. Although this surfactant solves the issue of precipitation, it shows less effectiveness when HCl acid concentration exceeds 5 wt%.

Li et al. (2009)[9] evaluated an amphoteric amine oxide surfactant that can be crosslinked as a result of Ca (II) and Mg (II) concentration increases after the acid-rock reaction. When the pH and concentration of salts increase, the surfactant changes its shape and forms a rod-like shape that increases the viscosity. After a while, the concentration of salts decrease as a result of dilution, which helps in changing the surfactant shape to a spherical again. They also found that it is sensitive to Fe concentration, and if it exceeds 0.3%, the phase separation and precipitation will form.

Foam can be used as an acid diverter where the gas in the discontinuous phase can clog the fractures and reduce acid permeability in the zone. This will enhance the acid treatment as the acid will reach to the lower permeable zones. Foams also require the use of a surfactant to be stable, and the most significant limitation is the reduction in the foam quality when it reaches the wellbore[8].

This study discusses using in situ foam generation as an acid diverter and its application in the field. Exothermal reaction between sodium nitrite and ammonium chloride has been used where it generates nitrogen gas, which helps in generating the foam downhole and overcoming the injection limitation of the foam.

Concept

Several diversion techniques have been developed for effective matrix acidizing in carbonate formations. As most of the wells nowadays are horizontal with very long intervals, effective diversion has become a key for successful acidizing. During matrix acidizing, acid will flow through the highest permeable zone, leaving other intervals untreated. Therefore, diverters are used to temporarily block treated areas, so acid will be redirected to other intervals. Subsequently, during matrix acidizing, multiple stages are pumped by alternating acid and diverter to enable the maximum homogeneous treatment.

Foam diversion is one of the techniques used to divert acid as foam creates viscous diversion by trapped gas to temporarily block the acidized zone, and divert the acid to untreated areas, Fig. 1. An associated challenge with foam diversion, is the surface operation and pumping. Squeezing foam into the formation in long horizontal wells is a major challenge. Due to back pressure, pumps experience several trips and may sometimes fail to squeeze foam into the formation. Surface mixing and the preparation stage for foam prior to pumping is also a challenge. When foam collapses prematurely, during pumping, no diversion will take place downhole, which means that the acid is pumped into a limited number of intervals.

Discussion

In Situ Foam Generation

The newly developed method is based on generating foam in situ using reactive fluids. The fluid system generates foam at high temperatures. Therefore, the fluid will be pumped at the surface as liquid and once it hits the formation, foam will be generated and squeezed into the formation. This method will overcome encountered challenges with surface pumping of foam.

With in situ foam generation, it is practical to squeeze the fluid into the formation, as the fluid will have high hydrostatic pressure, e.g., 3,000 psi, which supports pumping. There are no operation challenges for surface preparation, as no foam will be prepared on the surface. The fluid system is pumped as one liquid phase, and generates gas and foam by itself in situ, therefore, no gas pumping is required to generate the foam.

Coreflood Test

A single coreflood system was used to conduct this study. Figure 2 shows the inside and outside view of the system. Figure 3 shows the schematic diagram of the system, where it contains three transfer cells (80 ml each), for brine, acid, and the in situ foam generation system, to be injected in a core holder through separate lines. The fluids were injected at a constant rate of 1 ml or 2 ml per minute, depending on the

Fig. 1 *Mechanism for in situ foam generation and acid diversion.*
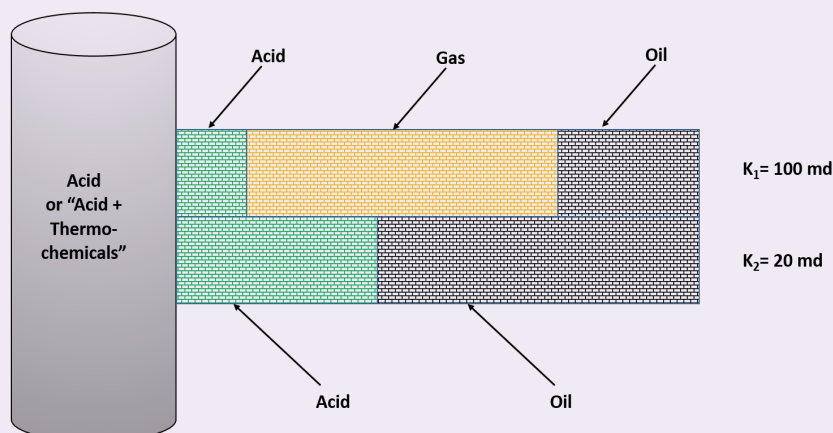
Fig. 2 *An inside and outside view of the coreflood system.*
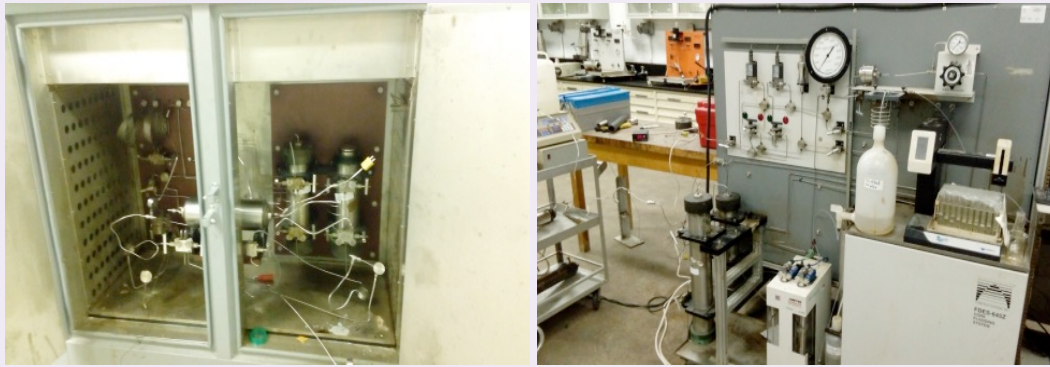
Fig. 3 *Coreflood experimental setup.*
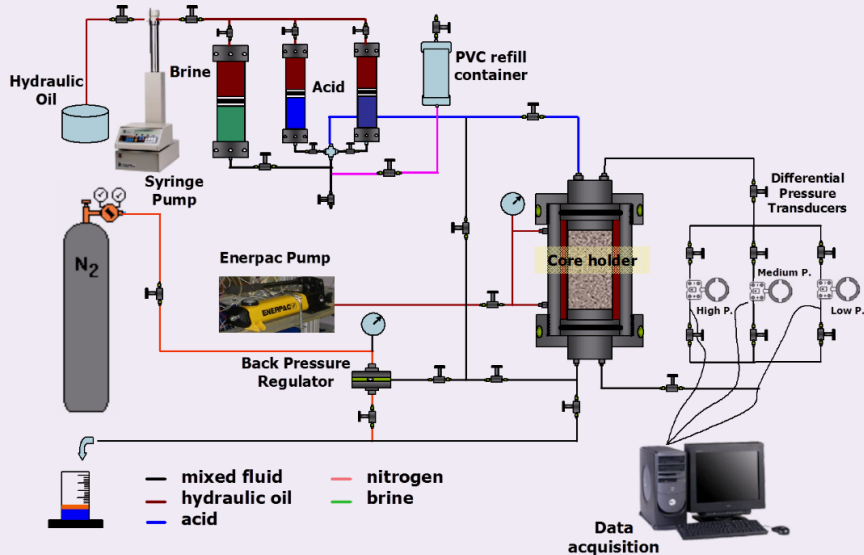
core permeability. Fluid coming out from the outlet valve was monitored for foam generation, collected in a beaker, and sent for analysis.

A 1,000-psi confining pressure was constantly set for the entire experiment duration. Pressure gauges were used at the inlet and outlet of the core holder to monitor pressure. The core holder was kept inside the oven, which is set to 200 °F to simulate downhole conditions. At this temperature, the in situ generation foam system was activated upon hitting the core sample face and foam was generated. A pressure difference between the inlet and outlet was built up and continuously recorded during the experiment. When the reaction was activated, there was a pressure build up inside the core holder. During the experiment, pressure and temperature were continuously recorded. Once the chemical injection was completed, and a breakthrough was observed, the injection was stopped and the system

was shut down. The core plug was removed from the core holder carefully, cleaned with toluene and then alcohol. A computed tomography (CT scan), micro-CT scan, and nuclear magnetic resonance analyses were conducted on the sample.

The technology was studied on both dolomite and calcite cores using a coreflooding system. In this study, the acid was injected and compared with and without a foam generation system. Cores were analyzed using a CT scan before and after the treatment.

Dolomite Core Samples

Standard dolomite core plugs were selected and scanned using a CT scan to compare the effect of in situ foam diversion.

Acid Injection

The first test was conducted by injecting 31 wt% HCl acid on the dolomite core, Fig. 4. The reaction was

slow and it took approximately 120 minutes for the breakthrough to take place. The generated differential pressure due to acid reactivity with the rock was 60 psi, at the peak. Once the breakthrough was observed, the system was shut down, the effluent collected, and the core samples were sent for CT scan imaging.

Injection of an in Situ Foam Generating System

The second test was conducted using an in situ foam generating system. As shown in Fig. 5a, the fluid contains no foam prior to injection, which will make it easy to pump in the lab and downhole in an actual field well. The fluid was placed in the accumulator and pumped down to dolomite rock at a fixed rate. Once the fluid hit the core, a reaction started to take place, as foam was generated and the differential pressure was increased from zero to 1,400 psi, Fig. 6.

The in situ generated foam created back pressure, which would force the next acid injection stage to divert to another zone. A reduced fluid volume was used in this experiment — approximately 60% — compared to the basic acid injection, which can be explained by a low leakoff of the in situ foam generating fluid system. The effluent after the flood test was purely foam, Fig. 5b. Once the breakthrough was observed, the system was shut down and samples were sent for analysis.

CT Scan Images

Post-treatment core samples were sent for CT scan analysis. Figure 7a shows the CT scan image of a dolomite core after plain acid injection, which shows some face dissolution at the injection face of the core. It is also observed that there was high leakoff of the acid with many created channels around the main wormhole. This can explain the large quantity of acid injected to get to the breakthrough. Therefore, the CT scan images show high leakoff for the core sample treated with pure HCl acid.

When the in situ foam generation fluid was used, minimal leakoff was observed, Fig. 7b. Therefore, less fluid volume was injected to get to the breakthrough. A low leakoff with generated back pressure, due to foam, will help to divert the acid stages.

Carbonate Core Samples

Acid Injection

The same approach that had been done with the dolomite cores was done on a carbonate core. In the first experiment, 30 wt% of HCl acid was injected on the carbonate rock at a fixed rate of 1 ml per minute, using the coreflood system with an oven set temperature at 115 °F, Fig. 8. This experiment was fast where the injection took around 9 minutes to breakthrough, which reflects the fast reactivity of the acid with calcite rock. The pressure drop across the core increased to 15 psi only, due to the reaction of acid with the core.

Injection of in Situ Foam Generating System

In another experiment, an in situ foam generating system was injected into a carbonate core sample using the coreflood system at a fixed rate off 1 ml/minute with an oven set to 115 °F. Once the fluid system hit

Fig. 4 *The coreflood experiment result from injecting HCl acid on a dolomite core.*
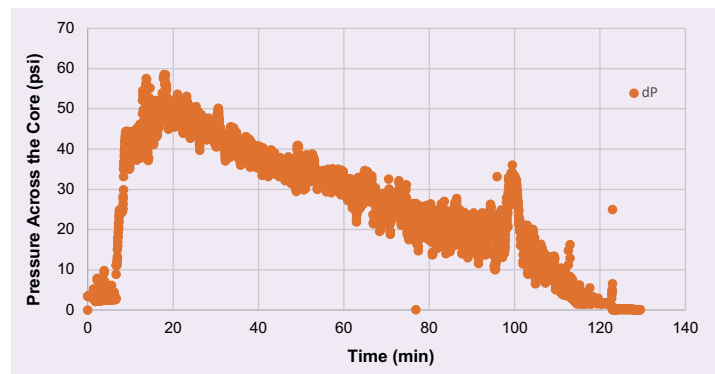
Fig. 5 *In situ foam generating system: (a) Pre-injection fluid, and (b) post-injection foam fluid.*
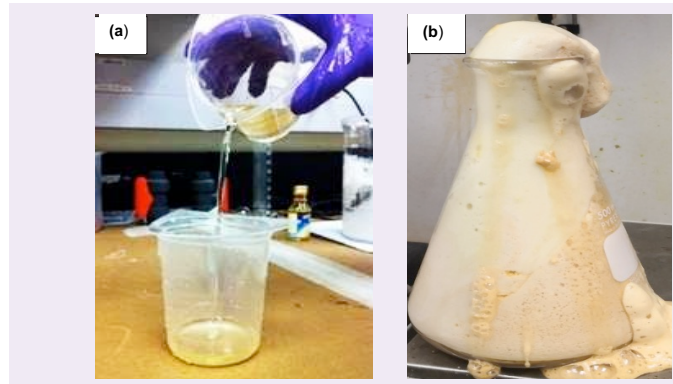
Fig. 6 *Coreflood experiment results from injecting an in situ foam generating system down to the dolomite core.*
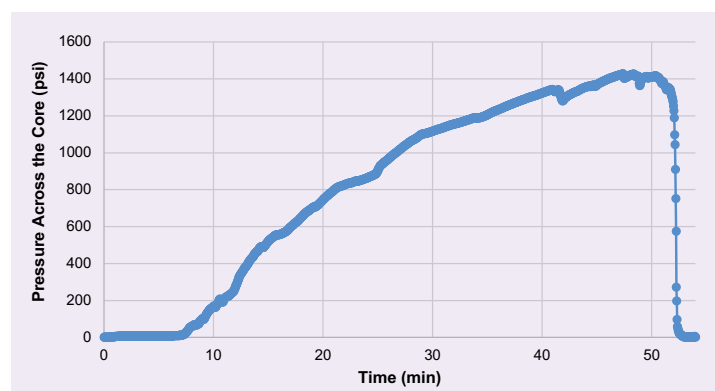
the rock face at the inlet, foam was generated and differential pressure increased to 250 psi, which is 500% of the generated pressure with plain acid, Fig. 9. The developed pressure will help to divert the following acid stage to another zone in a real oil well.

CT Scan

Collected samples post-plain acid injection were sent for CT scan analysis. Figure 10 shows the photos and CT scan images that show the high reactivity of the acid and carbonate rock, with no significant resistance

Fig. 7 *CT scan images of dolomite post-treatment with (a) acid, and (b) with an in situ foam generating system.*
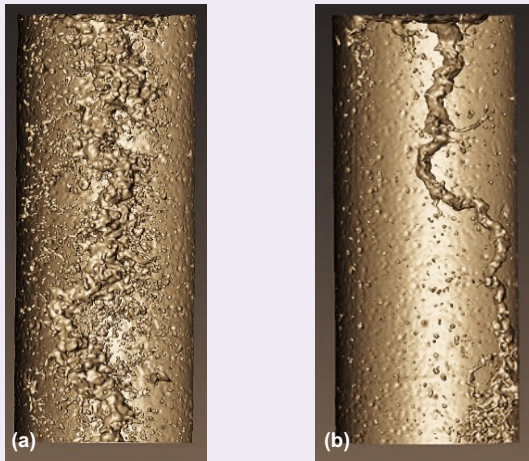
Fig. 8 *The results of the coreflood experiment from injecting HCl acid on the calcite core.*
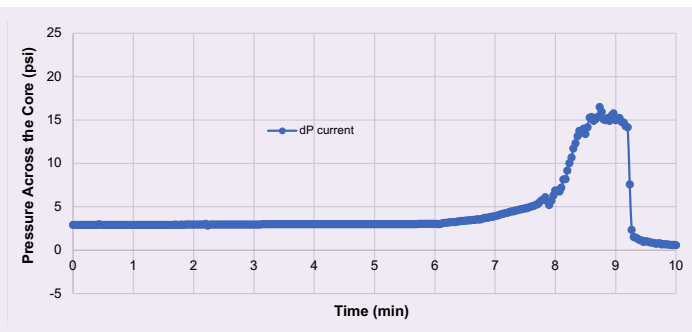
Fig. 9 *The results of the coreflood experiment from injecting an in situ foam generating system on the calcite core.*
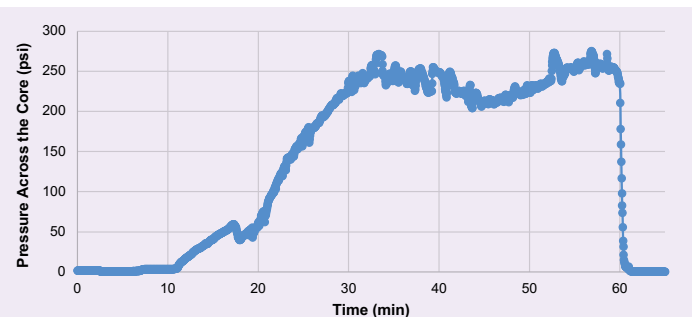
to help diversion. This can be elaborated from the large wormhole created, and face dissolution.

For core samples tested with the in situ foam generating system, CT scan analysis showed a much smaller wormhole and great diversion effect, Fig. 11. Most of the acid reactivity was at the top part of the inlet side, which explains the help of foam to minimize acid penetration and delay breakthrough, which is also reflected in the high differential pressure of a coreflood test.

Field Application

The treatment recipe was extensively tested in the lab to ensure compatibility with reservoir brine, pressure, and temperature. The job was designed to be conducted without flowing back acid, as the well is a horizontal water injector. The recipe was designed to have the in situ generated foam expand up to thirtyfold of the original fluid volume.

Another test was conducted on-site with actual chemical batches for QA/QC. Drums were tested one by one, and any expired chemical batches were replaced with fresh ones. Figure 12 shows the system prepared on the surface prior to pumping. As a spot test on the surface, the reaction was triggered by an activator, foam was generated, and the solution volume expands 30 times its original volume, Fig. 12.

The pretreatment well injectivity was measured. Then, acid and an in situ foam generation system were pumped in stages until the whole interval was treated. After completing the job, it was rigged down, connecting the well to the injection system. Successfully, the treatment increased the well injectivity up by eighteenfold of the original injectivity. The system is more cost-effective compared to a viscoelastic diverting system, with a minimal surface mixing operation compared to emulsified acid.

Conclusions

1. A novel acid diverting system was developed using an in situ foam generation system.

2. The technology eliminates the need for costly VES, with effective acid diversion and homogeneous treatment.

3. In situ foam generation represents an excellent diversion system with no damage effect, as there is no leftover. The new system also eliminates the need for flow back, so it significantly reduces the treatment time and cost.

4. The new system can easily be mixed on the surface compared to emulsified acids.

5. Lab testing showed effective acid diversion using an in situ steam generation system in dolomite and carbonate rocks.

6. Field application of the new system (in situ foam generation) outperformed rivals by eighteenfold, and increased in injectivity.

Fig. 10 *The CT scan images of the carbonate core with plain acid post-treatment.*
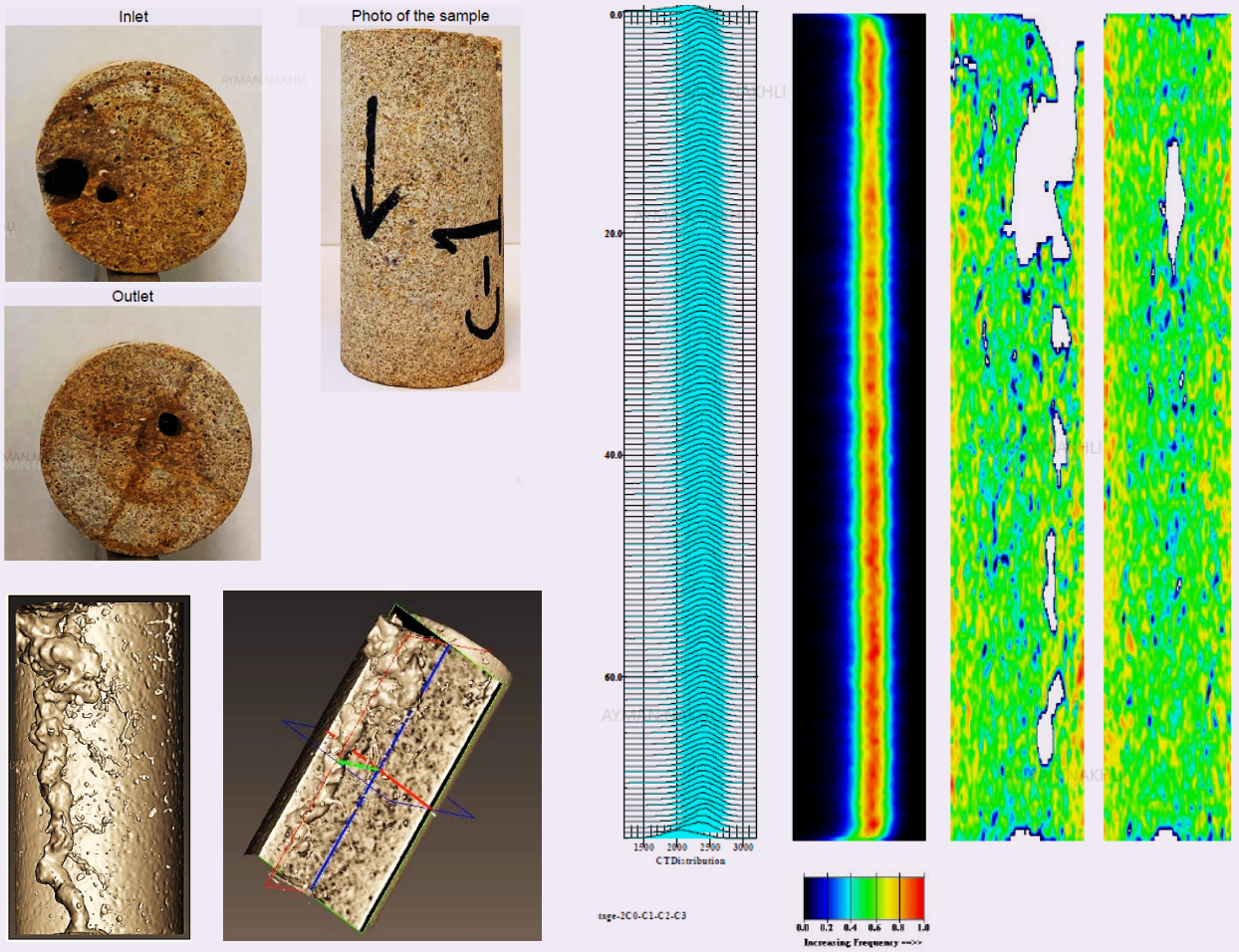
Fig. 11 *The CT scan images of the carbonate core with in situ foam generating system post-treatment.*

Fig. 12 *The lab and field testing of an in situ foam generating system, expanding up to thirtyfold of the original fluid volume.*

References

1. Sarmah, A., Ahmed, A.F., Nasr-El-Din, H.A. and Jackson, J.: "A Novel Cationic Polymer System That Improves Acid Diversion in Heterogeneous Carbonate Reservoirs," SPE paper 194647, presented at the SPE Oil and Gas India Conference and Exhibition, Mumbai, India, April 9-11, 2019.

2. Schechter, R.S.: *Oil Well Stimulation*, 1st edition, Englewood Cliffs, N.J.: Prentice Hall, 1992, 602 p.

3. Economides, M.J., Hill, A.D. and Ehlig-Economides, C.: *Petroleum Production Systems*, Englewood Cliffs, N.J.: Prentice Hall, 1993.

4. Abdrazakov, D., Kalabayev, R., Stepanov, V., Juldugulov, Y., et al.: "Integrated Approach to Diversion during Acid Treatments in Extended Intervals, High Temperature and Fractured Reservoirs," SPE paper 196969, presented at the SPE Russian Petroleum Technology Conference, Moscow, Russia, October 22-24, 2019.

5. Taylor, K.C. and Nasr-El-Din, H.A.: "Coreflood Evaluation of In Situ Gelled Acids," SPE paper 73707, presented at the International Symposium and Exhibition on Formation Damage Control, Lafayette, Louisiana, February 20-21, 2002.

6. Alghamdi, A., Nasr-El-Din, M.A., Hill, A.D. and Nasr-El-Din, H.A.: "Diversion and Propagation of Viscoelastic Surfactant-Based Acid in Carbonate Cores," SPE paper 121713, presented at the SPE International Symposium on Oil Field Chemistry, The Woodlands, Texas, April 20-22, 2009.

7. Bazin, B., Charbonnel, P. and Onaisi, A.: "Strategy Optimization for Matrix Treatments of Horizontal Drains in Carbonate Reservoirs, Use of Self-Gelling Acid Diverter," SPE paper 54720, presented at the SPE European Formation Damage Conference, The Hague, the Netherlands, May 31-June 1, 1999.

8. Ba Alawi, M., Hassan, A., Aljawad, M.S., Kamal, M.S., et al.: "A Novel Approach to Improve Acid Diversion in Carbonate Rocks Using Thermochemical Fluids: Experimental and Numerical Study," *Molecules*, Vol. 25, Issue 13, June 2020.

9. Li, L.: "Impact of Acid Additives and Fe (III) on the Rheological Properties of a New Class of Viscoelastic Surfactant," SPE paper 121716, presented at the SPE International Symposium on Oil Field Chemistry, The Woodlands, Texas, April 20-22, 2009.

10. Sultan, A.S., Balbuena, P.B., Hill, A.D. and Nasr-El-Din, H.A.: "Theoretical Study on the Properties of Cationic, Amidoamine Oxide and Betaine Viscoelastic Diverting Surfactants in Gas Phase and Water Solution," SPE paper 121727, presented at the SPE International Symposium on Oil Field Chemistry, The Woodlands, Texas, April 20-22, 2009.

11. Al-Nakhli, A.R., Nasr-El-Din, H.A. and Al-Baiyat, I.A.: "Interactions of Iron and Viscoelastic Surfactants: A New Formation Damage Mechanism," SPE paper 112465, presented at the SPE International Symposium and Exhibition on Formation Damage Control, Lafayette, Louisiana, February 13-15, 2008.

About the Authors

Ayman R. Al-Nakhli

M.S. in Entrepreneurship for New Business Development, Open University Malaysia

Ayman R. Al-Nakhli is a Petroleum Scientist in Saudi Aramco's Exploration and Petroleum Engineering Center – Advanced Research Center (EXPEC ARC), where he leads the research program on thermochemicals and develops technologies related to conventional and unconventional reservoirs such as pulse fracturing, stimulation, diverting agents, and heavy oil.

Ayman has developed and field deployed several novel technologies, with four of them being commercialized with international service companies. He received the World Oil Award for Best Production Chemical in 2015.

Ayman has filed more than 20 patents, published 35 journal papers, and 40 conference papers.

He received his B.S. degree in Industrial Chemistry from King Fahd University of Petroleum and Minerals (KFUPM), Dhahran, Saudi Arabia, and an M.S. degree in Entrepreneurship for New Business Development from Open University Malaysia, Bahrain.

Abdualilah I. Albaiz

B.S. in Chemistry, King Fahd University of Petroleum and Minerals

Abdualilah I. Albaiz is a Petroleum Scientist working with the Production Technology Team of Saudi Aramco's Exploration and Petroleum Engineering Center – Advanced Research Center (EXPEC ARC). He is working on several research projects that utilizes thermochemicals in stimulation and production enhancement.

In 2020, Abdualilah received his B.S. degree in Chemistry from King Fahd University of Petroleum and Minerals (KFUPM), Dhahran, Saudi Arabia.

Mohammed Al-Yami

A.S. in Chemistry, Jubail Industrial College

Mohammed Al-Yami is a Lab Technician working with the Production Technology Team of Saudi Aramco's Exploration and Petroleum Engineering Center – Advanced Research Center (EXPEC ARC). His work focuses on smart fluids.

In 2017, Mohammed received his A.S. degree in Chemistry from the Jubail Industrial Collage, Jubail, Saudi Arabia.

Mohannad A. Gizany

M.S. in Petroleum Engineering, University of New South Wales

Mohannad A. Gizany is a Petroleum Engineer currently assigned as a Lead Production Engineer for four fields in Saudi Aramco's Northern Area Production Engineering Department.

His experience includes work as a Reservoir and Production Engineer.

In 2010, Mohannad received his B.S. degree in Petroleum and Natural Gas Engineering from West Virginia University, Morgantown, WV. He received his M.S. degree in Petroleum Engineering from the University of New South Wales, Sydney, New South Wales, Australia, in 2017.

Wajdi Buheazah

A.S. in Chemistry, Jubail Industrial College

Wajdi Buheazah is a Lab Technician working with the Production Technology Team of Saudi Aramco's Exploration and Petroleum Engineering Center – Advanced Research Center (EXPEC ARC). His work focuses on smart fluids. Prior to joining Saudi Aramco in 2019, Wajdi worked for several service companies, including Schlumberger.

In 2012, Wajdi received his A.S. degree in Chemistry from the Jubail Industrial Collage, Jubail, Saudi Arabia.

Achieving Uniform Fluid Distribution with a Custom-Designed Organic Solvent Maximizing Coiled Tubing Reach during Matrix Acid Stimulations

Hussain A. Al-Saiood, Laurie S. Duthie, Umut Aybar and Nestor Molero

Abstract /

The success of stimulation fluid placement in open hole extended reach wells through coiled tubing (CT) is highly dependent on the depth achieved. Friction forces and helical buckling typically cause early CT lockup, which limits the reach. Organic deposits in the wellbore increases frictional forces causing premature lockup or in some cases even complete blockage. Efficient removal of organic deposits enables the CT to reach maximum depth to perform the matrix stimulation.

An analysis of these organic deposits was conducted, and following a thorough comparative test, a new solvent external phase emulsion inhibitor was selected to treat the wellbore prior to matrix stimulation. An optimum clean out methodology was identified for the CT run with a high-pressure jetting nozzle (HPJN) combined with a chemical dissolution effect of the chosen solvent. Focused, high energy fluid streams loosen any compacted deposits, while the high rate of fluid passing through the tool allows for an efficient clean out. A matrix stimulation treatment with CT was then executed in the open hole section of the extended reach well with a total depth (TD) of 18,773 ft (9,800 ft horizontal lateral section) with hydrochloric (HCl) acid and emulsified acid systems.

By using a solvent external phase emulsion, only the external phase of the emulsion containing the dissolver is in contact with organic deposits; the remaining internal phase fluid is not. This therefore allows a reduction in total solvent volume. The proposed wellbore clean out treatment with a HPJN reduced the friction coefficient between the CT and the completion by 10%. In turn, it was verified that during the operation, an additional 3,320 ft of reach was achieved in the open hole section. Combined with other extended reach techniques, i.e., mechanical agitator tools and friction reducers, it allowed the 2.0" CT pipe to reach the TD of the well, 18,773 ft.

These efforts together maximized the reservoir contact during the matrix stimulation in the open hole section with HCl acid and emulsified acid systems. Distributed temperature sensing (DTS) methodology was used with the aid of fiber optic installed CT, and the intake profile of the open hole section was mapped. Analysis of the data was applied to optimize the pumping schedule to obtain uniform production contribution across the open hole section.

The systematic engineering workflow presented includes the organic deposit diagnostic procedure, laboratory testing, chemical selection, and treatment application. This yields a wellbore treatment that minimizes friction for the remainder of the operation and enables maximum CT reach. This provides more insights of integrated matrix stimulation treatment with CT to overcome the serious challenges present in extended reach open hole wells.

Introduction

Coil tubing (CT) lockup is a challenge that is often encountered in extended reach wells during CT interventions. Saiood et al. (2019)[1] summarized that frictional forces are applied in the opposite direction while CT is running in hole (RIH). CT buckling originates when axial compressive forces over a certain threshold are applied. Buckling initiates with a sinusoidal wave shape and the CT deforms into a helix. The required force to push the CT further exponentially increases when the CT buckles into a helix.

When the frictional force between the CT and the casing or formation reaches a critical point exceeding external axial pushing forces, CT lockup occurs, and the CT will cease to RIH any further. In earlier publications[1, 2], the impact of downhole tool technology advancements was explored on maximizing CT reach in complex extended reach well completions. Maximizing the reach in these extended reach wells requires a multifaceted approach, and examining this from the fluid technology perspective — by removing organic deposits — is another important area to cover.

Organic deposition is a phenomenon that may limit the CT reach when it occurs in the wellbore. Organic deposits increase the friction coefficient in the wellbore during CT interventions. These organic deposits can block the access of the wellbore and the open hole section for any type of intervention, including slick line, wireline, and CT, and need to be treated prior to the CT matrix stimulation. Therefore, an additional wellbore deposit removal run was implemented to reduce the friction from the end of the tubing to the end of the liner shoe section. This additional run with a high-pressure jetting nozzle (HPJN), combined with the chemical dissolution effect of the chosen chemical, set the average reach limit to 90% of the open hole.

Ortiz et al. (2017)[3] stated that tar-like deposits and sludge can occur at the wellbore, in the perforations, and in the completion accessories. This is in addition to the reservoir level and how critical it is to identify the location of these deposits, Fig. 1. In the same study[3], the authors stated three chemical control agents to dissolve these deposits: (1) aromatic solvents, (2) asphaltene dispersants, and (3) asphaltene inhibitors.

Identification of deposit locations is also important in planning the treatment. It is possible to identify the exact location of an organic obstruction during an intervention operation as it will be blocking the access to the wellbore. The inclusion of real-time downhole readings from a tension compression tool helps to identify the exact location instantaneously. This of course then becomes the main challenge to overcome before proceeding with the main intervention objective. For instance, the main objective of this intervention was to stimulate the open hole section of an extended reach well (measured depth/true vertical depth > 2), however, after observing the tar-like sludge materials, the workflow was revised to open the access to the wellbore.

Background

The main objective of the intervention was to perform a CT matrix stimulation in a horizontal extended reach well located in a carbonate formation. The well is completed with a 4½" tubing, an electric submersible pump (ESP) Y-tool assembly with a 2.441" and 7" liner shoe to 15,485 ft. The 6⅛" open hole section starts from 15,485 ft and extends to 18,770 ft, Fig. 2. Matrix stimulation with the CT in extended reach open hole wells strive to reach the total depth (TD) of the wells to maximize the reservoir contact for an efficient stimulation.

A CT well intervention in the subject field observed some tags during the operation in the wellbore, however, the CT was still able to pass the obstruction. Tar-like material was observed on the bottom-hole assembly (BHA) after reaching the surface, Fig. 3. The samples were sent to the lab to identify the material to allow an efficient treatment with the compatible fluid system.

Fig. 2 *Typical open hole completion.*

4½" tubing with ESP

7" liner

6⅛" open hole

Fig. 1 *The location of the organic deposits[3].*
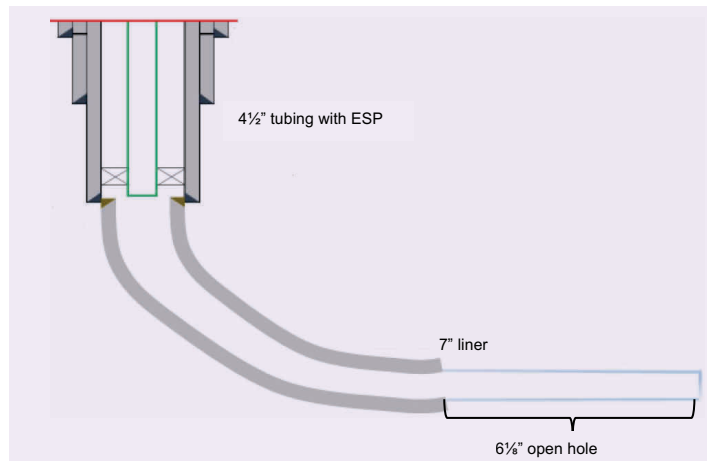
Organic Deposits

Fig. 3 *The deposits observed on the BHA.*
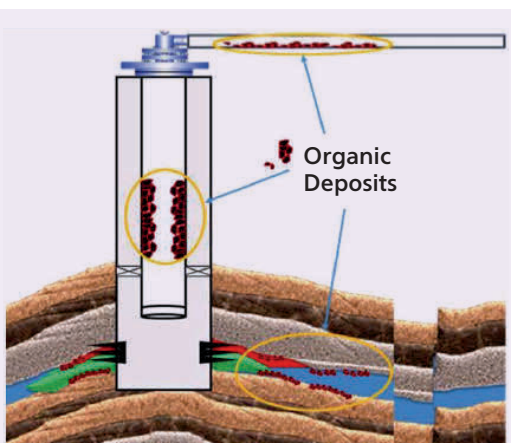
Methodology

Once samples of the deposits were collected, a comprehensive study was performed. This methodology became a fundamental step to optimize the CT reach by reducing the wellbore deposit induced friction inside the wellbore. The methodology, Fig. 4, starts with collecting the samples and sending them to a specialist laboratory with the capabilities to run multiple tests to characterize the samples.

From these results, the applicable chemical treatment is selected to identify the optimum dissolution (with time) and total percentage of the dissolution. A design aided computer simulation is performed to see the impact of removing these deposits on the CT reach performance. An additional wellbore clean out run prior to matrix stimulation is added. Finally, the matrix stimulation is completed utilizing distributed temperature sensing (DTS) to identify the intake profile to optimize the pumping schedule.

Diagnostics and Fluid Selection

To characterize the collected materials, a detailed lab study was performed, which included multiple steps. The diagnostics can be summarized as:

1. **Analytical Techniques:** Inductively coupled plasma − optical emission spectroscopy was preferred to measure cations in the samples. Suppressed ion chromatography was then used to identify sulfate and low-level chloride ion content. The pH measurements were conducted using an Accumet AR-15 pH meter. Alkalinity measurements were performed using a potentiometric titration where the endpoint determinations are done for both phenolphthalein and methyl orange. Density measurements were done utilizing an Anton Paar DMA 48 density meter.

2. **Asphaltene Content:** The asphaltene content in the organic part of the sludge sample was determined using the petroleum assessment pyrolysis method. A detailed solubility test was performed, which calculated the solubility by Eqn. 1:

$$Solubility\ (\%) =$$
$$\frac{Orginal\ weight\ (g) - residual\ weight\ (g)}{Orginal\ weight\ (g)} x100 \quad \boxed{1}$$

3. **Thermal Gravimetric Analysis:** A heating rate of 20 °C/min between 25 °C to 900 °C under air atmosphere for the compositional analysis was used.

4. **X-ray Diffraction (XRD) Analysis:** A crystalline dry obstruction material XRD analysis was performed.

The diagnostic results showed that the sample, Fig. 5, consists of both organic and inorganic material. The inorganic portion of the sample showed mainly corrosion products in the forms of iron sulfides and iron oxide based on the XRD analysis. The sources of iron species identified as the interaction of hydrogen sulfide (H_2S) and carbon dioxide with production tubing steel. It was observed that the two-stage solubility test dissolved more than 70% of the sludge sample. A two-stage treatment includes 15% hydrochloric (HCl) acid (with iron content) followed by a mutual solvent.

The two-stage treatment, including solvent wash, removes the organic phase covering the inorganic material followed with 15% HCl acid. A pre-flush/

Fig. 5 *A sample of the obstruction material collected from a representative well.*

Fig. 4 *Deposits removal prior to matrix stimulation methodology.*
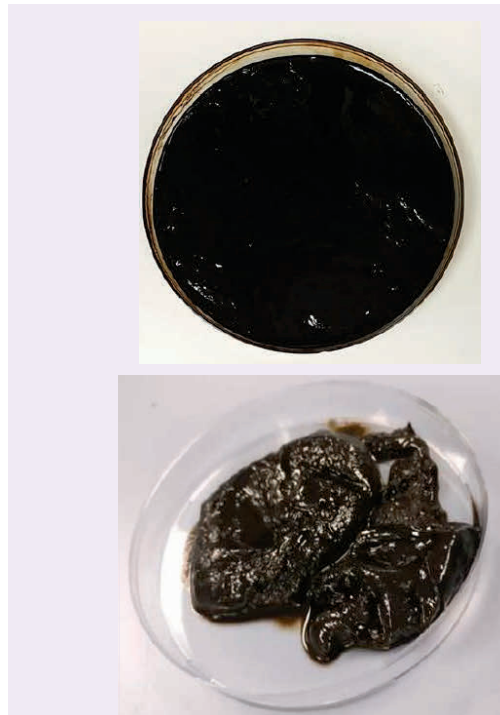
post-flush of freshwater containing a water wetting surfactant, H_2S scavenger, and mutual solvent is conducted prior to and after the acid treatment. The acid recipe also includes a mutual solvent, a water-wetting surfactant, a corrosion inhibitor, iron control agents, and a H_2S scavenger.

Based on the diagnostic recommendations, two chemical treatment options were further evaluated in consecutive lab studies. The first option was a non-aromatic solvent (treatment A), which readily dissolves or disperses paraffinic deposits, heavy residual oil fractions, asphalts, and waxes from oil wells. The non-aromatic solvent is a combination of natural extracts that is particularly effective on residual pipe-dope deposits used for wellbore pickling operations prior to interventions. It is equally effective on paraffin wax buildups and is applied directly to clean the formation and well equipment.

The second option was a solvent external phase emulsion inhibitor (treatment B). One of the factors that often limits the efficient removal of organic deposits in the wellbore is the volume of solvent in contact with the organic deposits. In general, the mass of the asphaltene or wax deposit on the wall of the tubulars is much greater than can be dissolved by the volume of solvent in contact with the deposit. This means that an additional volume of solvent must be displaced in the wellbore to have enough solvent in contact with the organic deposit to completely dissolve it.

By using a solvent external phase emulsion, only the external phase of the emulsion is in contact with the organic deposit; the remaining fluid (the internal phase) not in contact with asphaltene or wax deposits is water. Using a solvent external phase emulsion greatly reduces the volume and cost of the solvent, while ensuring that the asphaltene deposits are removed efficiently.

To test the effectiveness of these two options, solvent strength tests were performed followed by 15% HCl acid. The solvent strength test can be summarized as per the following steps:

1. Four samples of 40 mL of both treatments A and B were prepared.

2. Four grams of the sludge were added to each sample of treatments A and B.

3. The mixtures were placed in a water bath set at 65 °C.

4. The four samples of treatments A and B were kept in the water bath for their designated time intervals: 1 hour, 3 hours, 5 hours, and 24 hours, respectively.

5. After removing each sample from the water bath, the sample is then filtered using filter paper.

6. The filtered samples were kept in the oven for 24 hours.

7. The samples were then weighed.

8. 40 mL of 15% HCl acid spearhead was added to each of the samples.

9. The samples were then placed for 1 hour in the water bath at 65 °C.

10. The samples were then re-filtered using filter paper.

11. The filtered samples were kept in the oven for 24 hours.

12. The samples were then re-weighed.

Figures 6 and 7 shows the lab test results for Treatment A without HCl acid, and Figs. 8 and 9 shows the lab test results for Treatment B with HCl acid. One can notice that treatment B gives a favorable dissolution — up to 80% while treatment A is at 60% dissolution. Also adding 15% HCl acid into the treatment schedule shows a remarkable increase in the dissolution of the obstruction material. The results after the comprehensive lab work was that treatment B was more effective, therefore, this solvent external phase emulsion inhibitor followed by 15% HCl acid was selected for implementation.

Fig. 6 *Dissolution vs. soaking time (solvent only).*

Fig. 7 *Treatment A test results, without HCl acid.*

Fig. 8 *Dissolution vs. soaking time (solvent and 15% HCl acid).*
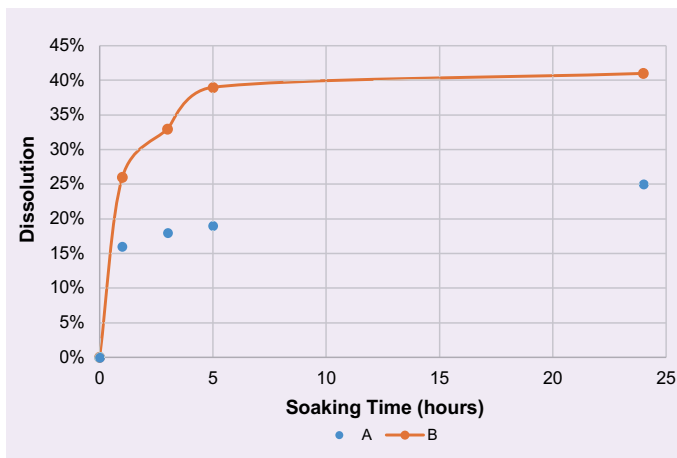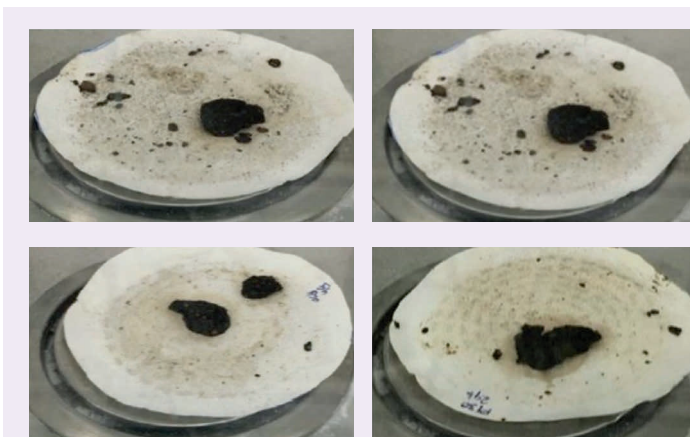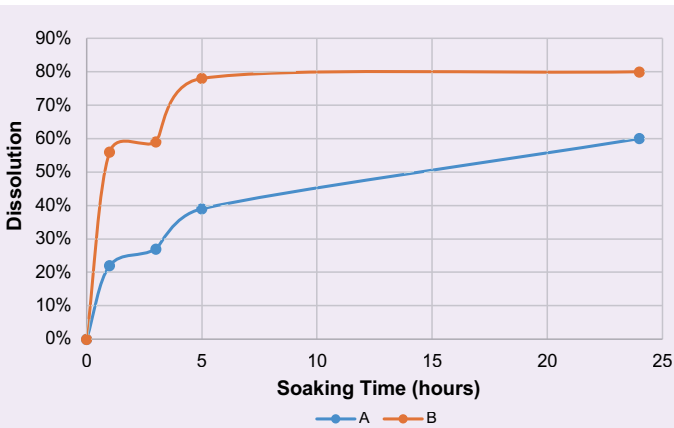

Fig. 9 *Treatment B test results, with HCl acid.*
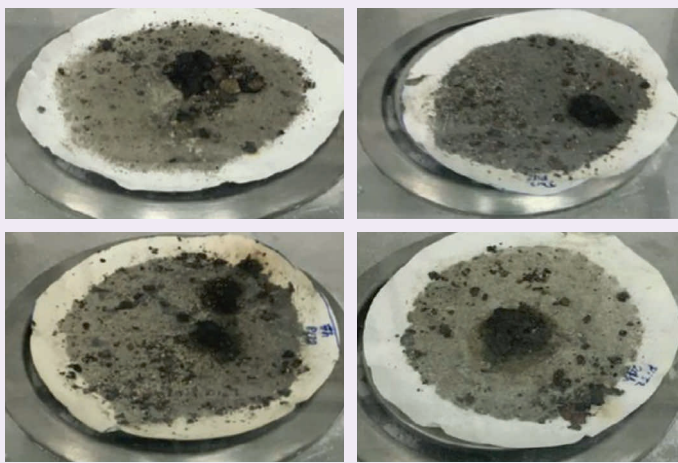
CT Agitator Tool Description

The buckling state of the CT string can be eliminated or delayed by reducing the induced friction due to the CT string and wellbore contact area. The CT agitator tool is used as a friction reduction tool to reduce the drag and frictional forces between the wellbore and the CT string while RIH. The agitator working principle is to break the static friction and convert it to a lower amount of friction in a dynamic form.

This is accomplished by generating continuous pressure pulses while pumping fluid through the tool. The CT string reacts with these traveling excitation waves as continuous mechanical motions. The friction is reduced in the part of the string where the pressure waves are traveling through the system. This friction reduction mechanism will result in improved weight transfer, faster CT tripping in speed, and delayed CT buckling occurrence, thereby extending the CT reach.

The agitator consists of two main sections: a power

section and valve assembly. The tool is activated by pumping a fluid through it and both tool sections work together converting the hydraulic energy to produce a series of pressure fluctuation waves that travel up and down in the coil. When the pumped fluid is passing through the tool, the rotor inside the power section rotates. The rotor's rotation, which occurs at a frequency proportional to the flow rate, will drive the oscillation valve plate in a continuous dynamic track relative to a stationary valve plate. This movement creates cyclic variation of the fluid's total flow area. This total flow area variation initiates a series of repetitive pressure pulses that are carried by the pumped fluid, Fig. 10[4].

Field Example

The optimum wellbore clean out treatment was designed based on the specific well parameters and the expected deposits. The treatment is combined with the mechanical effectiveness of the clean out BHA; the tool selected to perform this procedure was the HPJN, Fig. 11. Focused, high-energy fluid streams loosen any compacted deposits, while the high rate of fluid passing through the tool allows for an efficient clean out[5].

Design aided simulations were then performed to identify the CT reach for the 2.0" CT with different conditions. The various scenarios compared cases without a HPJN clean out run, with the HPJN clean out run with the selected wellbore treatment B followed by 15% HCl acid, and the matrix stimulation run with a vibrating agitator tool. The historical CT reach database was used to identify friction coefficients. The CT reach analysis results for various scenarios are given in Table 1.

Figure 12 shows the parameters of the clean out operation. The CT starts to RIH to 5,000 ft where the HPJN is activated to clean out the wellbore, continuing to RIH to 13,627 ft. A hard tag was observed before the expected lockup depth of 16,094 ft. Treatment B was performed followed by a 15% HCl acid wash in the wellbore. This enabled access to the rest of the wellbore, which was then confirmed during the matrix stimulation run with the CT agitator tool. During the matrix stimulation run, the CT continued to RIH while pumping friction reducer in the cased hole section and pre-flush in the open hole section, reaching 18,773 ft — the TD of the well.

This result showed the direct impact of clearing the wellbore obstruction with an effective treatment strategy developed with the characterization and fluid selection. In turn, this enabled a uniform fluid distribution during matrix stimulation, with DTS utilized to identify the intake profile to update the pumping schedule on the fly, Fig. 13.

Conclusions

Matrix stimulation in horizontal extended reach wells with open hole completions are complex operations, including several elements and challenges. In this article, we focused on how critical it is to identify the wellbore deposits and select the most effective treatment strategy. This in turn clearly impacts positively

Fig. 10 *A schematic of the agitator and cyclic pressure waves signature.*
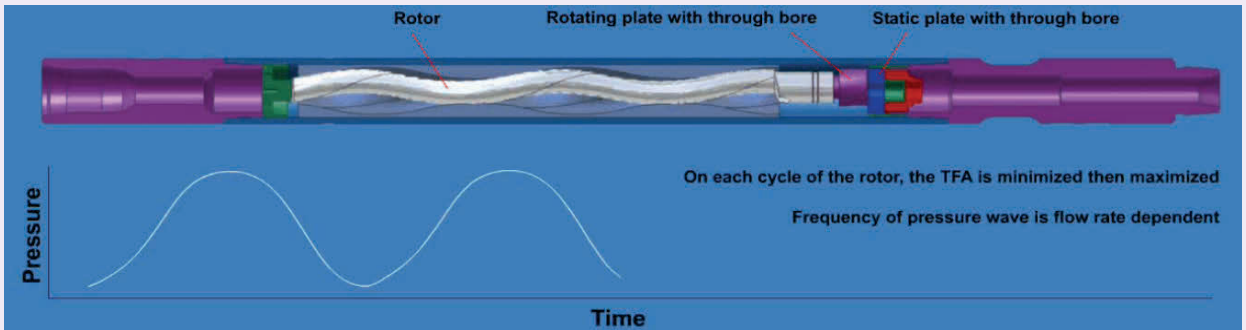
Fig. 11 *Clean out the BHA. (a) Fiber optics connector head and release sub, (b) Pressure temperature sub, (c) Casing collar locator sub, (d) Tension compression sub, providing axial load readings, (e) Downhole filter, (f) Motor head assembly, and (g) Engineered HPJN.*
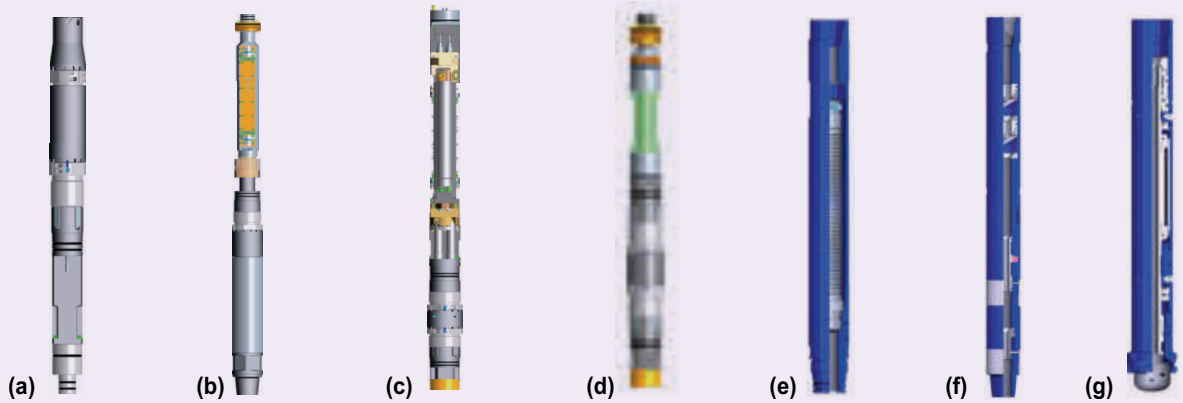
Table 1 *CT reach analysis for various scenarios.*

	Friction Coefficients		
Scenarios	**Cased Hole**	**Open Hole**	**Reach (ft)**
Without HPJN	0.27	0.27	13,465
With HPJN	0.22	0.27	16,094
With HPJN + 2⅛" agitator	0.20	0.27	17,700

on reaching the TD of the well during the matrix stimulation. This would not be possible if the access to the open hole was not established during the clean out run. The outcome can be classified as follows:

- Wellbore obstruction samples were used from representative wells in the field to characterize the material content. This enabled taking proactive contingency actions during matrix stimulation operations.
- Using a solvent external phase emulsion, only the external phase of the emulsion containing the

dissolver is in contact with organic deposits; the remaining internal phase fluid is not. This in turn reduces the required solvent volume.

- Clearing the wellbore efficiently enabled reaching the TD of the well during matrix stimulation operation.
- The combined effect of chemical systems and downhole tool advancements set the standards for challenging the extended reach wells' CT intervention operations.

Fig. 12 *The CT parameters for the clean out run.*
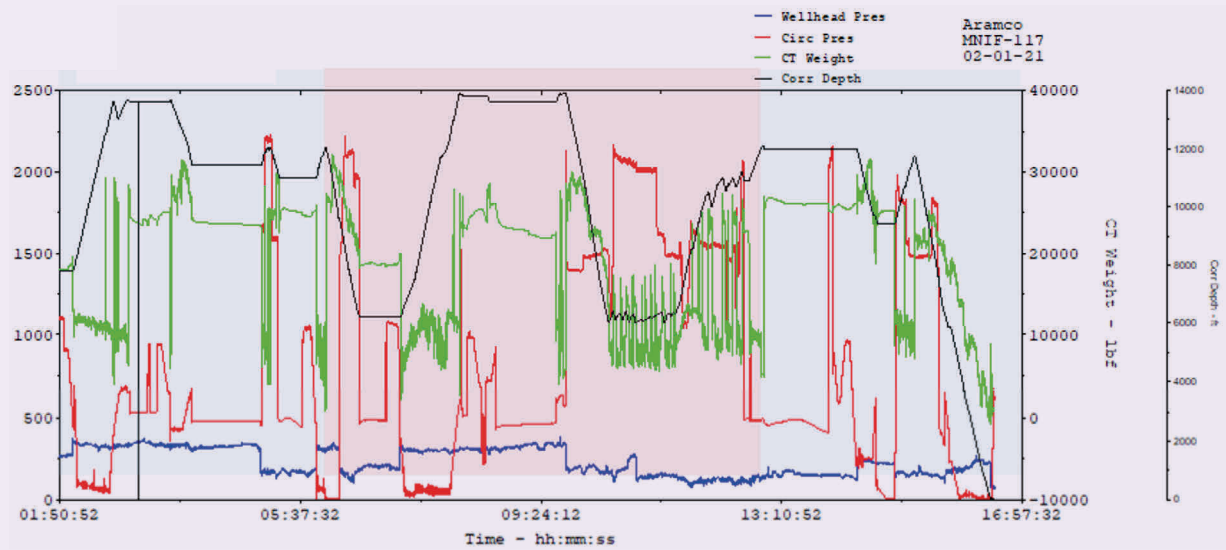
Fig. 13 *The DTS prior to matrix stimulation.*
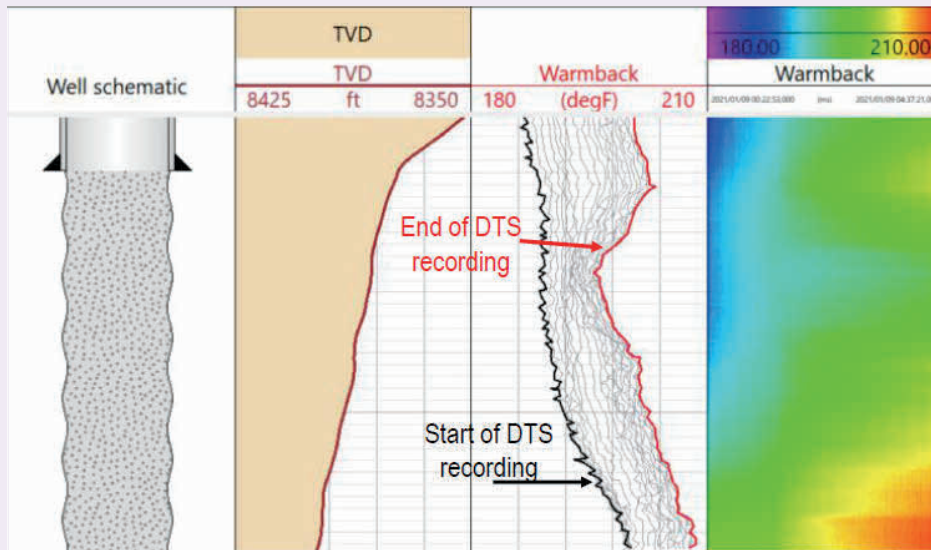
Acknowledgments

References

1. Saiood, H., Duthie, L., Aybar, U. and Bal, M.: "Incremental Gains in Coil Tubing Reachability for Highly Restricted Extended Reach Open Hole Completions," SPE paper 194259, presented at the SPE/ICoTA Well Intervention Conference and Exhibition, The Woodlands, Texas, March 26-27, 2019.

2. Saiood, H., Otaibi, A., Duthie, L., Aybar, U., et al.: "Powerful Hydraulic Coil Tubing Tractor Facilitates Stimulation Application in Extended Reach Wells through Completion Operations," SPE paper 199851, presented at the SPE/ICoTA Well Intervention Conference and Exhibition, The Woodlands, Texas, March 24-25, 2020.

3. Ortiz, R., Perez, C., Sánchez, O., Aybar, U., et al.: "Asphaltene Prevention Work Flow Enhances Oil Production in High Temperature Fractured Carbonate Reservoirs," *SPE Production & Operations*, Vol. 32, Issue 4, November 2017, pp. 476-490.

4. Saiood, H., Duthie, L., Albaqshi, A. and Ahsan, M.: "Design Optimization for Hydraulically Driven

Agitation Tool in Extended Coiled Tubing Reach Application," SPE paper 204425, presented at the SPE/ICoTA Well Intervention Conference and Exhibition, Virtual, March 22-25, 2021.

5. Dahroug, A., Brown, B. and Shaheen, M.: "Optimizing Acid Treatments with the Use of Jet Blasting Tool," SPE paper 68364, presented at the SPE/ICoTA Coiled Tubing Roundtable, Houston, Texas, March 7-8, 2001.

About the Authors

Hussain A. Al-Saiood

B.S. in Petroleum Engineering, University of Oklahoma

Hussain A. Al-Saiood is a Production Engineer working in the Manifa Production Engineering Division of Saudi Aramco's Northern Area Production Engineering and Well Services Department. He joined Saudi Aramco as a Petroleum Engineer, but has also held several drilling and reservoir engineering positions, covering several onshore and offshore fields. Hussain's areas of interest include rigless intervention with coiled tubing (CT), wireline, and hydraulic workover operations.

Throughout his career, he has worked on multiple projects, including the change out of electric submersible pumps utilizing the hydraulic workover unit, and developing downhole equipment to enhance the CT reach, i.e., CT tractors and pulsation tools, in extended reach wells for stimulation and logging applications.

Hussain received his B.S. degree in Petroleum Engineering from the University of Oklahoma, Norman, OK.

Laurie S. Duthie

M.S. in Petroleum Engineering, University of New South Wales

Laurie S. Duthie joined Saudi Aramco in 2011 as a Petroleum Engineer and works in the Manifa Production Engineering Unit of the Northern Area Production Engineering Department. His focus is on the development and production of a large offshore field in the Northern Area.

Laurie started his career in 1986 working on offshore installations in the U.K. North Sea as a Field Engineer in well testing and wireline operations. He has a strong background in reservoir surveillance, well intervention, acid stimulation, well testing, completions, and cased hole logging. Laurie has gained extensive operational experience in diverse remote onshore and offshore locations — across Africa, Central Asia, the former Soviet Union, Asia Pacific, and in the Middle East region — since 2009.

In 2005, Laurie received his M.S. degree in Petroleum Engineering from the University of New South Wales, Sydney, Australia.

Umut Aybar

M.S. in Petroleum Engineering, University of Texas at Austin

Umut Aybar is a Completions Technology Development Engineer at Schlumberger based in Houston, TX. Previously, he held the role of Senior Technical Sales Engineer at Schlumberger based in Dhahran, Saudi Arabia. Umut's 10 years of experience includes various global assignments in the USA, Turkey, Japan, and Saudi Arabia.

His area of expertise is extended reach horizontal wells, completions technology, matrix stimulation, intervention diagnostics, and data interpretation for distributed measurements.

Umut has authored and coauthored more than 20 conference proceedings and peer-reviewed journal papers. He serves as an Associate Editor at the *Journal of Natural Gas Science & Engineering*, and as a committee member for the Society of Petroleum Engineers (SPE)/Intervention and Coiled Tubing Association (ICoTA) Middle East and North Africa.

Umut received his B.S. degree from Istanbul Technical University, Istanbul, Turkey, and an M.S. degree from the University of Texas at Austin, Austin, TX, both in Petroleum Engineering.

Nestor Molero

B.S. in Mechanical Engineering, Universidad del Zulia

Nestor Molero is currently the Well Intervention Regional Domain for Schlumberger Middle East and North Africa, acting as Technical Advisor for Coiled Tubing and Matrix Stimulation services in the region.

He has also been serving as co-chairman for the Intervention and Coiled Tubing Association (ICoTA) Middle East and North Africa since 2019.

Nestor is a Principal Well Intervention Technical Engineer with more than 22 years of experience in coiled tubing and matrix stimulation operations. During the last 7 years, he has played a key role on the introduction of several new technologies and value solutions for well intervention at a global level.

Nestor has coauthored over 25 Society of Petroleum Engineers (SPE) papers and technical articles published in various industry magazines.

In 1999, he received his B.S. degree in Mechanical Engineering from Universidad del Zulia, Maracaibo, Venezuela.

NanoGram Detection of Drilling Fluids Additives for Uncertainty Reduction in Surface Logging

Dr. S. Sherry Zhu, Marta Antoniv, Dr. Martin E. Poitzsch, Dr. Nouf M. Aljabri and Dr. Alberto F. Marsala

Abstract /

The manual sampling of rock cuttings off the shale shaker for lithology and petrophysical characterization is performed frequently during mud logging. Knowing the depth origin where the cuttings were generated is very important for correlating the cuttings to the petrophysical characterization of the formation. It is a challenge to accurately determine the depth origin of the cuttings, especially in horizontal sections and in coiled tubing drilling, where conventional logging while drilling is not accessible.

Additionally, even in less challenging drilling conditions, many factors can contribute to an inaccurate assessment of the depth origin of the cuttings. Inaccuracies can be caused by the variation of the annulus dimension used to determine the lag time, and therefore, the depth of the cuttings, by the shifting or scrambling of cuttings during their return trip back to the surface, and by the mislabeling of the cuttings during sampling.

In this work, we report the synthesis and application of polystyrenic nanoparticles (NanoTags) in labeling cuttings for depth origin assessment. We have successfully tagged cuttings using two Nano-Tags during a drilling field-test in a carbonate gas well and demonstrated nanogram detection capability of the tags via pyrolysis-gas chromatography-mass spectrometry (Py-GC-MS) using an internally developed workflow. The cuttings depth determined using our tags correlates well with the depth calculated by conventional mud logging techniques.

Introduction

During drilling operations, oil companies rely on mud logging services to gather important data about the formation and location of hydrocarbons[1]. Surface logging companies provide information such as lithology data, minerology, reservoir connectivity, and the presence of oil, which helps them to make informed decisions about the optimum well placement and drilling, and therefore, maximum oil recovery[2].

Many of the above-mentioned characterizations depend on the collection of cuttings during the mud logging process because cuttings carry key information about the subsurface layers[3]. The petrophysical properties of the cuttings, combined with the calculation of the cuttings' depth origin, generate an understanding of the formation[4], however, an improper depth assessment may cause misleading mapping of the reservoir. Therefore, determination of the true location of hydrocarbons and proper mapping of the formation's petrophysical properties hinge on the accurate assessment of the drill cuttings' depth.

Many factors impact the cuttings' depth determination, causing uncertainties in the depth origin. For example, the depth calculation depends on the cuttings' return trip up the annulus[5]. The return trip lag time may be miscalculated due to hole caving, overgauge drilling, spiraling, and settling of cuttings in the return trip to the surface. Furthermore, gravitational debris accumulation, hydraulics, and hole cleaning can cause errors in horizontal intervals. These combined factors result in depth inaccuracies of 20 ft or more, depending on the length of the return trip. Mislabeling of collected cuttings can further increase these inaccuracies. Despite these errors, mud logging serves as a valuable tool for understanding the formation during drilling.

Unfortunately, traditional mud logging cannot be applied to some drilling conditions, but would be very beneficial for achieving improved well placement and oil recovery. Logging while drilling is currently not available for coiled tubing drilling, where logging tools are not accessible in the small diameter hole sizes, e.g., 3". Affordable logging options are also not available for extended reach horizontal drilling and underbalanced gas drilling.

Using polymeric tags to label the cuttings when they are formed at the drill bit is a promising technology for accurate determination of the depth origin of the drilled cuttings and for formation evaluation in operations where logging while drilling is not yet applied. The unique barcoded labels on the cuttings correlate to the exact depth of the cutting's origin in wells that are thousands of feet long with an accuracy of +/- 2 ft.

This innovative technology consists of: (1) barcoded NanoTags, (2) an extraction process, and (3) a detection method for precisely and distinctively labeling the drill cuttings at the exact time of their generation at the drill

bit. The NanoTagging approach also uses the downward trip time through an accurately known drillpipe's inside diameter to estimate the depth origin instead of the longer upward trip time traditionally used by mud logging. The NanoTagging method can improve the depth correlation to +/- 2 ft, matching the accuracy of wireline logging. More importantly, the NanoTags adsorb into the cuttings until collection and analysis, increasing certainty in depth assessment, even if the cuttings become shuffled during transport.

We successfully synthesized polymeric "NanoTags" using a simple, scalable emulsion polymerization method. Notably, the sizes of the as-made NanoTags were narrowly distributed in the range of 20 nm to 60 nm, and were proven to be compatible with drilling fluids without affecting the rheology of the drilling mud, and were safe for handling and disposal due to their low toxicity. The tags were designed such that they would adhere to the rocks and remain stable in downhole conditions; the tags would only depolymerize by thermal treatment, i.e., pyrolysis, for chromatographic separation and mass spectral analysis after cuttings collection. We used a pyrolysis-gas chromatography-mass spectrometry (Py-GC-MS) system to identify the tags at nanogram quantities on the drill cuttings.

Our NanoTagging technology shows promise for ultimately helping to maximize oil recovery. Improved depth correlation accuracy can allow oil and gas operators to: (1) improve the quality of lithological and petrophysical analyses, (2) enhance formation evaluation and geosteering practices, and (3) control well placement. These advantages can be achieved by injecting ppm levels of the NanoTags into drilling fluids without any interruption to the drilling operation. Additionally, the detection of the nanoparticles can be automated using an auto-sampler, showing the potential for quick sample analysis close to the well site.

The NanoTagging technology can be seamlessly integrated into the already employed mud logging process, Fig. 1. The tagging innovation uses a modified approach to calculate the tag and cuttings arrival time. In conventional mud logging, the depth from which cuttings were generated, L_g, is estimated using annular volume, V_a, in barrels (m^3), and the mud flow rate, f, in m^3/min, to compute the lag time, t_l. The lag time is given by Eqn. 1:

$$t_l = \frac{V_a}{f} = \frac{L_g(\pi R_a^2 - \pi R_p^2)}{f} \quad \boxed{1}$$

The drillpipe and the V_a correlate to the cuttings' depth, L_g, and to the annular and drillpipe radius, R_a and R_p, Eqn. 1. The L_g is estimated by the drill bit depth at the time the cuttings are collected, L_c, minus the distance the drill bit moves during the lag time, t_l, i.e., the lag time multiplied by the drill speed, v (meter/minute), Eqn. 2:

$$L_g = L_c - t_l v = L_c - \frac{L_g(\pi R_a^2 - \pi R_p^2)}{f} v$$

$$L_g = \frac{f L_c}{f - (\pi R_a^2 - \pi R_p^2) v} \quad \boxed{2}$$

Unfortunately, the V_a (radius) is not always accurately
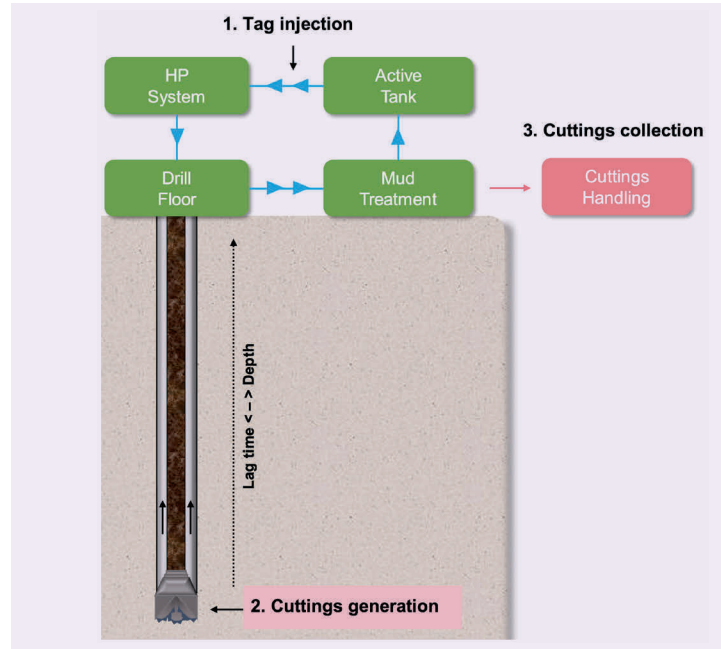
known, due to borehole enlargement during drilling, whirling of the bit, spiraling, or radial fracturing; these factors can cause minutes of lag time error, or as much as 10 ft to 20 ft of depth error, depending on the drilling rate of penetration.

The new NanoTag technology improves on this depth correlation by using the drillpipe interior volume, V_d, and the f, to calculate the downward going lag time, t_i, as given by the following:

$$t_i = \frac{V_d}{f} = \frac{L_i \pi R_p^2}{f} \quad \boxed{3}$$

When a particular barcode, i, is pumped at time, t_i, at the drill bit depth of L_i, the depth of the cuttings tagged with that same barcode, L_{bi}, is the L_i plus the distance of the drill bit moved during the downward lag time:

$$L_{bi} = t_i v + L_i$$

$$L_{bi} = \frac{L_i \pi R_p^2}{f} v + L_i \quad \boxed{4}$$

The downward going lag time is shorter than the upward going lag time and depends only on the internal dimensions of the drillpipe and the bottom-hole assembly (BHA) elements, which are accurately known and not subject to change during drilling. The NanoTags mark the cuttings, preventing any confusion due to shifting, settling, or mislabeling in handling, transport, and storage.

Materials and Methods

All the chemicals were purchased from Sigma Aldrich

Co. and used without further purification. The solution of sodium dodecyl sulfate (2.55% in water) was degassed under vacuum overnight before being used as an emulsion for the polymerization reactions.

We synthesized two NanoTags: poly(4-bromostyrene-co-acrylamide) (P(BrSt-AM)) and poly(4-chlorostyrene-co-acrylamide) (P(ClSt-AM)), at a large-scale using an internally developed synthetic method[6]. To improve the colloidal stability of the NanoTags in water and brine, 20 mol% of a water-soluble acrylamide monomer was introduced to the emulsion polymerization to form copolymers with bromostyrene and chlorostyrene. Figure 2 shows the synthetic method for making the two NanoTags in field-test quantities.

The incorporation of acrylamide into the tags also improves the long-term stability of the nanoparticles in aqueous solution even at elevated temperatures. As an example, Fig. 3 shows the particle size of the PClSt nanoparticles at 45 °C over time. The particle size in water was measured using a dynamic light scattering experiment at 25 °C in a polystyrene cuvette with a 90° angle, 659 nm laser. The reported data for each point shows an average of three repeated measurements. As illustrated in Fig. 3, only small changes occur to the particle size over the course of three months, indicating that the nanoparticles have a long enough shelf life (colloidal stability) for long-distance shipping, on-site storage, and testing in the field. The two NanoTags were dispersed in water at 1 wt% for shipping to the field site and were further diluted to 0.2 wt% to 0.4 wt% with tap water right before the injection in the well with the drilling mud.

We designed a nonintrusive protocol to inject the tags and collect the tagged cuttings for a field-test carried out during the drilling of a gas well. The well was a near vertical well on land in a carbonate formation, drilled 8⅜" gauge initially, and later drilled 5⅞" gauge through a lower section of the same formation. We manually pumped two distinctly barcoded NanoTags, one at a time, using a pneumatically powered, explosion-proof reciprocating pump, at just near atmospheric pressure, into the mud suction line upstream of the array of high-pressure "triplex" mud pumps.

The mud pumps, which brought the mud from atmospheric pressure up to 2,000 psi to 4,000 psi while
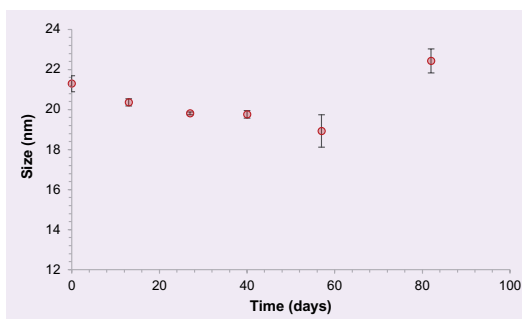
feeding into the drillpipe, were operated to maintain a flow of water-based mud at a normal ~600 gal/min flow rate into the drillpipe. The injection of each tag lasted 3 to 4 minutes, pumped at a rate of 1 gal/min to 1.5 gal/min. Immediately after completing the injection of the premeasured ~4.5 gal of NanoTag suspension, we pumped tap water for a few minutes to flush out the 20 ft long line leading from the pump to the injection port on the mud suction line.

The NanoTags were diluted by the water-based mud to a concentration of a few ppm when they reached the drill bit and mixed with the newly generated cuttings upon impact. We then collected cuttings off the shale shakers, located at the surface of the drilling operation. We estimated the sampling window based on the mud flow rate and modeling of all the BHA dimensions including a ~1,158 ft long "pendulum" BHA, which is designed to maintain a natural vertical drilling tendency. We collected the samples every two minutes from 16 minutes prior to 18 minutes after the "optimal" arrival time predicted.

The sample R1 was collected at the pre-computed nominal arrival time of the NanoTags back to the surface, Eqn. 2. Sample R2 started 2 minutes after; sample R3, two additional minutes after, and sample R4, two additional minutes later. Samples 1, 2, and 3 were collected 6 minutes, 4 minutes, and 2 minutes before sample R1; and the control sample #0 was collected 16 mins before sample R1. Samples 4, 5, 6, 7, 8,

Fig. 2   The synthetic method for making the two NanoTags used for a field-test pilot.
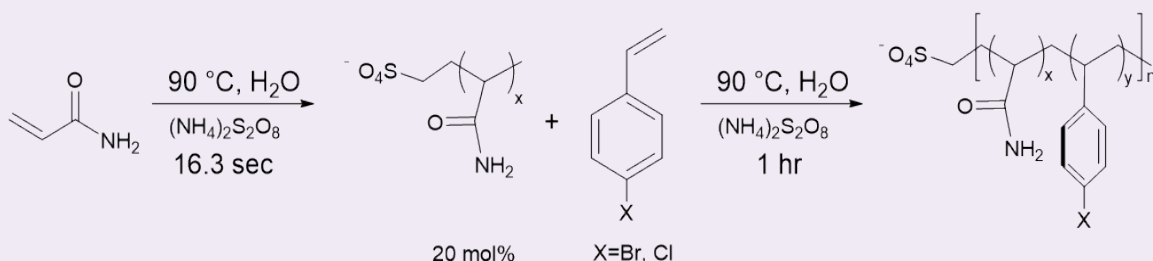
and 9 were collected 8, 10, 12, 14, 16, and 18 minutes, respectively, after sample R1. Therefore, the ensemble of these bottles covered 26 minutes of continuous sampling, with an additional control (null) sample #0 taken 10 minutes before this collection interval.

A major service company also computed the downward and upward going lag times of the mud using their proprietary mud logging software that displayed all the drilling parameters from the rig, including the bit depth, and counts of actual strokes of the mud pumps — which can give more accurate lag times in case the mud flow rate varies. We compared their computed lag time numbers with our own independently developed mud hydraulics modeling spreadsheet and found the two numbers in agreement to within a couple tenths of a minute, except for a systematic disagreement discovered later that we will explain in detail later.

In the lab, we applied an internally developed workflow to separate the cuttings from the mud and extract the tags from the cuttings. The workflow, as reported elsewhere[7], consists of multiple water washing steps, a tetrahydrofuran extraction, and the thermal removal of small volatile molecules. The workflow removes most polymers and small molecule additives normally present in the mud, and therefore reduces matrix interferences in the final Py-GC-MS analysis[7].

Results

NanoTags Injection during the Field-Test

Table 1 and Fig. 4 show the two tags that were injected at two different concentrations when drilling the caprock and the reservoir section, respectively.

The cuttings collected at the computed arrival time (lag time) were packed in bottles and shipped to our lab for tag identification via Py-GC-MS analysis. The cuttings were separated from the mud as described previously, and the tags were extracted from the cuttings as reported previously[7]. The calibration curve for each tag was established by plotting a series of tag solutions at different concentrations vs. their respective GC-MS signal-to-noise (S/N) ratio values. Next, we determined the criteria for identifying the presence of a tag on a sample. A Py-GC-MS peak with a S/N

ratio of 10 was established as the detection minimum for confirming the presence of a tag, in addition to the presence of the tag's unique molecular ion and isotope pattern on the MS[7]. Using the calibration curve, we also calculated the nanogram quantity of tags per gram of cuttings (ng/g cuttings) in the samples.

In an ideal situation, we expected to detect the tags only in samples R1 and R2, assuming a steady mud flow, sharp pulse injection of the tag, and perfect estimation of the lag times. Figure 5 shows the S/N values and the masses of the PBrSt tag detected on the cuttings collected during the drilling of the reservoir section of the formation. We clearly detected the PBrSt tag on the cuttings from samples R1 and R2, which show

Fig. 4 *The sequence in which the two distinct barcodes were injected as single 3 to 4 minute pulses.*
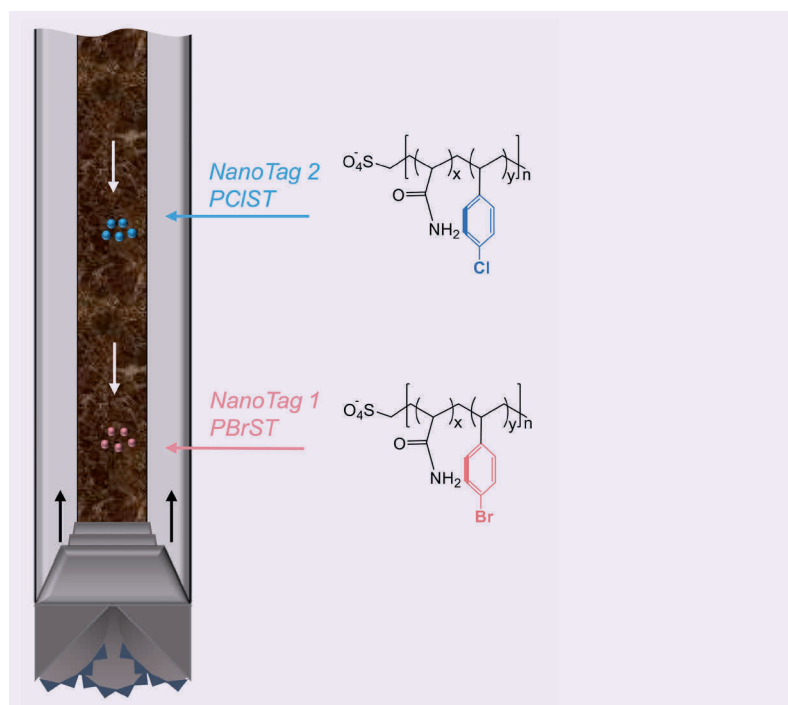
Table 1 *The sequence of NanoTag barcodes injected to tag the caprock and reservoir sections. The NanoTags designed for this field-test were poly(4-bromostyrene-co-acrylamide) (PBrSt) and poly(4-chlorostyrene-co-acrylamide) (PClSt) nanoparticles.*

Formation	NanoTag	Concentration in Mud (ppm)	Time Elapsed from Injection to Sample Collection (hr:min)
Caprock section	PBrSt	5	0:41
Caprock section	PBrSt	10	0:41
Caprock section	PClSt	5	0:40
Caprock section	PClSt	10	0:40
Reservoir section	PBrSt	10	0:48
Reservoir section	PClSt	10	0:48

Fig. 5 *The masses (orange square) and GC S/N ratios (blue circle) of PBrSt tags on the cuttings collected during the drilling of a reservoir section. The orange short dashed line and the blue wide dashed line mark the mass and S/N detection limits, respectively.*
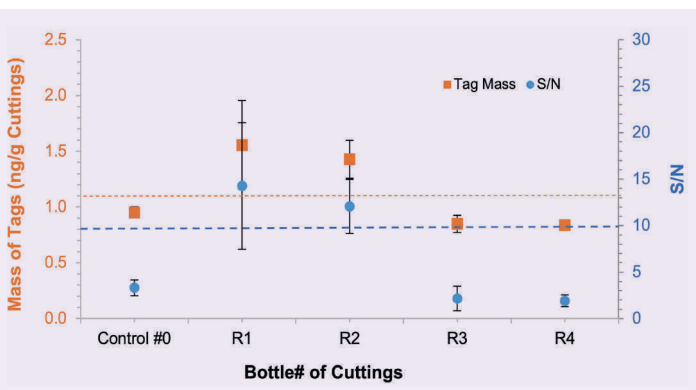
Fig. 6 *The masses (orange square markers) and detected GC S/N ratios (blue circle markers) of PBrSt tags on the cuttings collected during the drilling of the caprock section. The orange short dashed line and the blue wide dashed line mark the mass and S/N detection limits, respectively.*
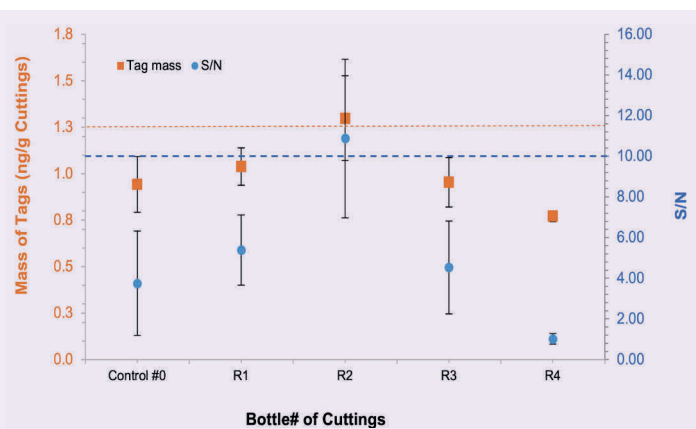
significantly higher signals on the GC-MS results compared to the control sample #0 and the R3 and R4 cuttings. On the other hand, we detected the PBrSt tag on the sample R2 cuttings that were collected during the drilling of the caprock section of the formation, Fig. 6. We further examine the time-depth correlation in more detail below by juxtaposing a representative subset of the Py-GC-MS detection results with the time-depth correlation results.

NanoTag Depth Correlation Compared to Mud Logging Depth Correlation

Table 2 shows a typical time-depth log data that we used for our analysis of the estimated cuttings arrival correlated to the tagged cuttings. Column 1 shows the date and time from the mud logger's data acquisition system. At each time (row), Column 2 shows the instantaneous drill bit depth (ft), measured from the rig's depth encoding system. Column 3 shows the total hole depth drilled to date (total depth).

When Column 2 matches Column 3, then the bit is on bottom and drilling a new hole; in that case, we color these cells green. When Column 2 decreases relative to Column 3, this indicates that the drill bit is off the bottom, typically in a tripping or reaming operation. Column 4 shows the lagged bit depth computed (as in our Eqn. 2) by the service company's software from the mud flow rate and the counting of pump strokes.

At the time shown in Column 1, the lagged bit depth represents the bit depth at which the currently returning cuttings were drilled. So, for example, at 17:30:02, the bit is at X559.04 ft and on the bottom, drilling. The cuttings arriving on the shakers were generated by the bit at X539.9 ft.

Field Pilot Injection Test

We start with the later portion of the field-test, the deeper interval drilled into the carbonate reservoir. The first pulse of 10 ppm PBrSt ("bromo") NanoTags was nominally injected for three minutes. As previously mentioned, it was actually injected with a small start delay and a total duration of four minutes. The mud logger's software showed about a 17-minute delay for the bromo NanoTags to arrive at the bit face, Eqn. 4.

Then, after the upward trip time to the surface, Eqn. 2, the expected cuttings with the bromo NanoTags were collected, at the same time as the second pulse of 10 ppm PClSt ("chloro") NanoTags was injected. In Fig. 7, we compare the nominal arrivals of bins R1, R2, R3, and R4, computed from the mud logging service company's predicted lag times, i.e., using both Eqn. 2 and Eqn. 4, to the NanoTag signals detected by Py-GC-MS analysis, indicating positive detection with a green checkmark and a null detection result with a red X. As indicated by a complete overlap, the mud logger's lag time approximations and the NanoTag depth correlation show close agreement.

We apply the NanoTag method by taking the bit depths where the cuttings were tagged after the downward lag time, Eqn. 4, and then plotting those depths with the red bar. The corrected calculation is about 4 minutes in duration and accounts for about an additional one-third minute of lag for the NanoTags to traverse the transfer line into the mud pump's suction line.

Similarly, we compared the NanoTags' detection and depth assignment from the 10 ppm PClSt injection with the mud logging depth correlation. There also, the computed lag time approximations and the NanoTag depth correlation show good agreement, with no statistically significant shift.

Caprocks Tagging Process

We had first begun the injections of the NanoTags two days earlier and about 1,300 ft shallower in depth, while drilling the carbonate caprock section. At the beginning, we were comparing carefully our own lag times from our independently written modeling spreadsheet with the mud logger's software; and at that time, we found a close agreement, to within a couple tenths of a minute. For that reason, we used the mud logger's

Table 2 *Format of drilling time-depth records from the mud logger, where X represents feet (thousands digit).*

Service Company Time (GMT)	Bit Depth (ft)	Total Depth (ft)	Lagged Bit Depth, i.e., Cuttings' Depth Origin (ft)
2019-12-02 17:30:02	X559.04	X559.0	X539.9
2019-12-02 17:30:09	X559.22	X559.2	X540.2
2019-12-02 17:30:18	X559.39	X559.4	X540.3
2019-12-02 17:30:27	X559.57	X559.6	X540.4
2019-12-02 17:30:38	X559.74	X559.7	X540.6
2019-12-02 17:30:50	X559.91	X559.9	X540.8

computed lag times for planning the sample acquisition windows for all the injections. In the first injection, for example, the service company estimated 15.5 minutes downward lag time (Eqn. 4) and 31.2 minutes return lag time (Eqn. 2) for a total round-trip travel time of almost 47 minutes for the NanoTags.

Figure 8 shows the detection of the PBrSt-AM Nano-Tags, which were injected at 0.2 wt% and diluted to a final concentration of 5 ppm in the flowing drilling mud. After careful analysis of the drill cuttings samples back in the lab, this case appeared to differ significantly from that in the reservoir region. The cuttings' arrival as estimated by the mud loggers (Eqn. 2) occurs almost 2 minutes earlier than the Py-GC-MS NanoTags detection reveals from analysis of the drill cuttings' samples.

In this caprock, drilled at about 60 ft/hr, that is almost 2 ft of depth error for the cuttings collected. Using the more reliable downward trip tagging with the NanoTags — depths assigned by Eqn. 4 and identified with the samples showing positive Py-GC-MS detection — the samples showing the NanoTags can be confidently assigned to their true depths of origin. The mud logger's software, however, by using a return

Fig. 7 *A comparison of the mud logger's software computed cuttings' depth assignments and the region where the PBrSt tags were detected. The shown depths were recorded while drilling on the bottom.*
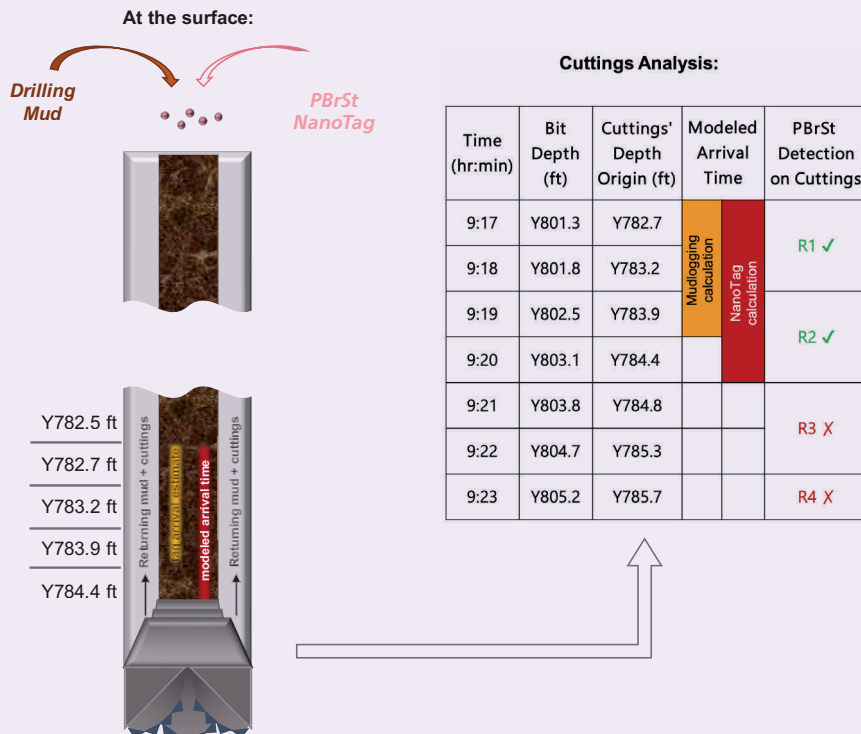
Fig. 8 *A comparison of the mud logger's software computed cuttings' depth assignment and the region where the PBrSt tags were detected. The shown depths were recorded while drilling on the bottom. The two depth correlation methods show an almost 2-minute difference in cuttings assignment.*

At the surface:

Drilling Mud

PBrSt NanoTag

X601.0 ft
X601.9 ft
X602.7 ft
X603.6 ft
X604.7 ft

Returning mud + cuttings | lag arrival estimate | modeled arrival time | Returning mud + cuttings

Cuttings Analysis:

Time (hr:min)	Bit Depth (ft)	Cuttings' Depth Origin (ft)	Modeled Arrival Time	PBrSt Detection on Cuttings
18:38	X633.6	X601.9	Mudlogging calculation / NanoTag calculation	R1 X
18:39	X634.3	X602.7		
18:40	X635.1	X603.6		R2 ✓
18:41	X636.2	X604.7		
18:42	X637.2	X606.3		R3 ✓
18:43	X638.0	X607.2		
18:44	X638.9	X608.0		R4 X
18:45	X639.6	X608.7		

lag time about 2 minutes too short, would assign those depths to samples collected 2 minutes (and 2 ft) too early. At higher drilling speeds, such a 2-minute difference can introduce proportionally greater depth assignment errors.

Similarly, for the final and fourth caprock injection of the 10 ppm chloro NanoTags, we saw a clear and slightly larger delay of between 2.5 and 3 minutes in the arrival of the NanoTagged cuttings relative to their predicted arrival time. In fact, three of the four caprock injections performed showed clear delays, slowly increasing from 2 to 3 minutes. The second injection was inconclusive due to some operational errors in the NanoTags injection.

How can we explain that our NanoTags arrive almost exactly as predicted by the mud logging software during tagging the reservoir section, but show a clear and increasing (with depth) delay lag of 2 to 3 minutes in the majority of the earlier injections in the caprock? The answer lies in the modeling of the lag times, specifically, in the input parameters used in the software. In the caprock section, our estimate of 46 to 47 minutes total travel time agreed closely with the mud logging software's prediction. In the reservoir formation, our estimate of ~52 minutes total travel time was significantly less than the 54 minutes

estimated by their software. Since we could not resolve the unexpected disagreement at that time, we used the longer lag time from the mud logger to program the samples acquisition timing (of the collection bins R1, R2, etc.).

We have already mentioned that the mud logger had carefully addressed the mud flow rate with auxiliary measurements, applying a more accurate value of 565 gal/min instead of the driller's nominal 600 gal/min control setting. The most likely cause of an increased return lag time of the cuttings returning to the surface is hole enlargement. A bit typically drills the hole slightly overgauge, with the amount of hole enlargement depending on the hardness of the formation, rate of penetration, and various whirling or resonance conditions. Since drilling rates were fairly low on both days, about 60 ft/hr in the caprock and 20 ft/hr in the reservoir, it is likely that the hole was enlarged by a few tenths of an inch overgauge, as the bit rotated many times while making its slow forward penetration.

Our hydraulics-based lag time calculations indicate that an enlarged open hole diameter of 9" (enlarged from the nominal 8⅜" bit gauge) gives a round-trip time of 54 minutes at the depths drilled in the reservoir. It is therefore our belief that this parameter was adjusted in the service company's software prior to

drilling the reservoir interval based on their experience over the intervening days of drilling. This 9" hole size then also accounts for the 2 to 2.5 minute shift that we observed in the caprocks. Had we used this input in the modeling software in the caprocks, very probably no shifts would have been observed in the NanoTagged samples.

Conclusions

This world first tagging while drilling field trial, performed in both caprock and reservoir sections of a vertical carbonate gas well, provided a convincing demonstration of the feasibility of NanoTagging drill cuttings for improved depth correlation accuracy during mud logging operations. The trial showed that this technology does not interfere with mud rheology and normal drilling operations; the NanoTags are clearly detectable on the collected cuttings by lab analyses; and the NanoTags can accurately assign the cuttings' depths.

In comparing these NanoTag assisted cuttings depths with depths conventionally assigned using mud logging software, the NanoTagging system revealed a 2-minute disagreement, corresponding to about a 2 ft depth difference, in the interval drilled in the caprock. This time difference could have resulted in a much larger difference in depth assignment if the drilling rate had been faster. Therefore, the test illustrated how this NanoTagging technology can play an important role in the cuttings' depth assignment when conditions like overgauge hole drilling create uncertainties in calculating the return trip lag time of cuttings up the annulus.

The test in the reservoir section, on the other hand, showed good agreement of the NanoTagging system, as it accurately assigned depths in agreement with traditional mud logging when drilling conditions were as expected. Based on these initial results, we see the potential for further developing and testing the NanoTagging technology in more challenging drilling conditions. An upcoming test will dispense a repeating sequence of different NanoTag barcodes into the drilling mud with accurate control of volumes and timings using an automated apparatus, again with no interference in the drilling operation[8].

This should be another step toward making this novel tagging process a routine operation available for improving mud logging data quality, with the goal of making it a convenient and viable option for real-time formation evaluation in wells where that is presently difficult or unavailable.

Acknowledgments

References

1. Santarelli, F.J., Marsala, A.F., Brignoli, M., Rossi, E., et al.: "Formation Evaluation from Logging on Cuttings," *SPE Reservoir Evaluation & Engineering*, Vol. 1, Issue 3, June 1998, pp. 238-244.

2. Malik, M., Hanson, S.A. and Clinch, S.: "Maximizing Value from Mud Logs: Integrated Approach to Determine Net Pay," paper presented at the SPWLA 61st Annual Logging Symposium, Virtual, June 24-29, 2020.

3. Georgi, D.T., Harville, D.G. and Robertson, H.A.: "Advances in Cuttings Collection and Analysis," paper presented at the SPWLA 34th Annual Logging Symposium, Calgary, Alberta, Canada, June 13-16, 1993.

4. Loermans, T., Bradford, C.M., Kimour, F., Karoum, R., et al.: "Advanced Mud Logging (AML) Aids Formation Evaluation and Drilling, and Yields Precise Hydrocarbon Fluid Composition," SPE paper 141277, presented at the SPE Middle East Oil and Gas Show and Conference, Manama, Kingdom of Bahrain, September 25-28, 2011.

5. Wilson, A.: "Cuttings Lag Distribution in Directional Wells Affects Depth Resolution of Mud Logging," *Journal of Petroleum Technology*, October 2018, pp. 1-4.

6. Antoniv, M., Chang, S., Al-Jabri, N. and Zhu, S.S.: "Surfactant-Free Synthesis of Poly (styrene-co-acrylamide) Monodisperse Nanoparticles Using Hybrid Flow-to-Batch Chemistry," *Journal of Applied Polymer Science*, Vol. 138, Issue 9, September 2020.

7. Antoniv, M., Zhu, S.S., Chang, S., Poitzsch, M.E., et al.: "Method for Detecting Nanoparticles on Cuttings Recovered from a Gas Reservoir," *Energy Fuels*, Vol. 35, Issue 9, April 2021, pp. 7708-7716.

8. Marsala, A.F., Li, B. and Alqattan, H.: "Robotics and Automation for Rock Sampling and Characterization: A Paradigm Shift in Real Time Formation Evaluation," paper presented at the AAPG International Conference and Exhibition, Cape Town, Africa, November 4-11, 2018.

About the Authors

Dr. S. Sherry Zhu

Ph.D. in Chemistry,
University of Pennsylvania

Dr. S. Sherry Zhu is a Research Scientist Specialist at the Aramco Americas Boston Research Center. Her current research focuses on the development of novel sustainable materials and nanotechnologies for oil field applications. Sherry and coworkers have recently developed NanoTags for labeling drill cuttings with improved accuracy in depth determination, which won the Institute of Chemical Engineers (IChemE) "Highly Commended" Award for the Oil & Gas 2020 division.

She has had a long career in chemical and oil industries and acquired broad experiences in the Research and Development and manufacturing of functional materials. Sherry has developed degradable polymers, derived from renewable resources, for applications downhole, which has contributed to the commercial success of degradable polymers as diverters for multistage stimulations.

She is one of the officers in the Boston Chapter of the Society of Petrophysicists and Well Log Analysts (SPWLA) and is an active member and symposium organizer in the American Chemical Society.

Sherry has authored and coauthored over 50 patents, patent applications, and a peer-reviewed book chapter and numerous papers.

She received her Ph.D. in Chemistry from the University of Pennsylvania, Philadelphia, PA. Sherry worked as a Postdoctoral fellow at the Massachusetts Institute of Technology before she moved to work in the oil and gas industry.

Marta Antoniv

B.A. in Chemistry,
Hamilton College

Marta Antoniv joined the Reservoir Engineering Technology team in the Aramco Americas Boston Research Center as a Chemist in 2018. At Aramco, she actively engages in design, synthesis, and the characterization of functional materials for oil field applications.

Marta has published two peer-reviewed papers and filed four patent applications.

In 2017, she received her B.A. degree in Chemistry from Hamilton College, Clinton, NY.

Dr. Martin E. Poitzsch

Ph.D. in Experimental Atomic
Physics,
Harvard University

Dr. Martin E. Poitzsch has been the Reservoir Engineering Technology Leader in the Aramco Americas Boston Research Center since 2014, leading a team applying nanomaterials and related methods to the challenges of improving reservoir surveillance and recovery.

Prior to his work at Aramco, Martin had a 20-year R&D career in Schlumberger, developing new technologies in logging while drilling, wireline logging, sensors research, and smart well completions in Houston, Paris, Connecticut, and Boston.

He also worked at the National Institute of Standards and Technology (NIST) in Boulder, CO, where he developed a novel prototype cold-ion primary atomic frequency standard.

Martin received his Ph.D. degree in Experimental Atomic Physics from Harvard University, Cambridge, MA.

Dr. Nouf M. AlJabri

Ph.D. in Chemical Engineering,
King Abdullah University of
Science and Technology

Dr. Nouf M. AlJabri is a Petroleum Engineer with the Reservoir Engineering Technology Division at Saudi Aramco's Exploration and Petroleum Engineering Center – Advanced Research Center (EXPEC ARC). Nouf is spearheading research efforts on novel functionalization of nanomaterials for targeted delivery of enhanced oil recovery chemicals.

Her research is focused on developing new disruptive concepts for upstream nanotechnologies and nanomaterials.

Previously, Nouf was a visiting scientist with Professor Timothy M. Swager at MIT to design and synthesize novel advanced materials to resolve key upstream challenges.

She received her M.S. degree and Ph.D. degree in Chemical Engineering from King Abdullah University of Science and Technology (KAUST), Thuwal, Saudi Arabia.

Dr. Alberto F. Marsala

Ph.D. in Nuclear Physics,
University of Milan

Dr. Alberto F. Marsala has more than 29 years of oil industry experience. For the last 15 years, he has been working in Saudi Aramco's Exploration and Petroleum Engineering Center – Advanced Research Center (EXPEC ARC) as the Deep Diagnostics Focus Area Champion, with responsibilities covering R&D and innovation in formation evaluation and deep reservoir characterization.

Alberto previously work with Eni and Agip, where he had technical and managerial responsibilities in geoscience, including 4D seismic, reservoir characterization, petrophysics, geomechanics, core analysis, drilling, and construction in environmentally sensitive areas. Alberto worked in the Technology Planning and R&D committee of Eni. He was also the Head of Performance Improvement of the KCO Joint Venture (Shell, ExxonMobil, Total, and others) for the development of giant fields in the northern Caspian Sea.

Alberto has authored a book on *Value of Innovation*, 100+ papers, and 30+ patents.

In 1991, Alberto received his Ph.D. degree in Nuclear Physics from the University of Milan, Milan, Italy, and in 1996, he received an MBA in Quality Management from the University of Pisa, Pisa, Italy. He also holds a Specialization in Innovation Management, received in 2001.

Some of Alberto's recent recognitions are the Society of Petrophysics and Well Log Analysts (SPWLA) Meritorious Award, the Society of Petroleum Engineers (SPE) Regional Formation Evaluation Award, Hart's E&P Engineering Innovation Award, and the World Oil Award for Best Exploration Technology.

Automatable High Sensitivity Tracer Detection: Toward Tracer Data Enriched Production Management of Hydrocarbon Reservoirs

Dr. Hooisweng Ow, Dr. Sehoon Chang, Gawain Thomas, Dr. Wei Wang, Dr. Afnan A. Mashat and Hussein A. Shateeb

Abstract /

The development of automatable high sensitivity analytical methods for tracer detection has been one of the most central challenges to realize ubiquitous full-field tracer deployment to study reservoirs with many cross-communicating injector and producer wells. Herein we report a tracer analysis approach, inspired by strategies commonly utilized in the biotechnology industry, which directly addresses the key limitations in process throughput, detection sensitivity, and the automation potential of state-of-the-art technologies.

A 2D high performance liquid chromatography (2D-HPLC) method was developed for the rapid fluorescence detection and simultaneous identification of a class of novel barcoded tracers in produced water down to ultra-trace concentration ranges (< 1 ppb), matching the sensitivity of tracer technologies currently used in the oil industry. The sample preparation process throughput was significantly intensified by judicious adaptations of off-the-shelf biopharma automation solutions. The optical detection sensitivity was further improved by the time resolved luminescence of the novel tracer materials that allows the negation of residual background signals from the produced water.

To showcase the potential, we applied this powerful separation and detection methodology to analyze field samples from two recent field validations of a novel class of optically detectable tracers, in which two novel tracers were injected along with a benchmarking conventional fluorobenzoic acid (FBA)-based tracer. The enhanced resolving power of the 2D chromatographic separation drastically suppressed the background signal, enabling the optical detection of a tracer species injected at 10x lower concentration.

Further, we orthogonally confirmed the detection of this tracer species by the industry standard high-resolution accurate mass (HRAM) spectrometry technique, demonstrating comparable limits of detection. The tracer detection profile indicated that the transport behavior of the novel optical tracers through a highly saline and retentive reservoir was similar to that of FBAs, validating the performance of this new class of tracers. Promising steps toward the complete automation of the tracer separation and detection procedure have drastically reduced manual interventions and decreased the analysis cycle time, laying a solid foundation to full-field deployment of tracers for better reservoir characterizations to inform decisions made on production optimization.

This article outlines the automatable tracer detection methodology that has been developed for robustness and simplicity, so that efficient utilization of the resultant high-resolution tracer data can be applied toward improving the production strategy via intelligent and active rate adjustments.

Introduction

Despite the advent of many intelligent well logging management technologies, tracers remain the most direct method to identify interwell communications. To manage the effectiveness of waterflooding operations, full-field tracer campaigns have been proposed as a surveillance technique to improve the fidelity of history matching for the reservoir with the objective of enhancing the production optimization algorithms[1]. While the reservoir simulation tools used are different, the addition of high-fidelity tracer data that describe movement of the injected water has proven beneficial to optimize hydrocarbon production, both in silico and in the field by reallocating injection water to high efficiency injectors[2, 3].

Many examples of informative tracer campaigns have been reported in the literature[4, 5]. To date, fluorobenzoic acid (FBA)-based tracer materials remain the most prevalently used in siliciclastic and carbonate reservoirs, due to their highly conservative transport behavior and extremely low detection limits[6, 7]. Subsequently, the analysis procedure for this class of materials is tedious and error prone, requiring complex sample preparations (clean up and chemical derivatization) and expert knowledge of sophisticated analytical equipment, i.e., gas chromatography-tandem mass spectrometry (GC-MS-MS)[8].

A tracer materials platform that can be detected and analyzed in near real-time would alleviate most of the

known drawbacks of FBAs, e.g., limited number of unique tracers and ease of analysis, especially for full-field deployment in which many samples would need to be collected and analyzed using a tedious analysis procedure with a long cycle time. To this end, we have developed an automatable high sensitivity analysis method designed specifically to expedite the processing of produced water samples that contain mixtures of a novel class of optically detectable tracer molecules.

Time Resolved Luminescent Tracer Molecules for the Oil Field

Currently, state-of-the-art tracer technology for the oil field is based on mass spectrometry-based detection of FBA-based molecules[6, 8]. The desirable attributes of optically detectable tracer materials, e.g., ultra-trace detectability and facile analysis approach, for the applications in a hydrocarbon reservoir are evident in the many recent research and development efforts to identify, study, and field deploy fluorescent materials as tracers as reported in the literature[9, 10].

We have previously described the development of a water tracer materials platform tailored for stability in a high temperature environment and transportability in highly saline and retentive carbonate formations[11]. The chemical structures of the prototype materials we recently field-tested, dipicolinic acid (DPA) and

4,7-diphenyl-1,10-phenanthroline-2,9-dicarboxylic acid disulfonate (BSPPDA), are depicted in Fig. la. In these field validations, we also injected a reference water tracer, 2-FBA, to compare the transport behavior of the materials.

These materials are designed to be analyzed and quantified by time resolved luminescence, which enables higher detection sensitivity down to sub-ppb levels without the use of high-resolution accurate mass (HRAM) spectrometry, in spite of the presence of many optically active dissolved organic compounds in produced water from a hydrocarbon reservoir. The general principle of how time resolved luminescence is used to eliminate fluorescence background in difficult matrices is outlined in Fig. lb.

Briefly, the novel chromophoric tracer molecules are designed to bind lanthanide ions. The binding of the chromophore sensitizes the ions and enhances their emissions, allowing achievement of low detection and quantification limits. Further, due to the longer luminescence lifetimes (typically in the micro- to milliseconds) of these lanthanide ions, the luminescence measurement window can be time gated to completely eliminate any background fluorescence (typically in the pico- to nanoseconds), rendering this approach extremely attractive for fluorescence-based quantifications in complex matrices[12, 13].

Fig. 1 *(a) Molecular structures of DPA (novel water tracer 1), BSPPDA (novel water tracer 2) and 2-FBA (reference water tracer), and (b) Principle of time resolved luminescence in which the long-lived luminescence of the sensitized lanthanide ions allows for the gating of the measurement window that enables the negation of obfuscating background fluorescence.*
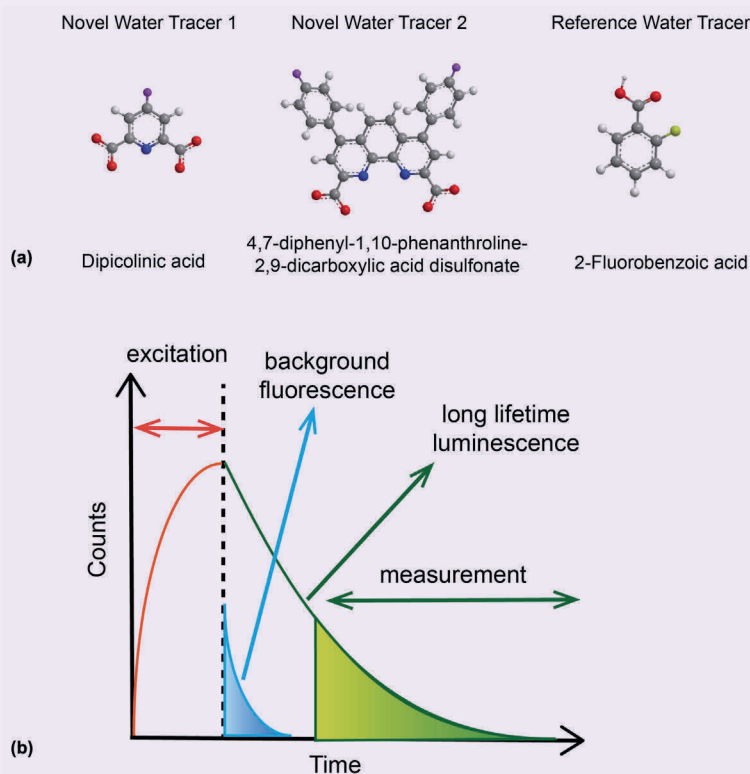
Optical-Based Tracer Detection and Quantification

For the success of ubiquitous full-field tracer deployment, the challenges can be categorized as:

1. Materials: The number of unique tracer species to adequately label injectors in a large reservoir for a full description of fluid flow underground.

2. Analysis: The burden of sample collection as well as the time it takes for each sample to be quantified.

3. Tracer data management: Value creation from applying high fidelity tracer data to production optimization for the management of waterflood fields.

We have previously reported on the molecular design principle we adopted to address the materials challenge 1, in which a modular derivatization approach could yield multiple unique tracers from the same molecular core[11]. We believe a tracer platform that can be detected and quantified optically addresses the analytics challenge 2, as previously mentioned. It should be emphasized that in the development of the detection and quantification methodologies for our optically detectable tracer platform, we specifically sought off-the-shelf mature analytical technologies from the chemical and biotech industries to facilitate facile adoption and deployment.

Figure 2 details the three-step procedure we developed to analyze the produced water collected from the field trials. To ensure success, the key considerations are: (a) The high salt content in the fluids may interfere with the analysis, (b) the complex mixtures contain many organic interferents in higher concentrations than the tracers (most often present at ultra-trace amounts), (c) the detection sensitivity of the spectrofluorometer to quantify tracer concentrations, and (d) the total analysis cycle time for the three-step process.

Step 1 of the process, solid phase extraction, is designed to largely desalt the field samples while they are pre-concentrated simultaneously. This step is critical to elevate the concentration of the tracers above the detection limits of the instrument from otherwise undetectable levels. Some removal of organic interferents occurs at this step as well[14]. In Step 2, the pre-concentrated sample is introduced into a multidimensional high performance liquid chromatography (HPLC) to separate the tracers from any residual organic compounds that are present. Details on the necessity of a multidimensional HPLC for the analysis of these samples are described next. Here, the fractions of interest are collected and processed through a solvent exchange before Step 3, where a buffered solution containing a lanthanide ion at a predetermined concentration is added to reconstitute the sample at pH 5.5.

The fluorescence signal of the sample is then measured in a spectrofluorometer for quantification. A typical process time for all three steps is approximately 12 hours. Development to automate some of the steps as described will further reduce sample cycle time to approach near real-time analysis. As compared to state-of-the-art methodologies, e.g., the analysis of
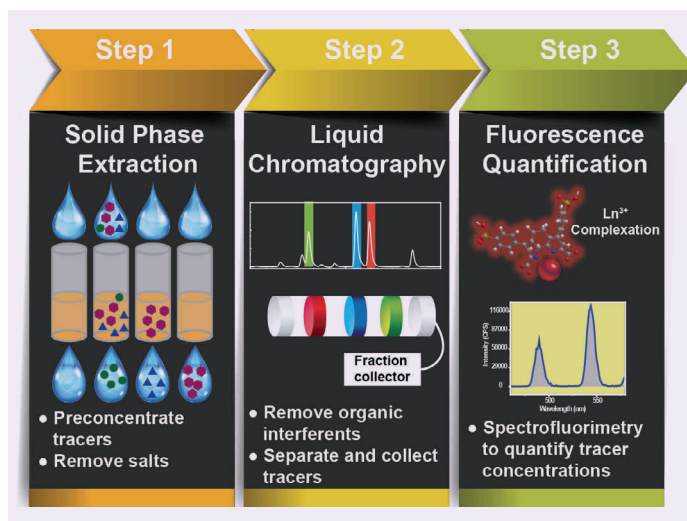
FBA-based tracers via GC-MS-MS, this represents major improvements throughout[15].

2D Liquid Chromatography for Tracer Analysis

Liquid chromatography (LC), as an analytical separation tool, has benefitted from a renaissance of innovations in the last two decades. This includes size (sub-2 μm particles for ultra-HPLC) and functionalities (advent of different separation modes, such as ion exchange, reversed phase, hydrophilic interaction liquid chromatography, and size exclusion chromatography) of the particles in the columns, as well as the instrumental advances from high efficiency pump modules and high throughput sample handling[16]. While LC is an incredibly competent approach to separate a mixture containing 10 to 20 components of interest within hours, in complex samples that either have significant matrix effects and/or containing upward of hundreds of species, the application of 2D-LC may become necessary[17].

While multidimensional LC technology development was originally spurred by the biotechnology industry in the quest for analytical tools that enable simultaneous and high throughput separation of complex proteomics samples, its utility in high sensitivity analysis of multicomponent environmental samples has been proven as well[18]. Fluid samples from the reservoir are typically highly complex, consisting of a plethora of dissolved organic matter, e.g., polycyclic aromatic hydrocarbons, which have a multitude of chemical functionalities, which usually manifest as high background signals in optical detection methodologies, masking, and obfuscating the detection of the analytes of interest. To separate and detect the tracer materials effectively from this background, we rely on the astounding separation prowess offered by 2D-LC, whereby a second column

affords orthogonal selectivity and additional capacity of separation.

Figure 3 shows the basic principle of 2D-LC. Peaks of interest from the 1D-LC, either identified by retention time or a predetermined signal threshold, are fractionated in-line and sent into a second column via a 2D injector valve for further separation. If the fractionated samples from the 1D-LC contain co-eluting species, the 2D separation should resolve them with a judicious choice of mobile and stationary phases.

For produced water samples from a hydrocarbon reservoir, this allows for highly effective isolation of the tracer compounds from other polycyclic aromatic hydrocarbons present in the fluids, suppressing background signals and enabling high sensitivity detection of the tracers down to ultra-trace concentration levels.

Results and Discussions

Produced water samples were collected from the field-test twice weekly, except when the wells were shut down. The samples were first subjected to a cursory clean up that separates the oil and water phases. The aqueous portion of the samples were then processed through the three-step extraction, separation, and quantification procedure as described previously.

Figure 4 shows the significant benefits of 2D-LC in the removal of background noise in the chromatograms. Figure 4a depicts the chromatogram of a representative field sample after 1D-LC separation. Peaks from the three injected tracers are highlighted in blue (DPA), red (BSPPDA), and green (FBA), respectively. What is

Fig. 3 *Schematic on the operating principle of 2D-LC in which the sample containing the analyte of interest undergoes two chromatographic separations.*
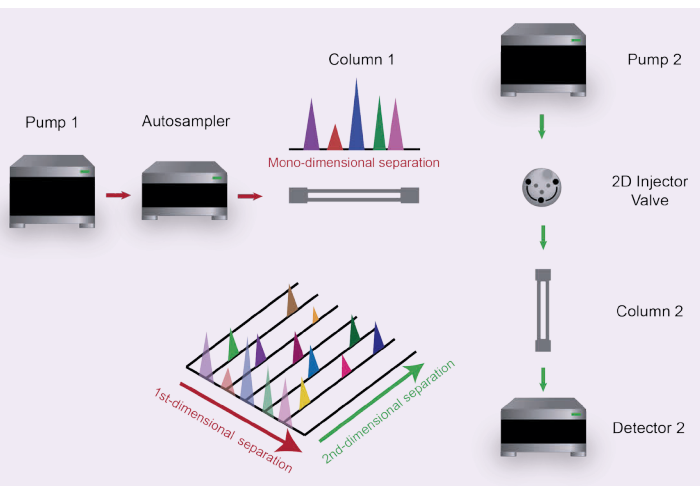
Fig. 4 *(a) Representative 1D-LC UV-Vis chromatogram of a field sample containing DPA (blue), BSPPDA (red), and 2-FBA (green) with a prevalent presence of organic interferents that make up the high background. (b) The 2D-LC chromatogram for DPA after peaking from the 1D separation, separated in the second column. (c) The 2D-LC chromatogram for BSPPDA after peaking from the 1D separation, separated in the second column. (d) The 2D-LC chromatogram for 2-FBA after peaking from the 1D separation, separated in the second column. As depicted in panels (b), (c), and (d), the background signal from the field sample was significantly suppressed after the powerful 2D separation.*
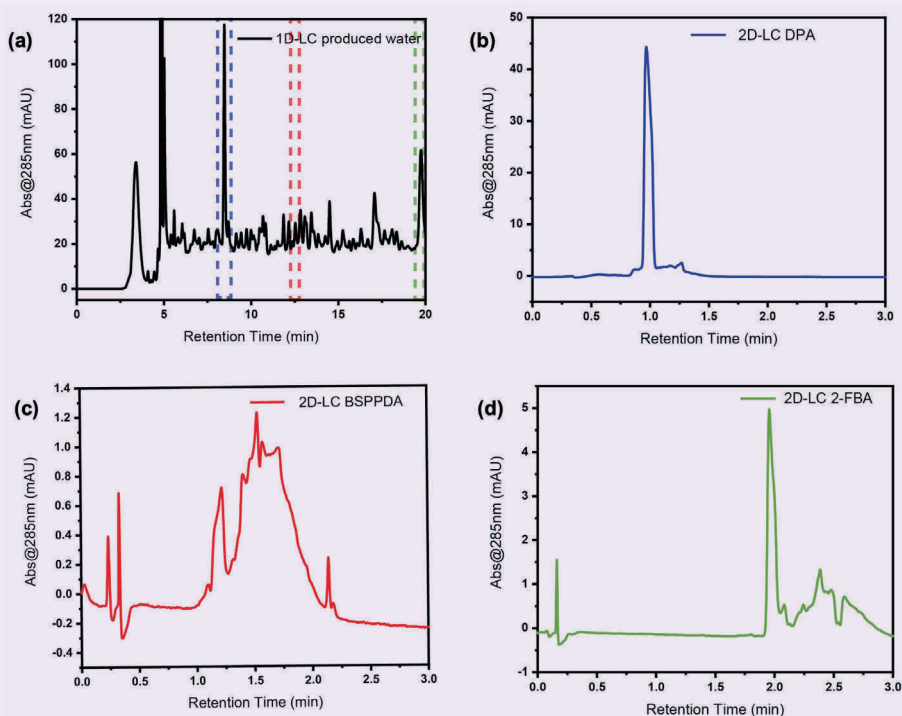
immediately obvious from retention time between 5 and 20 minutes is the formidable background signal, which will interfere with retention time-based fractionation. The 2D-LC system allows us to fractionate the peaks from our tracer after separation in the first column and further separate them again in the second column. As shown in Figs. 4b, 4c, and 4d, the chromatograms of the DPA, BSPPDA, and 2-FBA tracers exhibit much lower background after the 2D separation. The multiple peaks observable in Fig. 4c for the BSPPDA sample indicated that there indeed was other dissolved organic matter co-eluting with our tracer sample that would not have been resolvable without 2D-LC.

To quantify the concentrations of tracers in the field samples, we first generated standard curves for each of them by spiking known amounts of the tracers into pristine produced water and processing these standard samples through our three-step optical analysis procedure.

Figures 5a and 5b shows the linear regression plots for the standard curves of DPA and BSPPDA with high R-squared. The two FBA samples were fraction collected after the 2D-LC step and analyzed by a GC-MS-MS after a derivatization step — linear regression of standard curve data, not shown. Figure 5c shows the tracer recovery in the producer well. Even though we injected 10x less BSPPDA, consistent

above background signal from the tracers, it could be detected approximately 25 days after the injection and the signals trend relatively consistently among the three tracers injected.

To validate the three-step optical analysis approach, we opted to orthogonally verify the recovery of BSPPDA by the industry standard HRAM methodology. We subject a set of field samples through the extraction and chromatographic separation steps of the 3-step process, and fraction collected the samples for LC tandem mass spectrometry by a third-party lab.

Figure 6a is a representative total ion chromatogram of a sample, where the major mass-to-charge ion for BSPPDA is indicated in red, at 245.2 m/z. Figure 6b shows the BSPPDA molecular ion was identifiable at an identical retention time of ~3.6 s for both the 10 ppb standard and the field sample. Quantification was possible for the field sample with less than a 20% discrepancy between the quantifying (transition between 245.1 m/z to 212.9 m/z) and qualifying (245.1 m/z to 79.9 m/z) ion ratio. In this example in Fig. 6c, the concertation of BSPPDA in the field sample was approximately 3 ppb. This corresponds well with field samples from the same period as quantified by our three-step optical analysis procedure.

Conclusions

Following the development of a novel tracer materials

Fig. 5 *(a) Standard curve obtained from fluorescence spectrofluorimetry after 2D-LC for the determination of DPA concentrations in field samples. (b) Standard curve from fluorescence spectrofluorimetry after 2D-LC for the determination of BSPPDA concentrations in field samples. (c) Concentrations of tracers in field samples as measured by fluorescence (DPA and BSPPDA) and GC-tandem MS (FBA).*
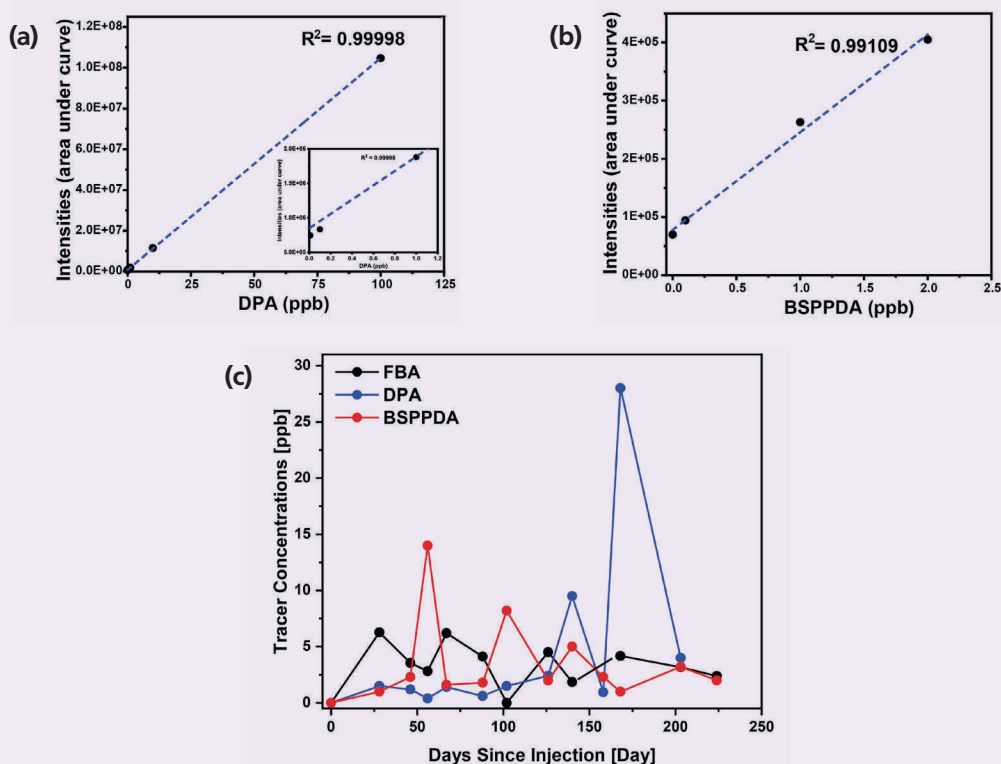
Fig. 6 *(a) Major mass-to-charge ion expected for the tracer BSPPDA is at 245.2 m/z. (b) A representative chromatogram of a 10 ppb standard of BSPPDA where the molecule could be identified by the retention time at ~3.6 s, and quantified with less than a 20% discrepancy for the qualifying and quantifying ion ratio. (c) Representative chromatogram of field samples containing the BSPPDA tracer identifiable at the retention time of 3.6 s.*
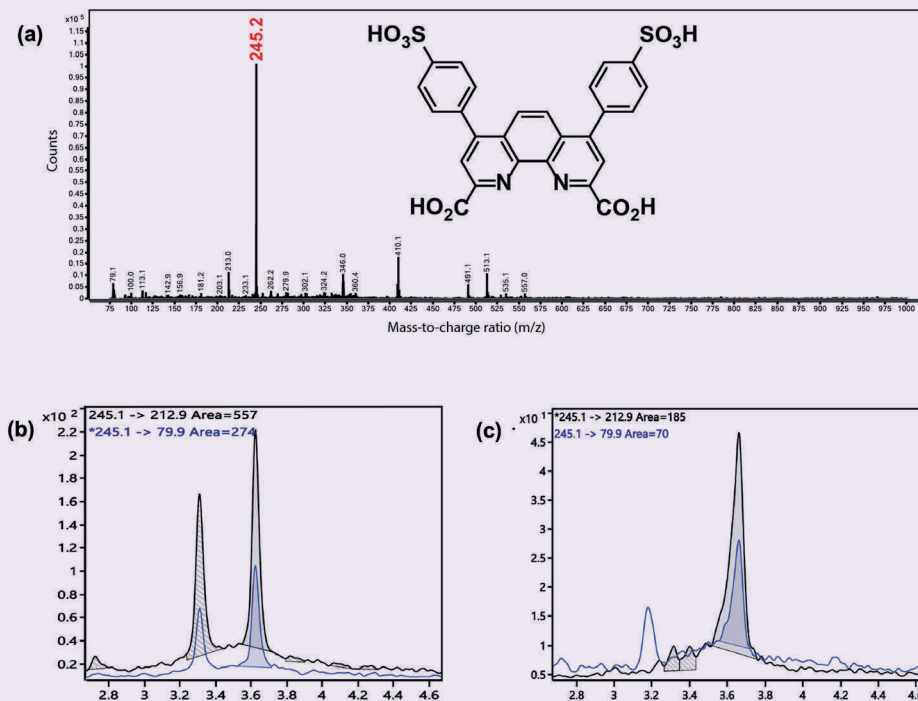
platform, which allows for high sensitivity detection at ultra-trace concentrations in produced water from hydrocarbon reservoirs, we refined the analysis protocol to an automatable three-step process that includes solid phase extraction, 2D-LC followed by time resolved luminescence spectrofluorometry for the tracer concentration quantification. The detection and analysis procedure were also validated by an orthogonal method widely accepted (LC tandem mass spectrometry).

Future work includes the complete automation of the solid phase extraction step and full integration to the 2D-HPLC with zero to minimal manual intervention, and the development of inline fluorescence quantification post-column to eliminate the need for a spectrofluorometer for the quantification step.

Acknowledgments

References

1. Chen, H. and Poitzsch, M.E.: "Improved Reservoir History Matching and Production Optimization with Tracer Data," SPE paper 191523, presented at the SPE Annual Technical Conference and Exhibition, Dallas, Texas, September 24-26, 2018.

2. Khan, S., Al Zaabi, N., Jani, Z., Tariq, S., et al.: "Optimizing Waterflood Management in a Giant UAE Carbonate Oil Field Using Simulation-Based Streamlines," SPE paper 171777, presented at the Abu Dhabi International Petroleum Exhibition and Conference, Abu Dhabi, UAE, November 10-13, 2014.

3. Kornberger, M. and Thiele, M.R.: "Experiences with an Efficient Rate Management Approach for the 8th Tortonian Reservoir in the Vienna Basin," *SPE Reservoir Evaluation & Engineering*, Vol. 17, Issue 2, May 2014, pp. 165-176.

4. Du, Y. and Guan, L.: "Interwell Tracer Tests: Lessons Learned from Past Field Studies," SPE paper 93140, presented at the SPE Asia Pacific Oil and Gas Conference and Exhibition, Jakarta, Indonesia, April 5-7, 2005.

5. Tayyib, D., Al-Qasim, A., Kokal, S.L. and Huseby, O.: "Overview of Tracer Applications in Oil and Gas Industry," SPE paper 198157, presented at the SPE Kuwait Oil and Gas Show and Conference, Mishref, Kuwait, October 13-16, 2019.

6. Galdiga, C.U. and Greibrokk, T.: "Ultra-Trace determination of Fluorinated Aromatic Carboxylic Acids in Aqueous Reservoir Fluids Using Solid-Phase Extraction in Combination with Gas Chromatography-Mass Spectrometry," *Journal of Chromatography A*, Vol. 793, Issue 2, January 1998, pp. 297-306.

7. Guan, L., Du, Y., Johnson, S.G. and Choudhary, M.: "Advances of Interwell Tracer Modeling in Petroleum Industry," paper presented at the Canadian International Petroleum Conference, Calgary, Alberta, Canada, June 8-10, 2004.

8. Serres-Piole, C., Moradi-Tehrani, N., Lobinski, R. and Preud'homme, H.: "Direct Sensitive Simultaneous determination of Fluorinated Benzoic Acids in Oil Reservoir Waters by Ultra High Performance Liquid

Chromatography-Tandem Mass Spectrometry," *Journal of Chromatography A*, Vol. 1218, Issue 34, August 2011, pp. 5872-5877.

9. Franco, C.A., Candela, C.H., Gallego, J., Marin, J., et al.: "Easy and Rapid Synthesis of Carbon Quantum Dots from Mortiño (Vaccinium Meridionale Swartz) Extract for Use as Green Tracers in the Oil and Gas Industry: Lab-to-Field Trial Development in Colombia," *Industrial & Engineering Chemistry Research*, Vol. 59, Issue 25, May 2020, pp. 11359-11369.

10. Kanj, M.Y. and Kosynkin, D.V.: "Oil Industry First Field Trial of Inter-Well Reservoir Nanoagent Tracers," *Proceedings of the SPIE*, The International Society for Optical Engineering, Vol. 9467, May 2015.

11. Ow, H., Chang, S., Thomas, G., Shi, R., et al.: "First Deployment of a Novel Advanced Tracers System for Improved Waterflood Recovery Optimization," SPE paper 192598, presented at the Abu Dhabi International Petroleum Exhibition and Conference, Abu Dhabi, UAE, November 12-15, 2018.

12. Georges, J.: "Lanthanide-Sensitized Luminescence and Applications to the determination of Organic Analytes. A Review," *Analyst*, Vol. 118, Issue 12, 1993, pp. 1481-1486.

13. Kaczmarek, M.: "Lanthanide-Sensitized Luminescence and Chemiluminescence in the Systems Containing Most Often Used Medicines; A Review," *Journal of Luminescence*, Vol. 222, June 2020.

14. Knoll, S., Rösch, T. and Huhn, C.: "Trends in Sample Preparation and Separation Methods for the Analysis of Very Polar and Ionic Compounds in Environmental Water and Biota Samples," *Analytical and Bioanalytical Chemistry*, Vol. 412, Issue 24, 2020, pp. 6149-6165.

15. Thomas, G., Ow, H., Chang, S., Shi, R., et al.: "Deployment and Detection of a Novel Barcoded Advanced Tracers System for the Optimization of Improved Waterflood Recovery in Hydrocarbon Reservoirs," SPE paper 194872, presented at the SPE Middle East Oil and Gas Show and Conference, Manama, Kingdom of Bahrain, March 18-21, 2019.

16. Pirok, B.W.J., Stoll, D.R. and Schoenmakers, P.J.: "Recent Developments in Two-Dimensional Liquid Chromatography: Fundamental Improvements for Practical Applications," *Analytical Chemistry*, Vol. 91, Issue 1, 2019, pp. 240-263.

17. Davis, J.M. and Stoll, D.R.: "Likelihood of Total Resolution in Liquid Chromatography: Evaluation of One-Dimensional, Comprehensive Two-Dimensional, and Selective Comprehensive Two-Dimensional Liquid Chromatography," *Journal of Chromatography A*, Vol. 1360, September 2014, pp. 128-142.

18. Horvatovich, P., Hoekman, B., Govorukhina, N. and Bischoff, R.: "Multidimensional Chromatography Coupled to Mass Spectrometry in Analyzing Complex Proteomics Samples," *Journal of Separation Science*, Vol. 33, Issue 10, 2010, pp. 1421-1437.

About the Authors

Dr. Hooisweng Ow

*Ph.D. in Materials Science and Engineering,
Cornell University*

Dr. Hooisweng Ow is a Research Science Specialist on the Reservoir Engineering and Technology Team, Aramco Americas, Aramco Research Center-Boston. Prior to joining Aramco Americas in November 2013, she was a co-founder and principal scientist at Hybrid Silica Technologies (HST) Inc., a nanotechnology startup company that commercialized the first-in-human multimodal C-dot nanoparticles from Cornell University for *in vivo* tumor margin marking applications. Sweng's research portfolio at HST also includes silicate adsorbent materials for explosives detection and luminescent nanomaterials for cross-well applications in highly saline and retentive carbonate reservoirs.

Her current research interests are in novel tracer materials for surveillance and production optimization for mature reservoirs, near real-time analysis of luminescent materials in highly complex matrices, and innovative techniques for characterizations of reservoir rocks.

Sweng is a recognized innovator with over 15 issued U.S. patents. She is also a contributor to more than 20 technical papers that have garnered over 6,000 citations. Sweng is an active member of the Division of Energy and Fuels of the American Chemical Society, where she has organized and chaired several symposia that focused on advanced materials and chemistries for oil field applications in the annual meetings.

Sweng received her Ph.D. in Materials Science and Engineering in 2005 from Cornell University, Ithaca, NY.

Dr. Sehoon Chang

Ph.D. in Materials Science and Engineering,
Georgia Institute of Technology

Dr. Sehoon Chang is a Senior Lab Scientist on the Reservoir Engineering Technology Team, Aramco Americas, Aramco Research Center-Boston.

He joined Aramco in 2015 and has been developing an integrated, real-time spectroscopic detection system for deploying advanced tracers to improve oil recovery. Sehoon also designed metal nanostructures for surface enhanced Raman scattering (SERS) detection of oil field chemicals, synthesized magnetic SERS composite nanoparticles for microfluidic detection, and fabricated reservoirs on-a-chip for enhanced oil recovery microfluidic imaging analysis.

Prior to joining Aramco, he led a multidisciplinary team as a postdoctoral associate at MIT's solar frontier center for the fabrication of highly efficient solar cells.

Sehoon is the author of more than 45 publications, including peer-reviewed journal articles and patents, with high impact factor journals such as *Advanced Energy Materials*, *Nano Letters*, *Advanced Materials*, and *ACS Nano*. His publications have received more than 2,000 citations.

Sehoon received his Ph.D. degree in Materials Science and Engineering from Georgia Institute of Technology, conducting research in the field of materials science and engineering with an emphasis on nanomaterials, specifically developing plasmonic sensors.

Gawain Thomas

M.S. in Physics,
Worcester Polytechnic Institute

Gawain Thomas is a Research Scientist on the Reservoir Engineering Technology Team, Aramco Americas, Aramco Research Center-Boston. Since joining the team in 2017, he has contributed to the development of several delivered technologies for the ultra-trace detection and quantification of advanced barcoded interwell tracers, as well as for pulsed injection of tracer tag fluids during drilling.

Gawain received his B.S. and M.S. degrees in Physics from Worcester Polytechnic Institute, Worcester, MA, where he investigated the effects of matrix elasticity on tissue cell physiology and signaling using atomic force microscopy.

Dr. Wei Wang

Ph.D. in Physical Chemistry,
Chinese Academy of Sciences

Dr. Wei Wang is a Research Science Consultant on the Reservoir Engineering and Technology Team, Aramco Americas, Aramco Research Center-Boston. Since he joined the Aramco Research Center-Boston as one of the founding members in 2012, Wei's research has been focused on the application of advanced materials and nanotechnology for reservoir engineering.

Prior to joining Aramco, he was a Staff R&D Scientist at the Oak Ridge National Laboratory (ORNL), where he was the PI or co-PI for 17 research projects funded by the U.S. Department of Energy and ORNL. Wei received the Stanley I. Auerbach Award for Excellence in Environmental Sciences in 2009.

He has published more than 160 peer-reviewed research papers, four book chapters, and 12 patents. Wei is a Fellow of the Industrial and Engineering Chemistry Division of the American Chemical Society (ACS), and serves as a Program Chair at Energy and Fuel Division of ACS and a Program Committee Member of the Society of Petroleum Engineers (SPE) Annual Technical Conference and Exhibition. He is also an Editorial Board Member of *Nature Scientific Reports*.

In 1993, Wei received his Ph.D. degree in Physical Chemistry from the Chinese Academy of Sciences, Changchun, China, with the honors.

Dr. Afnan A. Mashat

Ph.D. in Environmental Science and Engineering,
King Abdullah University of Science and Technology

Dr. Afnan A. Mashat joined the Reservoir Engineering Technology Division of Saudi Aramco's Exploration and Petroleum Engineering Center – Advanced Research Center (EXPEC ARC) in July 2015. Her research interest includes using nanomaterials for enhanced oil recovery/improved oil recovery applications.

Afnan received her B.S. degree in Microbiology from King Abdulaziz University, Jiddah, Saudi Arabia, and her M.S. and Ph.D. degrees in Environmental Science and Engineering from King Abdullah University of Science and Technology, where Afnan investigated nanomaterials for drug release and delivery applications.

Hussain A. Shateeb

A.S. in Industrial Chemistry Technology,
Jubail Industrial College

Hussain A. Shateeb joined Saudi Aramco as an Apprentice Technician in the Vocational College Graduates (VCGNE) Training Program in August 2014. Upon attaining his degree in 2016, he then then joined the Reservoir Engineering Technology Division of Saudi Aramco's Exploration and Petroleum Engineering Center – Advanced Research Center (EXPEC ARC), where he works as a Lab Technician.

Hussain received his A.S. degree in Industrial Chemistry Technology from Jubail Industrial College, Jubail, Saudi Arabia.

Injecting Cooling Agents to Reduce Breakdown Pressure for Open Hole Hydraulic Fracturing Treatment

Dr. Kaiming Xia, Dr. Tariq Mahmood, Dr. Saidi A. Hassani, Dr. Rajesh Goteti and Dr. Yaser A. Alzayer

Abstract /

For deep and tight gas reservoirs, horizontal wells are generally drilled for maximum reservoir contact. Also, transverse hydraulic fractures are strongly desired, which suggests that the horizontal part should be drilled in the minimal horizontal stress (σ_{hmin}) direction. In this situation, formation breakdown for initiating transverse fractures can be a challenging issue for zonal isolated open hole multistage hydraulic fracturing treatment.

This article presents an innovative idea on reducing breakdown pressure through cooling the borehole. It is achieved by injecting cooling agents and flowing them to the target open borehole fracturing interval. As a result, the cooling agent may lead to a temperature drop in the open borehole formation. The near borehole formation will exhibit thermal contraction, and accordingly, tensile stress increases along the borehole axial direction. Simultaneously, the thermal contraction leads to the compressive hoop stress increasing, which can inhibit the longitudinal fracture initiation.

Eventually, the breakdown pressure along the borehole axis direction can be reduced and becomes easy, which boosts the chance for initiating transverse hydraulic fractures. The required axial tensile stress changes along the borehole axis, and always varies from well to well and reservoir to reservoir.

For accurately estimating the required axial stress change along the borehole axis, a 3D fully coupled thermal displacement finite element model was specifically developed for facilitating the cooling agent design. Criteria to terminate the cooling process and timing of the breakdown are also offered. Examples are also provided to demonstrate the effectiveness of the method.

Introduction

Rock breakdown or fracture initiation should first be achieved for a successful hydraulic fracturing treatment. For a hydraulic fracturing treatment, reliable breakdown of the near borehole formation may affect the selection of right casing size, tubing size, wellhead, and burst pressure limits, as well as pump schedule design. The hydraulic fracturing pump schedule may not be able to be injected as planned if breakdown is an issue. Additionally, wellheads of a wellbore, e.g., an entrance portion of the wellbore, may have a pressure limit. In some situations, the pressure limit may be approximately 15,000 psi. For some deep and tight gas reservoirs, breakdown may be a challenge because it is difficult to get a pressure high enough to act on the wellbore without exceeding the wellhead pressure limit.

In the oil and gas industry, horizontal wells in deep and tight gas reservoirs are generally drilled for maximum reservoir contact. Also, transverse hydraulic fractures are strongly desired, which suggests that the horizontal part should be drilled in the minimum horizontal stress (σ_{hmin}) direction. In this situation, formation breakdown for initiating transverse fractures may be a challenging issue for zonal isolated open hole multistage hydraulic fracturing treatment, Fig. 1, which has no casing and no perforation clusters, unlike a cased well fractured with perforation and plug method.

For the open hole hydraulic fracturing method, the tubing is surrounded by an annulus within the open borehole, which has a spacing between the tubing and the formation. Expandable packers separate the fracturing stages. For open hole multistage hydraulic fracturing treatment, the bottom-hole fluid pressure from the hydraulic fracturing fluid injection cannot effectively stretch the formation along the wellbore axis direction if the borehole surface is smooth, or without significant notches. Fluid cannot effectively apply surface traction in the axial direction.

Only a small amount of pressure acting on the packers (in the axial direction) can induce axial tensile stress in the fracturing stage interval, but seems to be very limited. Therefore, fluid pressure acting on an open borehole may not be able to induce enough tensile stress along the borehole axis direction so that transverse hydraulic fractures can be initiated effectively. From a mechanics point of view, we can consider this case approximately as a plane strain mechanics problem if the borehole axis aligns at either the σ_{hmin} or maximum horizontal stress direction.

Based on mechanics, it can be reasonably inferred that the induced axial stress may be very low, i.e., approaching
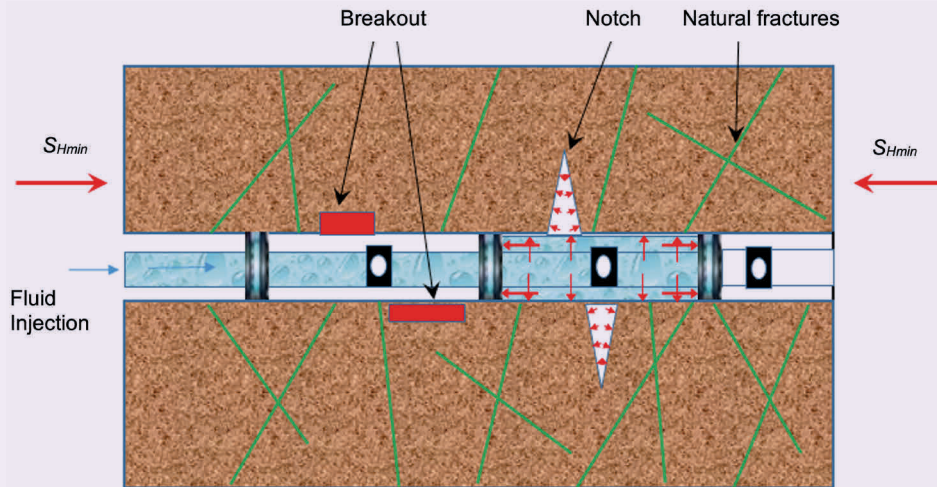
zero or negligible, compared with the induced hoop stress. For an open hole under this loading situation, the induced tensile stress may be appreciable only if there are weak locations, such as big and deep breakouts or notches existing on the zonal isolated borehole wall, Fig. 1, and little to no hydraulic fluid leaks off into the borehole formation.

In reality, fluid injection over the open hole fracturing stage can effectively induce hoop stress, which indicates a faster increase in tensional hoop stress than axial stress. Therefore, longitudinal hydraulic fractures may be initiated first. This is against the goal of hydraulic fracturing treatment for a transverse hydraulic fracture even though the horizontal well is drilled in the σ_{hmin} direction.

To address this issue, we developed a method relating to the reduced breakdown pressure prior to injecting the main pump schedule of the hydraulic fracturing treatment. Specifically, the technique relates to an approach on reducing breakdown pressure through cooling the open borehole first, which can be achieved by injecting cooling agents through the tubing and flowing them to the target open hole fracturing interval. As a result, the cooling agents may lead to a temperature drop near the borehole formation. The cooling agents may be or include one or more of: dry ice, ethanol, liquid nitrogen, water ice, slick water, etc.

Simultaneously, the near wellbore formation may exhibit thermal contraction and tensile stress increases in the borehole axial direction. Also, the thermal contraction leads to an increasing compressive hoop stress, which can inhibit the longitudinal fracture initiation. This can be ideal for a hydraulic fracturing treatment in horizontal wells. Eventually, the breakdown pressure along the borehole axis direction may be reduced, and facilitates the initiation of transverse hydraulic fractures for open hole hydraulic fracturing treatment. There are a few studies discussing the application of cold

nitrogen and foam for waterless stimulation purposes — and other purposes[1-3].

None of these studies directly addressed the idea of using cold liquid for the purpose of reducing breakdown pressure so that transverse fractures can be initiated successfully for horizontal wells. In real situations, the required axial tensile stress changes along the borehole axis, and may vary from well to well and reservoir to reservoir. Thermal shock or cold shock might not work as mentioned. For accurately estimating the required axial stress changes along the borehole axis, a 3D fully coupled thermal displacement finite element model is developed for facilitating the cooling agent injection design[4]. The criteria to terminate the cooling process is also proposed[4]. All of these will help to control the design of a cooling agent injection and a cooling process in an efficient manner.

Fracture Initiation Issues for Open Hole Hydraulic Fracturing Treatment

As previously mentioned, an open hole multistage hydraulic fracturing treatment seems to be inefficient on initiating transverse fractures. To verify the fracturing performance of the open hole hydraulic fracturing treatment, a finite element-based model on plane strain condition is built, Fig. 2, which assumes that the horizontal well aligns subparallel to the σ_{hmin} direction. From the simulation results of hoop stress and axial stress, we can see that induced hoop stress, S_{22}, Fig. 3, is approximately 56.03 MPa (tensile). The induced axial stress, S_{33}, is approximately 0.1277 MPa, Fig. 4, which is very small or negligible. The ratio of the induced axial stress over the induced hoop stress is approximately 0.22%.

From this simple finite element study, one can see the fluid injection over the open hole fracturing stage effectively inducing the hoop stress more than the axial stress, which indicates a faster increase in tensional

Fig. 2 *A finite element model for a horizontal well in plane strain condition (internal pressure loading).*
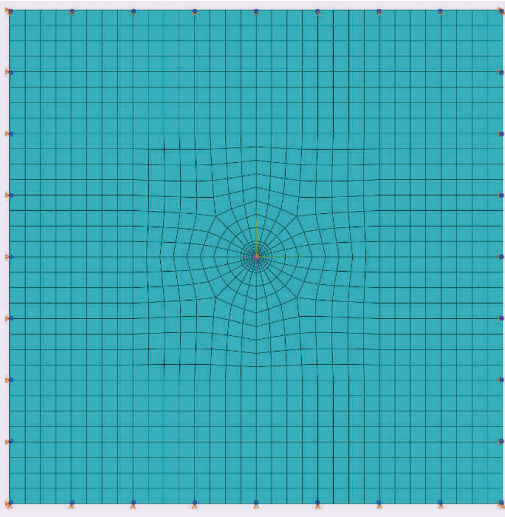
Fig. 3 *The induced hoop stress, S_{22}, for a horizontal well under the loading of internal pressure.*
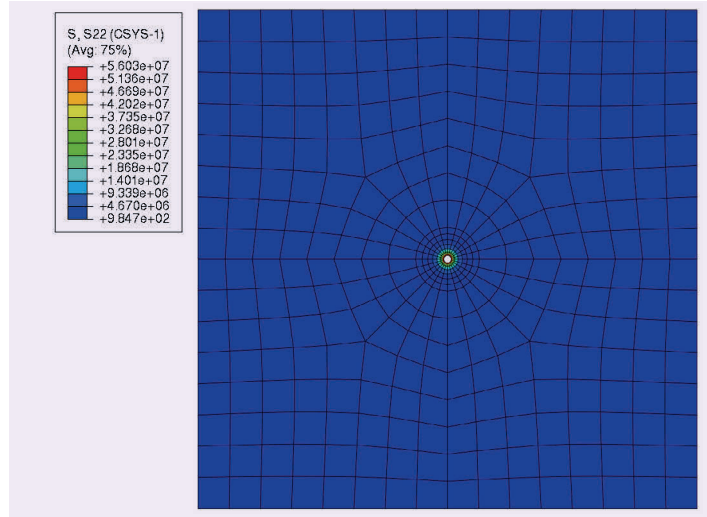
hoop stress than inducing axial stress. Hoop stress is used to generate a longitudinal fracture, and axial stress is used to initiate a transverse fracture, which clearly proves that a longitudinal fracture is very likely to initiate first instead of a transverse fracture. Once a longitudinal fracture initiates, injection fluid continues to drive the longitudinal fracture to propagate, with little chance for initiating transverse fractures.

This confirms the qualitative analysis about the potential issues that exist for the open hole fluid injection method. Also, it is likely for a longitudinal fracture to propagate to the neighboring fracturing stages, which causes a lot of stage communication issues for subsequent fracturing stages and is very difficult to stimulate the whole horizontal well for good production. Subsequently, the longitudinal fracture plane is horizontal if drilled at the σ_{hmin} direction, and it is very difficult to place proppant for good conductivity. This issue has not been well addressed to any extent in the past.

Inject Cooling Agents to Reduce Breakdown Pressure

To address the breakdown issue, we present a new procedure, which strives to reduce the breakdown pressure before injecting the pump schedule of the main hydraulic fracturing treatment. Figure 5 shows the mechanism on how cooling can effectively reduce breakdown pressure. As can be seen, cooling can be achieved by injecting the cooling agent and directing it to flow to the isolated zone of an open hole, which represents a fracturing interval and can directly interface with the borehole and quickly cool the targeted borehole formation. Then, thermal contraction will occur along the axis of the borehole direction and simultaneously induces tensile stress — inside the blue box area.

The cooling rate can be controlled based on numerical

Fig. 4 *The axial stress, S_{33}, for a horizontal well under the loading of internal pressure.*
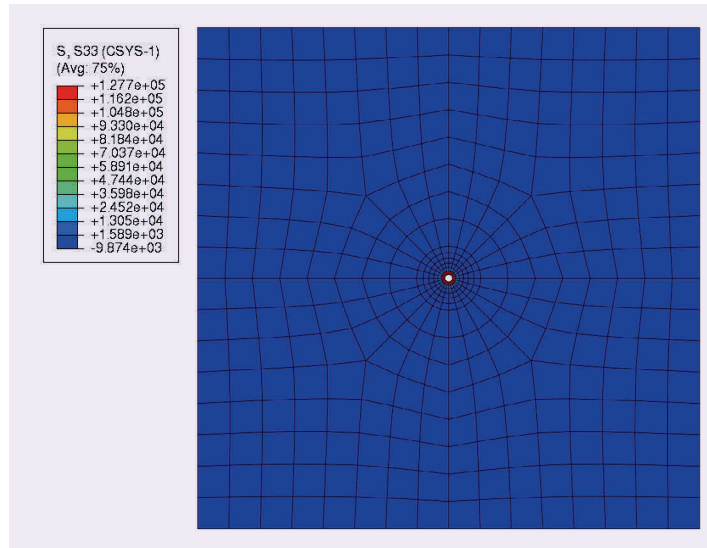
modeling, thermal energy transfer, and conversion. Increasing tensile stress in rock can reduce the breakdown pressure. The cooling process will be executed stage after stage, which should not be done for all stages simultaneously. For a reservoir, the reservoir temperature can be accurately measured through a downhole logging device. The thermal properties of the rock includes thermal expansion, thermal conductivity, and specific heat, which can be accurately tested in the lab. The rock mechanical properties can be extracted through the processing of sonic logs as well as lab tests. All of these properties need to be known before simulating the cooling process, which will be

Fig. 5 *The mechanical principle of cooling the targeted borehole formation.*

Condensate nitrogen liquid (cold temperature)   Open hole isolated packer

Injection of
cold nitrogen

Thermal contraction due to rapid
cooling around the near borehole
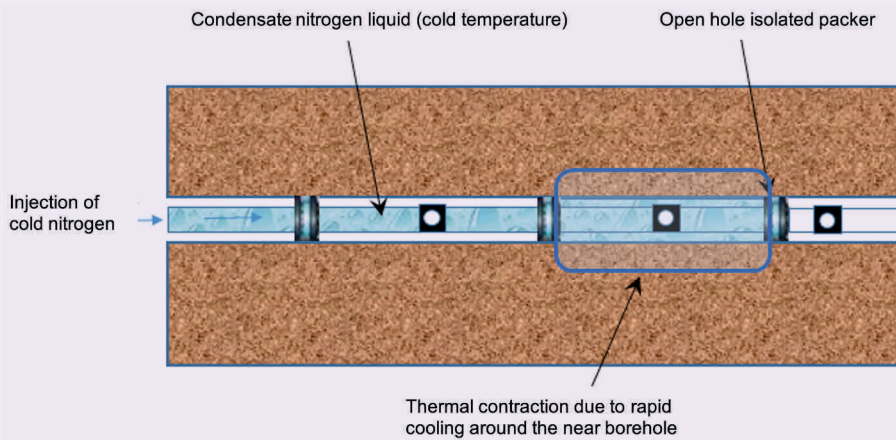
needed and accounted for, in the cooling agent design and injection process. Certainly, the injection schedule should be well designed and executed in detail, which will not be discussed in this article.

Dry ice is the solid form of carbon dioxide, which is used primarily as a cooling agent and has a lower temperature than that of water ice. Dry ice sublimates at -78.5 °C, at Earth atmospheric pressures. Liquid nitrogen is in a liquid state at low temperature, -195.79 °C, the boiling point at sea level and freezing point at -210 °C. Ethanol has a low freezing point, -114.14 °C, and a boiling point of 78.5 °C, which sometimes can be used with dry ice as a cooling agent. It is a colorless, low viscosity liquid and widely used as a coolant. Therefore, dry ice, ethanol, liquid nitrogen, and water ice can be good potential materials used for cooling the zonal isolated open borehole.

To quickly cool the borehole formation, different mixtures of dry ice, water ice, ethanol, or liquid nitrogen, and other chemical materials should be well prepared and mixed, and finally injected into the subsurface target fracking stage. The exact mixture of different materials should be accurately calculated based on the required temperature drop needed, the heat transfer process, the thermal energy equations, and rock thermal and mechanical properties.

3D Coupled Thermal Displacement Finite Element Model for Cooling Process

To estimate the cooling process, a 3D coupled thermal displacement finite element model was developed, which can be used to predict the cooling process and indicate transient temperature drop, stress change, etc. Figure 6 shows the developed finite element model, in which the red colored area represents a fracturing stage. Cooling agents are injected through a tube and flow out of an open port and then accumulate at the annulus.

The borehole will interface with injected cooling agents. The heat will be transferred from high reservoir temperature to the sink of cooling agents (lower temperature coolant in the borehole, which is modeled as surface film conditions. It is defined with a film coefficient — $(W/m^2/°C)$ — sink temperature and its distribution type. The coupled thermal displacement model needs the rock mechanical properties, including thermal conductivity, thermal expansion, and specific heat, besides the Young's modulus, Poisson ratio, and density. All these properties can be obtained from lab tests or log data.

Figure 7 represents an example of a temperature contour for the whole reservoir model, which shows only the interval of the borehole being cooled. The rest of the reservoir maintains its original temperature, as the cooling is limited to the area near the borehole. Figure 8 shows the temperature distribution around the borehole at an instant, which has a significant temperature drop due to cooling. After a certain cooling time, the temperature drops to 58 °C at the borehole wall.

Figure 9 shows the temperature gradient, which has a sharp temperature gradient around the borehole due to the cooling agent being present in the targeted borehole. Figure 10 shows an example of the induced axial stress change along the axis of the borehole during the cooling process, which exhibits axial tensile stress increasing to approximately 30 MPa, which represents enough change over the open borehole area. This change in axial stress in the near open hole may represent enough changes to significantly reduce the breakdown pressure for initiating transverse hydraulic fractures.

The numerical simulation confirms that the cooling borehole can reduce the potential breakdown pressure for initiating a transverse fracture. Consequently, the numerical modeling results show the formation needs to take a certain amount of time — a minimum of 10 minutes — to cool the formation and induce enough thermal contraction. Typically, the amount of time for the cooling process may be based on several factors, such as thermal mechanical properties of the rock, temperature of the reservoir rock, temperature of the

Fig. 6 *Coupled thermal displacement finite element model for simulating cooling process.*

Low temperature sink controlled by cooling agent injection
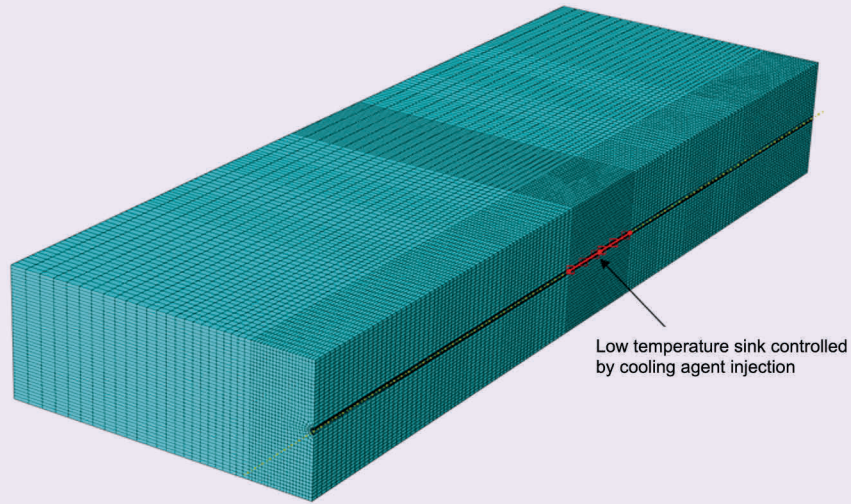
Fig. 7 *The temperature contour over the reservoir induced by the cooling agent.*
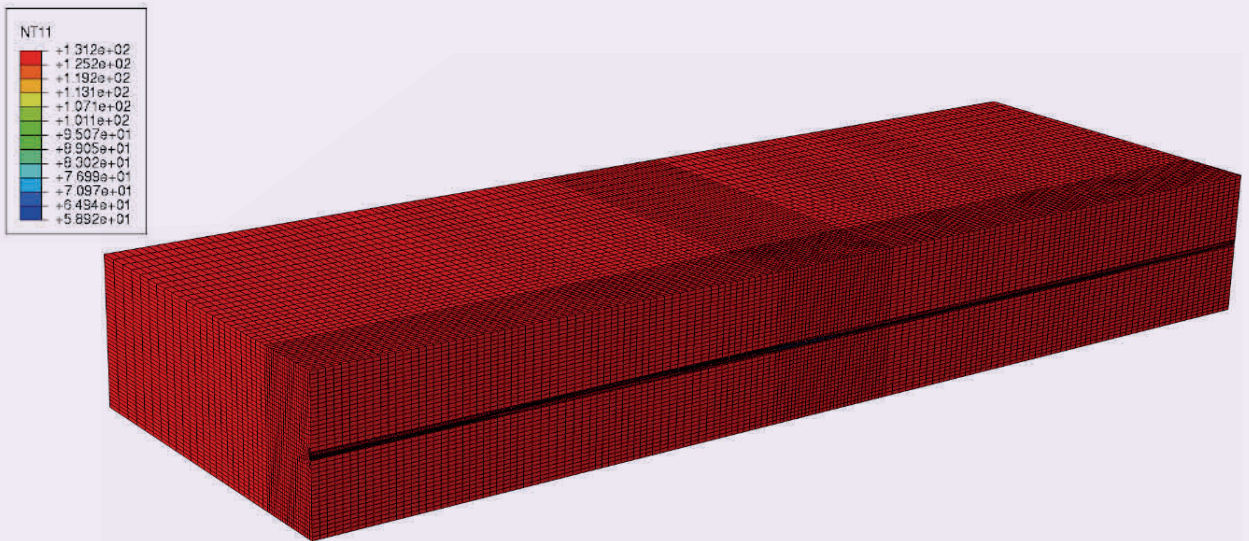
coolant, etc.

In other words, the effect of instantaneous thermal shock or cold shock due to injecting cold nitrogen stimulation to the subsurface formation seems to be negligible. Based on the simulation results, we can see the impacted area of thermal shock or cold shock for producing microscopic fractures is within a limited and small area.

Criteria to Terminate Cooling Process and Timing Injection for Breakdown

For a zonal isolated open hole, tensile fractures will be initiated from the open borehole once the cooling induced axial stress exceeds the threshold value, which is equal to the rock tensile strength, T, plus the effective in situ σ_{hmin} if the horizontal well is drilled subparallel to the σ_{hmin} direction. For open hole hydraulic fracturing, the cooling process may be stopped when the induced axial tensile stress meets the following condition:

$$\sigma_{\text{T\_axial}} = T + \sigma_{hmin} \hspace{2cm} \boxed{1}$$

For the cased hole/perforation hydraulic fracturing method, the induced axial tensile stress needs to be increased to a threshold value, which can guarantee enough bottom-hole pressure to breakdown the rock around the perforation tunnel and the surface treating pressure below the wellhead pressure limit. Based on the finite element modeling results, e.g., the models

Fig. 8 *The temperature distribution contour around the borehole.*
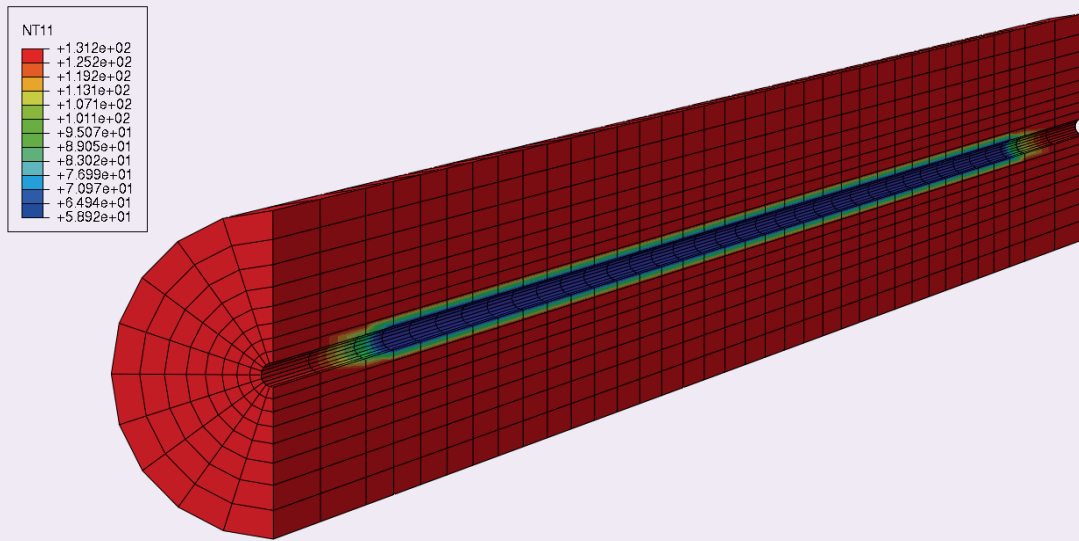
Fig. 9 *The temperature gradient contour around the borehole.*
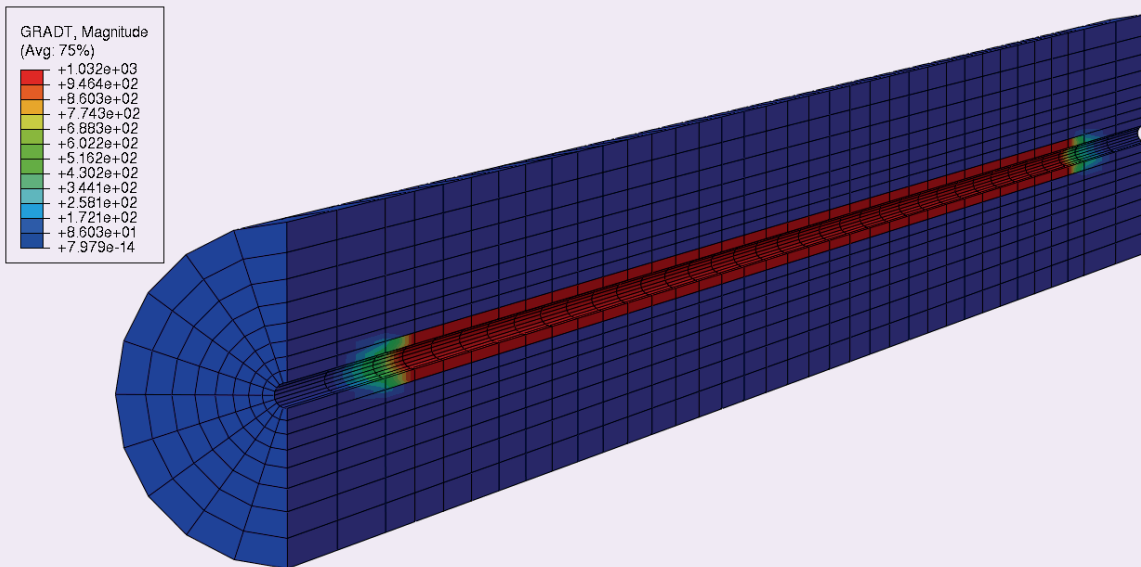
depicted in Figs. 6 to 9, one may be able to identify aspects of the cooling process such as the transient cooling process, temperature drop, or stress change. These aspects may be used to identify criteria to terminate the cooling process. For example, the criteria to terminate the cooling process may be a time span in which the cooling process should be performed. In some cases, the cooling process may take on the order of 10 minutes, while in other cases the cooling process may be longer or shorter.

In some cases, the cooling process may be performed for approximately 10 minutes to 20 minutes. Typically,

the amount of time for the cooling process may be based on the comprehensive factors such as thermal mechanical properties of the rock, temperature of the rock, temperature of the coolant, etc. To monitor the cooling process, the criteria to terminate the cooling process may be based on the induced axial tensile stress change along the borehole axis, which may allow the rock to break down without exceeding the pressure limit at the wellhead.

In this situation, σ_{T_axial} may represent the required or predefined change in induced axial tensile stress. T may refer to the tensile strength of the formation of

Fig. 10 *The induced axial stress along the borehole axis.*
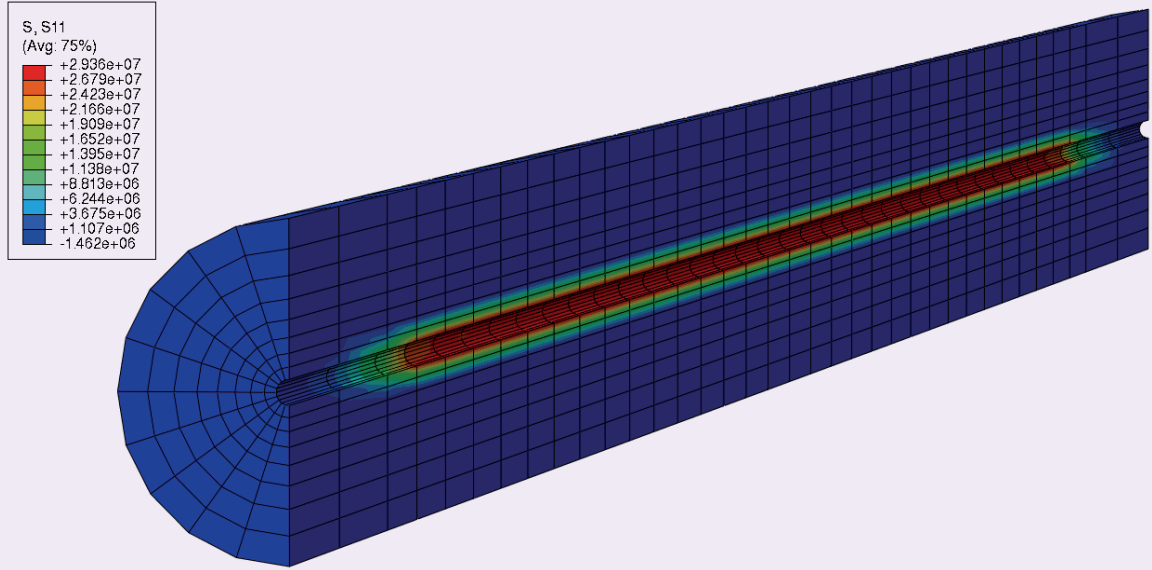
the borehole where the transverse hydraulic fracture is desired. σ_{hmin} denotes the effective in situ σ_{hmin}. For a perforation hydraulic fracturing method, it may be desirable to increase the induced axial tensile stress, e.g., σ_{T_axial}, to a threshold value that may allow bottom-hole pressure to break down the rock around the perforation tunnel, while keeping the surface pressure below the wellhead pressure limit. Once this induced axial tensile stress is achieved, the cooling process may be terminated, and injection of the main pump schedule for hydraulic fracturing should be started immediately.

In case the horizontal part of the borehole is not subparallel with the σ_{hmin} direction, the σ_{hmin} will be replaced by the component of in situ stress projected onto the borehole direction, which is named by $\sigma_{axial}^{In-situ}$. Based on the finite element model, we can see the transient cooling process in terms of temperature drop. To obtain the component $\sigma_{axial}^{In-situ}$ of the in situ projected stress, σ_{Pr}, onto the axial direction of the borehole, the two coordinate systems may be established: global coordinate system $(x_G y_G z_G)$ and borehole coordinate system $(x_B y_B z_B)$, Fig. 11.

The global coordinate system is defined as the x axis always aligning with the north, the y axis aligning with the east, and therefore the z axis aligns vertically downwards. Generally, one may assume the azimuth of the maximum principal stress is θ_{σ_H}, which is the angle turning clockwise from the north to the maximum principle stress. Therefore, the rotation matrix is given by:

$$R_{\sigma_H \to G} = \begin{pmatrix} \cos\theta_{\sigma_H} & -\sin\theta_{\sigma_H} & 0 \\ \sin\theta_{\sigma_H} & \cos\theta_{\sigma_H} & 0 \\ 0 & 0 & 1 \end{pmatrix} \quad \text{2}$$

Generally, θ_{σ_H} is positive if the maximum principal stress is clockwise to the x_G axis, and negative if it is counterclockwise to the x_G axis. For a well survey, any point along the well trajectory may be determined by three parameters: measured depth, wellbore deviation, α_D, and wellbore azimuth, α_A. The borehole coordinate system at any point along the well trajectory may be tracked and obtained by the following rotations about the global coordinate system, particularly following two steps: (1) rotation of the α_D about the y_G axis; and (2) rotation of the α_A about the z_G axis. The transformation matrix is given by:

$$R_{G \to B}(\alpha_A, \alpha_D) = R_y(\alpha_D)R_z(\alpha_A) =$$

$$\begin{pmatrix} \cos\alpha_D & 0 & -\sin\alpha_D \\ 0 & 1 & 0 \\ \sin\alpha_D & 0 & \cos\alpha_D \end{pmatrix} \begin{pmatrix} \cos\alpha_A & \sin\alpha_A & 0 \\ -\sin\alpha_A & \cos\alpha_A & 0 \\ 0 & 0 & 1 \end{pmatrix} \quad \text{3}$$

Then, the in situ stress tensor can be projected onto the borehole coordinate system by:

$$\sigma^{B,I} = R_{G \to B}(\alpha_D, \alpha_A)R_{\sigma_H \to G}\sigma_{Pr}R_{\sigma_H \to}^T$$

$$_G R_{G \to B}^T(\alpha_D, \alpha_A) \quad \text{4}$$

where $\sigma_{axial}^{In-situ}$ is the stress component at the direction of the z axis of the borehole coordinate system, which is calculated using Eqn. 4.

Conclusions

Determining the rock breakdown pressure can be a challenging task for hydraulic fracture treatment in deep and tight gas reservoirs. Zonal isolated open hole hydraulic fracturing treatment has been used to stimulate the horizontal wells. Consequently, the fracture initiation associated with this fracturing method has not been well addressed. Based on the loading, open hole fluid injection is more likely to initiate the

Fig. 11 *The coordinate systems for projecting in situ stress onto the borehole axial direction.*
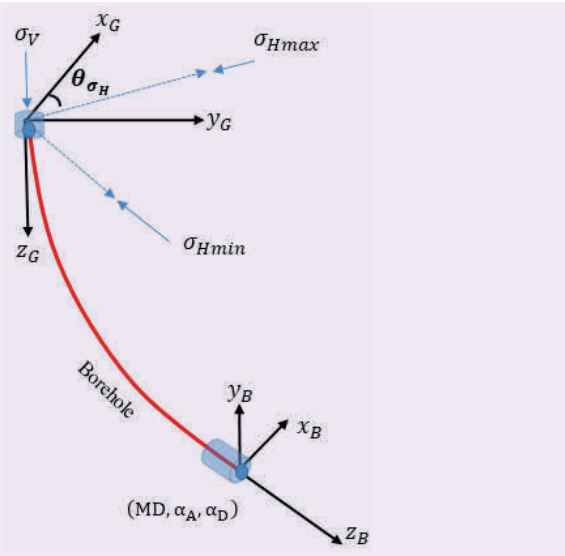
longitudinal fractures first, even though the horizontal well is drilled at the σ_{hmin} direction. Therefore, stage communications can happen for the subsequent fracturing stages.

In this article, a finite element modeling result is presented to verify this. To address this issue for an open hole hydraulic fracturing method, we recently developed an innovative method on injecting a cooling agent to reduce breakdown pressure first, and then proceed to inject the main pump schedule. The cooling agents can drop the temperature in the near borehole formation and leads to thermal contraction in the axial direction along the borehole fracturing interval. Therefore, the axial tensile stress can be induced by thermal contraction, which can lower the breakdown pressure for initiating transverse fractures. Also, thermal contraction of the open borehole leads to an increasing compressive hoop stress, which inhibits the longitudinal fracture initiation.

This exactly alleviates or minimizes the drawback of the open hole hydraulic fracturing method.

Additionally, a 3D fully coupled thermal displacement finite element model was developed for simulating the borehole cooling process as well as the criteria to control the cooling process. All of these parameters are very critical to direct the cooling agent injection design, and control the cooling process. This helps to determine the best breakdown moment so that the main pump schedule can be injected immediately thereafter.

Based on the finite element modeling study, we can see the idea of injecting cooling agents to reduce breakdown pressure works efficiently; however, it may take over 10 minutes to cool the borehole so that enough change in the induced axial stress can be achieved. The cooling time is dependent on thermal mechanical properties of the formation and cooling agents, and injection schedule, which may vary from reservoir to reservoir and well to well.

The required cooling time, based on simulation, seems to indicate that thermal cold shock to the subsurface formation to produce microscopic fractures might not be significant as previously thought. The subject matter described in this article can be implemented in field operations, so as to realize the following advantages. First, it may help reduce the breakdown pressure, and improve the success rate of breakdown for transverse fractures. Second, the method may present a computer modeling method and criteria to control the cooling process performed in a controlled and efficient manner.

References

1. Lai, B., Liang, F., Li, L. and Zhang, J.: "Conditioning a Subterranean Formation," U.S. Patent 10,415,358, September 2019.

2. Bacock, J.A. and Siess, C.P.: "Low Temperature Waterless Stimulation Fluid," U.S. Patent 10,428,263, October 2019.

3. Zhang, L., Ren, S.R., Fang, Z.K., Luo, J., et al.: "Cryogenic Gas Assists the Method for CBM Fracturing Technique," Chinese Patent 103,726,819B, 2016.

4. Xia, K., Mahmood, T. and Hassani, S.: "Breakdown Pressure Reduction Based on Injection of Cooling Agents," U.S. Patent Application 17,062,546, 2020.

About the Authors

Dr. Kaiming Xia

Ph.D. in Computational Mechanics,
University of Illinois at Chicago

Dr. Kaiming Xia is a Geophysicist working in Saudi Aramco's Gas Reservoir Characterization Department. His current focus is related to geomechanics and hydraulic fracturing treatment.

Prior to joining Saudi Aramco in 2019, Xia had worked with Caterpillar, Colorado School of Mines, Weatherford, and Shell Oil Company in U.S. His expertise has been on multidisciplinary areas, including finite element modeling,

geomechanics, soil/machine interactions, ground vehicle dynamics, downhole tool development, drilling dynamics, borehole stability, and hydraulic fracturing treatment.

Xia has published over 50 journal and conference papers.

He received his Ph.D. degree in Computational Mechanics from the University of Illinois at Chicago, Chicago, IL.

Dr. Tariq Mahmood

*Ph.D. in Geology,
University of Adelaide*

Dr. Tariq Mahmood joined Saudi Aramco in 2008 and currently works in the Gas Reservoir Characterization Department as a Geological Consultant. He began his career in 1996, working in Perth, Australia, specializing in fractures/faults characterization from borehole images. Tariq has provided consultancies to major oil companies in the Asia Pacific region and Australia, including Shell Brunei, Petronas, Chevron, Santos, Apache, Woodside, etc. Since joining Saudi Aramco, he has worked on many interesting projects addressing a variety of problems in both offshore and onshore gas fields.

Tariq is a member of the American Associa-tion of Petroleum Geologists (AAPG), the European Association of Geoscientists and Engineers (EAGE), and the Dhahran Geosciences Society (DGS). He is the coauthor of three patents.

Tariq received his Ph.D. degree in Geology from the University of Adelaide, Adelaide, South Australia, Australia, in 1996. Based on his Ph.D. research, an atlas on the "3D Analogue Modeling of Extensional Fault Systems plus Field Applications" was published by the University of Adelaide. Tariq was the recipient of the Harold Rhoda Scholarship during his studies in Australia.

Dr. Saidi A. Hassani

*Ph.D. in Geology,
University of South Carolina*

Dr. Saidi A. Hassani is a Chief Geologist for the Satellites Gas Fields Division in Saudi Aramco's Reservoir Characterization Department. He joined Saudi Aramco in 2002 and is currently responsible for integrated reservoir characteri-zation studies, in particular, 3D geological modeling, structural geology, geomechanics, and development planning of the gas fields.

Prior to joining Saudi Aramco Oil Company, Saidi worked for Qatar Petroleum, BP Explora-tion in Anchorage, Alaska, and Deepwater Gulf of Mexico in Houston, Texas, on various reservoir characterization and description projects, including field development studies.

He is an active member of the American Association of Petroleum Geologists (AAPG), Society of Petroleum Engineers (SPE) and Dhahran Geoscience Society (DGS). Saidi is the author and coauthor several technical publications.

He received his Ph.D. degree in Geology from the University of South Carolina, Columbia, SC.

Dr. Rajesh Goteti

*Ph.D. in Structural Geology and Geomechanics,
University of Rochester*

Dr. Rajesh Goteti is the Petroleum Systems Modeling Team Lead in the Aramco Americas Houston Research Center (HRC), Houston, TX. He joined the HRC in 2014, and his primary area of expertise is structural geology and geome-chanics. Since joining Aramco, Rajesh has worked in several diverse areas, including natural fracture prediction, salt tectonics, geomechanical forward modeling and regional in situ stress prediction.

Prior to joining Aramco, he worked as a Senior Geoscientist at the ExxonMobil Upstream Research Center. Rajesh's experience includes working in both conventional and unconven-tional basins worldwide.

He is an active member of the American Association of Petroleum Geologists (AAPG) and the American Rocks Mechanics Association (ARMA). Rajesh has published numerous papers in international journals, a book chapter, and was the co-editor for two special thematic articles in the *Petroleum Geoscience* journal.

He has received numerous internal and external recognitions for his work since joining Aramco, including the 2017 Exploration and Petroleum Engineering Center – Advanced Research Center (EXPEC ARC) Technology Milestone Award, the 2018 HRC Delivered Technology Award, and the 2019 ARMA Applied Rock Mechanics Award for his work on modeling salt tectonics in the Red Sea. Most recently, Rajesh was elected to the Petroleum Geoscience (Lyell Collection) Editorial Board in 2020.

Rajesh received his B.S. and M.S. degrees in Applied Geology from the Indian Institute of Technology, Kharagpur, India, and his Ph.D. degree in Structural Geology and Geomechanics from the University of Rochester, Rochester, NY.

He was the recipient of the Academic Postdoctoral Fellowship from Dalhousie University, Halifax, Nova Scotia, Canada.

Dr. Yaser A. Alzayer

*Ph.D. in Geological Sciences,
University of Texas*

Dr. Yaser A. Alzayer is Geoscientist leading the Unconventional Resources Focus Area in the Geology Technology Division of Saudi Aramco's Exploration and Petroleum Engineering Center – Advanced Research Center (EXPEC ARC). Prior to his current position, Yaser had multiple rotational assignments in the Southern Area Exploration, Wellsite Geology, and Geologic Solutions divisions.

Currently, he is leading several projects to enhance the mechanical and fracture character-ization of conventional and unconventional reservoirs. Yaser's research interests include mechanical stratigraphy, fracture characteriza-tion, and forward geomechanical modeling.

He is an active member of the American Association of Petroleum Geologists (AAPG) and the Society of Petroleum Engineers (SPE). Yaser regularly serves as a technical reviewer for the *Journal of Petroleum Science and Engineering* and several international conferences such as the AAPG Annual Convention and Exhibition, the International Petroleum Technology Conference, and the American Rock Mechanics Symposium.

Yaser received his B.S. degree in Geology from the University of Kansas, Lawrence, KS. He also received his M.S. and Ph.D. degrees in Geological Sciences from the University of Texas at Austin, Austin, TX.

Utilizing Novel Expandable Steel Packers to Overcome Multistage Fracturing Completion Deployment Challenges in Horizontal Gas Wells

Ebikebena M. Ombe, Ernesto S. Gomez, Aldia Syamsudhuha and Abdullah M. Alkwiter

Abstract /

This article discusses the successful deployment of multistage fracturing (MSF) completions, composed of novel expandable steel packers, in high-pressure, high temperature (HPHT) horizontal gas wells. The 5⅞" horizontal sections of these wells were drilled in HPHT gas-bearing formations. There were also washouts and high "doglegs" along their wellbores, due to constant geosteering required to keep the laterals within the hydrocarbon-bearing zones. These factors introduced challenges to deploying the conventional MSF completion in these laterals. Due to the delicate nature of their packer elastomers and their susceptibility to degradation at high temperature, these conventional MSF completions could not be run in such hostile downhole conditions without the risk of damage or getting stuck off bottom.

This article describes the deployment of a novel expandable steel packer MSF completion in these tough downhole conditions. These expandable steel packers could overcome these mentioned challenges because of the following unique features:

- High temperature durability.
- Enhanced ruggedness, which gave them the ability to be rotated and reciprocated without risk of damage.
- Reduced packer outer diameter (OD) of 5.500" as compared to the 5.625" OD of conventional elastomer MSF packers.
- Enhanced flexibility, which enabled them to be deployed in wellbores with high dogleg severity (DLS).

With the ability to rotate and reciprocate them while running in hole (RIH), coupled with their higher annular clearance and tolerance of high temperature, the expandable steel packers were key to overcoming the risk of damaging or getting stuck with the MSF completion while RIH. Also, due to the higher setting pressure of the expandable steel packers when compared to conventional elastomer packers, there was a reduced risk of prematurely setting the packers if high circulating pressure were encountered during deployment.

Another notable advantage of these expandable packers is that they provided an optimization opportunity to reduce the number of packers required in the MSF completion. In a conventional MSF completion, two elastomer packers are usually required to ensure optimum zonal isolation between each MSF stage. Subsequently, due to their superior sealing capability, only one expandable steel packer is required to ensure good interstage isolation. This greatly reduces the number of packers required in the MSF completion, thereby reducing its stiffness and ultimately reducing the probability of getting stuck while RIH.

The results of using these expandable steel packers is the successful deployment of the MSF completions in these harsh downhole conditions, elimination of nonproductive time associated with a stuck or damaged MSF completion as well as the safe and cost-effective completion in these critical horizontal gas wells.

Introduction

Deploying multistage fracturing (MSF) completions in horizontal high-pressure, high temperature (HPHT) gas wells can be a challenging operation when compared to deploying conventional cemented liner completions. The inclusion of multiple accessories in the MSF completion assemblies, e.g., open hole packers and fracture ports, increases its outer diameter (OD), and thereby reduces the clearance between the assembly and the open hole.

Coupled with the increased frictional factor due to these extra accessories and the presence of washouts

and localized high "doglegs" in the hole, a common occurrence in long horizontal sections, there is a very high risk of getting stuck with the MSF assembly before reaching its required setting depth. This is highly undesirable, since the positions of the MSF packers in the completion assembly are predetermined, such that when the MSF reaches its proposed setting depth, these packers would be positioned in areas of minimum hole internal diameter (ID), and therefore, would provide the most optimal sealing between the stages when they are finally activated.

With the resulting ineffective sealing between the stages, the MSF would not be able to achieve zonal isolation required for the multistage fracturing operation. Such stuck MSF assembly incidents may lead to significant nonproductive time, additional cost for remedial operations, and the possibility of compromising the well objective. In some cases, the completion may not be retrievable and this will require a sidetrack operation, which will delay the well delivery.

Even if the MSF is run to its setting depth, the packer may have been damaged due to exposure to these hostile open hole conditions. The elastomers commonly used in MSF completions are susceptible to heat damage when exposed to the high downhole temperatures as well as mechanical damage when interacting with the wellbore walls. This will also compromise the packer's ability to provide effective zonal isolation when they are set, and thereby compromise the MSF completion capacity to optimal MSF[1].

These challenges require a fit for purpose solution that will withstand the harsh conditions encountered by the MSF while being deployed, and at the same time, retain its ability to provide proper zonal isolation when required. The novel expandable steel packers are designed to meet the challenges in these tough downhole conditions. These expandable steel packers have higher temperature durability, enhanced ruggedness, and a lower OD, when compared to the conventional elastomer packers. All these factors help to reduce the risk of stuck pipe occurring while deploying the MSF completion in long horizontal laterals.

Technology

By placing the MSF packers in specific places in the horizontal wellbore, there is a greater ability to increase the cumulative production in a shorter time frame[2]. A typical MSF completion is deployed in the horizontal lateral and hung off the previous casing or liner via a liner hanger, similar to a cemented liner. It consists of multiple fracture valves with open hole packers positioned between them. These fracture ports serve as the conduit for which the fractures proppant is applied to the wellbore to create the fractures while the open hole packers provide zonal isolation between the fracture ports, thereby concentrating the fractures in the desired zones within the lateral.

There are three main categories of open hole packers available for MSF completions. These are mechanical open hole packers, swellable packers, and expandable packers. Mechanical open hole packers are similar to

the standard isolation packers used in oil and gas wells.

Figure 1a is an external view of an elastomer mechanical packer. Figure 1b shows the packer's internal setting mechanism consists of hydraulically actuated pistons placed either above or below the elastomer element. Figure 1c shows the packer's setting process. When the pistons are actuated they close in and squeeze the element, thereby forcing it to expand and fill the annular space between the fracture ports, thereby providing zonal isolation.

Swellable packers provide zonal isolation by swelling to fill up the annular space between the fracture ports. Figure 2a is an external view of a swellable packer. The swelling occurs when the packer elastomers come in contact and reacts with the fluid in the wellbore, Figs. 2b, 2c, and 2d. The expandable packers, unlike the previous categories, do not have elastomer elements, and achieve zonal isolation by the expansion of metallic sleeves. These sleeves deform and expand beyond the elastic limit of the metal when pressure is applied to them from within the string, Figs. 3a and 3b.

Elastomer-based packers, i.e., mechanical open hole packers and swellable packers, have two major disadvantages, which limits their deployment in long horizontal HPHT wells; their susceptibility to mechanical damage and their low tolerance to heat. Elastomers are typically softer than the formations they are deployed in, and during the deployment process, contact with these abrasive formations can lead to damage, especially when agitating or "worked" past constrictions and tight spots within the wellbore. This effect is further amplified when there are localized doglegs

---

Fig. 1 *(a) An external view of an elastomer mechanical packer, (b) a schematic of the packer's internal components, and (c) the packer setting process.*
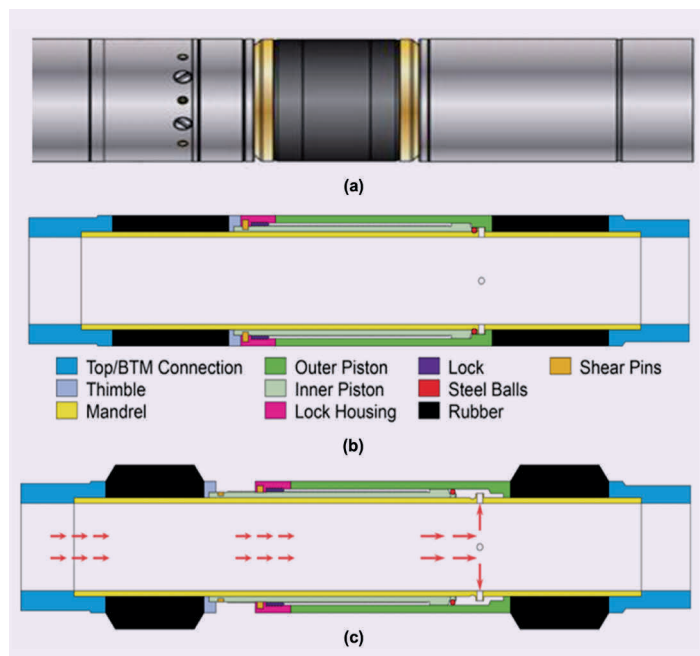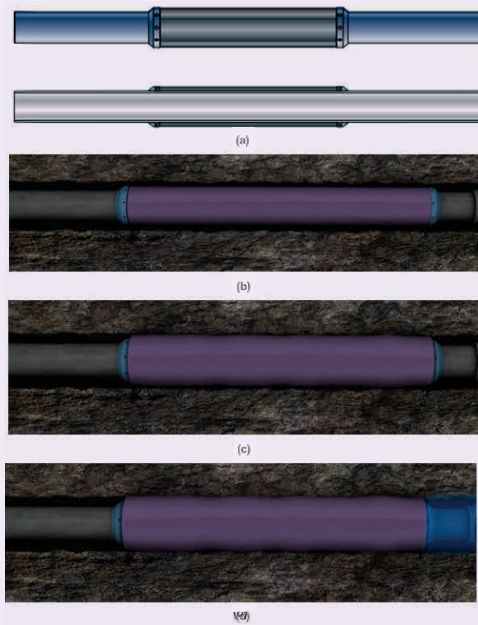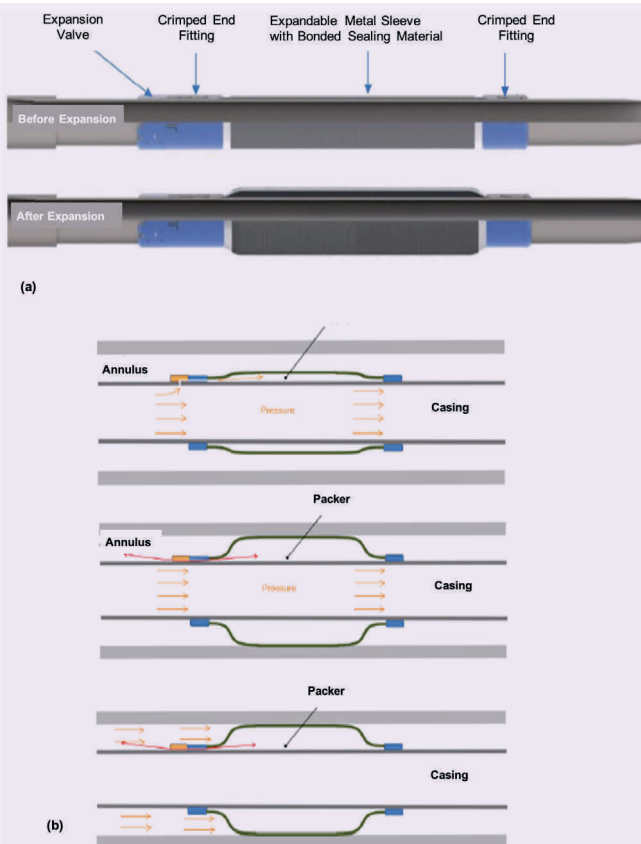
within the wellbore. Also, accelerated aging occurs in packer elastomers at high temperatures, since rubber molecules are prone to decompose at these elevated temperatures. The temperature degrading effect is even more pronounced if the elastomers are submerged in fluids[3]. In HPHT applications where bottom-hole temperatures may sometimes reach or even exceed this temperature, the packer may also be damaged when deployed.

Another limitation associated with the mechanical packers is inherent in their setting mechanism. Most open hole mechanical packers are set by applying hydraulic pressure from the surface, which is transmitted to the packers vial the wellbore fluids. While running the MSF completion in the wellbore, some circulation may be required to lubricate the MSF assembly and sweep the hole of any debris and obstructions in the wellbore.

Unfortunately, these circulating pressures will have to be controlled or the resulting circulating pressure could inadvertently initiate the packer setting process before the packer reaches its required setting depth.

For the swellable packers, the reaction between the packers and the wellbore fluids is time dependent and the packer elastomers are usually designed in such a way that the swelling process is delayed by a set time equal to the approximate time required to run the MSF assembly to its setting depth.

Consequently, in reality, the running time may far exceed the estimated time due to unpredictable downhole challenges like tight hole, well control events, and even surface equipment failures. If any of these challenges occur, the actual MSF assembly running time may exceed the swelling delay time. The packers may start swelling and ultimately wedge the MSF assembly in place before it reaches its setting depth.

The expandable steel packers do not have these disadvantages due to their unique design and setting process[4]. Due to the steel body and the lack of moving parts in the design, i.e., being built as a single metal part, the packers are inherently more robust and resistant to damage. The recessed sealing system of the packers also prevents damage to the sealing elements during deployment. They also have a high axial loading capability and torsional strength.

These properties afford the packers the ability to be rotated or "worked" while running in hole (RIH), if required, e.g., in restricted or undergauged sections of the horizontal wellbore[1]. They also give the packer an inherent toughness that further enhances its ruggedness and resistance to buckling when compared with the much shorter and bulkier mechanical packers. Because of this toughness, an expandable steel packer can be run in wellbores with up to 8°/100 ft dogleg severity (DLS). Additionally, the steel body of the packers also gives them a higher resistance to heat damage when compared with their elastomer counterparts.

Due to its unique design, the expandable steel packer can provide more effective sealing in irregular open hole conditions of ovality and out of gauge irregular

borehole shapes, when compared to mechanical packers and swell packers. This means that one expandable packer can effectively provide the same zonal isolation that will require two or more elastomer packers. This ultimately reduces the number of packers required in the MSF assembly, thereby reducing its frictional factor and increasing its deployment success rate.

The expansion process for setting the expandable steel packer requires a high amount of pressure (5,000 psi to 7,000 psi), which is usually much higher than the circulating pressure while RIH, thereby preventing the premature setting of the packer while circulating. Also, the expansion can only occur when the pressure is applied, so expansion occurs only when required. This is a clear advantage over the time dependent swellable packer where there is limited control on the swelling process.

Table 1 is a summary of the technical comparison of the mechanical packers, the swellable packers, and the expandable steel packers selected for deployment in the wells discussed in this article.

Case Study

This case study discusses the deployment of 4½" MSF completion assemblies comprising of expandable steel packers and fracture ports in a field of interest in the Middle East. These MSF assemblies were deployed in 5⅞" horizontal laterals of five HPHT horizontal gas wells with lateral lengths ranging from 3,000 ft to 7,000 ft and a total depth (TD) ranging from 17,000 ft to 19,000 ft.

Drilling these 5⅞" laterals in this field was associated with different downhole challenges that affected both the drilling operations and the subsequent MSF deployment operations. Some of these challenges are discussed next.

Formation Complexity

The 5⅞" laterals of the subject wells were drilled across the gas-bearing reservoirs toward the minimum stress direction (strike-slip tectonic regime). Information gathered from existing log data from wells previously drilled in the field indicated that the reservoir was highly heterogenous, Fig. 4, and compartmentalized, with varying porosity and formation pressures.

The laterals would be drilled across these varying reservoir characteristics, and due to the compartmentalization, the overbalance across the reservoir would range from 350 psi to 2,600 psi. Coupled with the maximum reservoir porosity of 12%, as observed from the offset wells, there was a high risk of differential stuck pipe occurring while drilling the laterals, and especially when deploying the MSF completions.

With this reservoir heterogeneity, a substantial amount of geosteering would be required while drilling to keep the lateral within the "sweet spots" of the reservoir. With geosteering comes excessive DLS, which could further complicate the MSF deployment operation.

Geomechanical Challenges

Geomechanic studies were carried out using the offset well data to understand the structural complexity of

---

Table 1 *MSF packer comparisons for 10K psi 4½" × 5⅞" open hole application.*

Description	Mechanical Packer	Swell Packer	Expandable Steel Packer
Construction	Aflas elements between the opposing hydraulic cylinders	Swellable elastomer vulcanized around the base pipe	Two double sleeve (Hastelloy) design with HNBR element vulcanized around the packer
Setting mechanism	Internal hydraulic pressure	Fluid activated swelling process	Internal hydraulic pressure
Pre-setting OD	5.625" (element)	5.600" (element)	5.500" (element)
Element length	2 ft	15 ft	8 ft
Ability to rotate while RIH	No	No	Yes
Maximum open hole ID tolerance for optimal sealing.	6.2"	6.25"	6.6"
Maximum allowable DLS	2°/100 ft	2°/100 ft	8°/100 ft
Maximum circulating rate	3 BPM	3 BPM	5 BPM
Maximum allowable circulating pressure to prevent premature setting	3,000 psi	No limitation	7,000 psi

Fig. 4 *The formation heterogeneity observed in the offset well logs.*
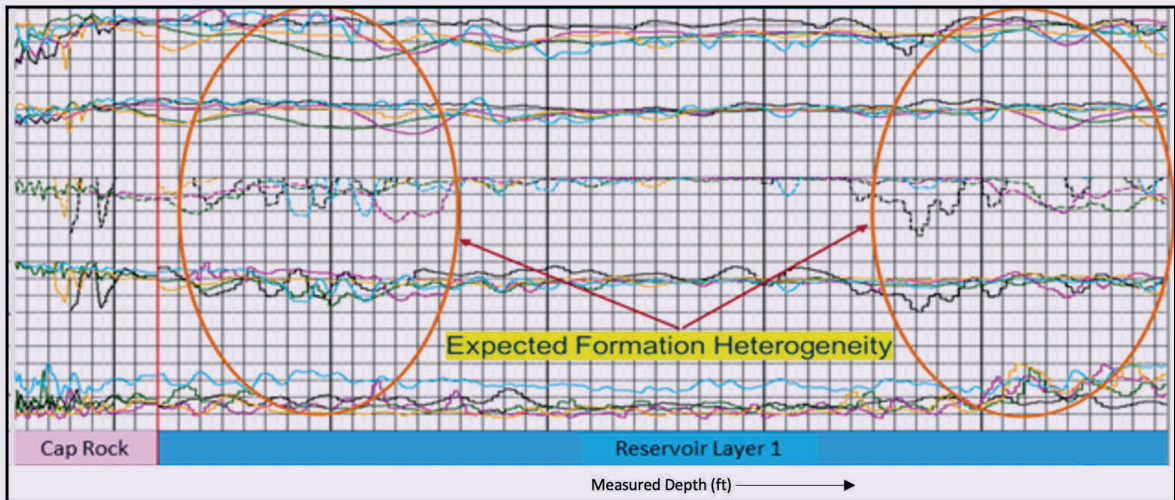
Fig. 5 *The planned vs. actual trajectory across the cap rock and reservoir rock.*
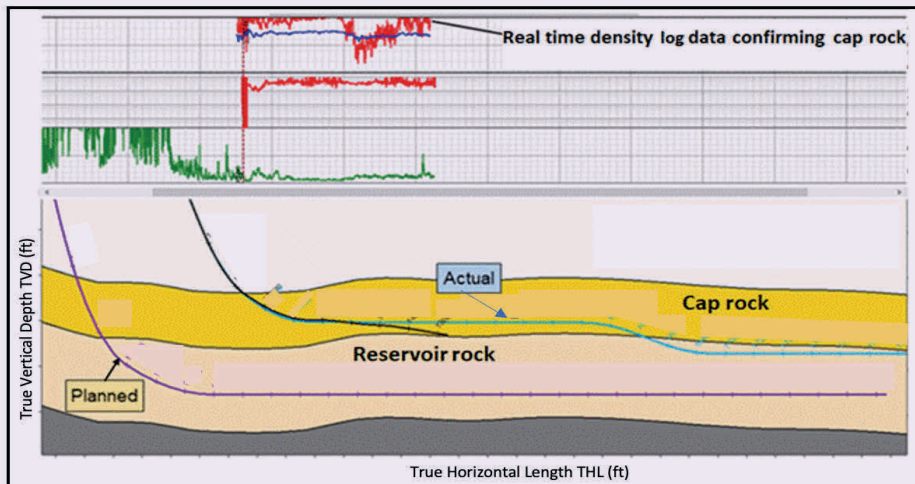
the reservoir, and thereby recommend the best ways to drill the laterals with minimum drilling challenges and improved wellbore quality for the subsequent MSF completions deployment. Subsequently, due to the limited number of relevant offset wells in the field, the geomechanical study was not as robust as desired to reduce the uncertainties in the geomechanical models. Also, some of the offset wells showed excessive hole enlargement across the logged reservoir sections, which negatively affected the log data quality and further introduced more uncertainties in the models.

The models recommended that the 5⅞" laterals should be drilled with a mud weight of 90 pcf. Another observation from the geomechanical studies was that the reservoir cap rock was very unstable and would require a very high mud weight to stabilize. The recommendation was to set the 7" liner shoe deeper within the reservoir cap rock above the target reservoir. This would minimize the amount of cap rock exposed in the 5⅞" lateral, and thereby improve the wellbore quality by reducing the risk of wellbore instability.

When the first of these wells were drilled, Well-A, the length of cap rock drilled was 1,375 ft as compared to the average anticipated length of 300 ft to 500 ft from the offset data and geological model. Drilling such a long cap rock interval in the lateral led to wellbore instability issues and numerous stuck pipe incidents while drilling. To mitigate these issues and improve wellbore quality, the mud weight was gradually increased from 90 pcf to 100 pcf to reduce the break out

Fig. 6 *Geomechanical models showing the Well-A pre-drilling (column 5), real-time (column 6) and postdrilling (column 7) wellbore breakout models for the lateral compared with the actual caliper logs (column 9).*
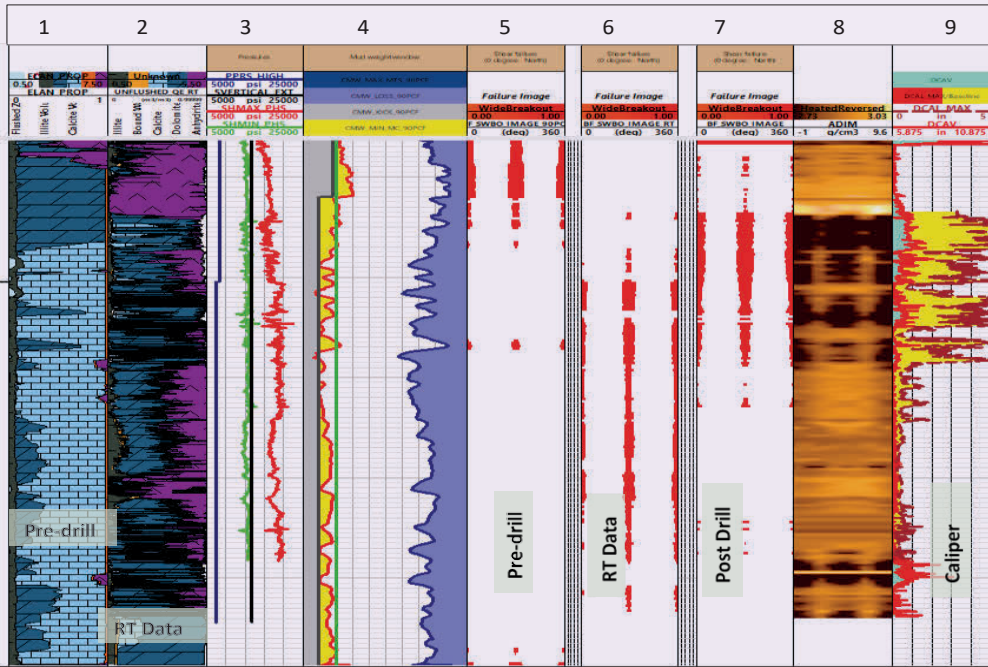
Fig. 7 *Real-time LWD temperature log showing high reservoir temperatures along the lateral.*
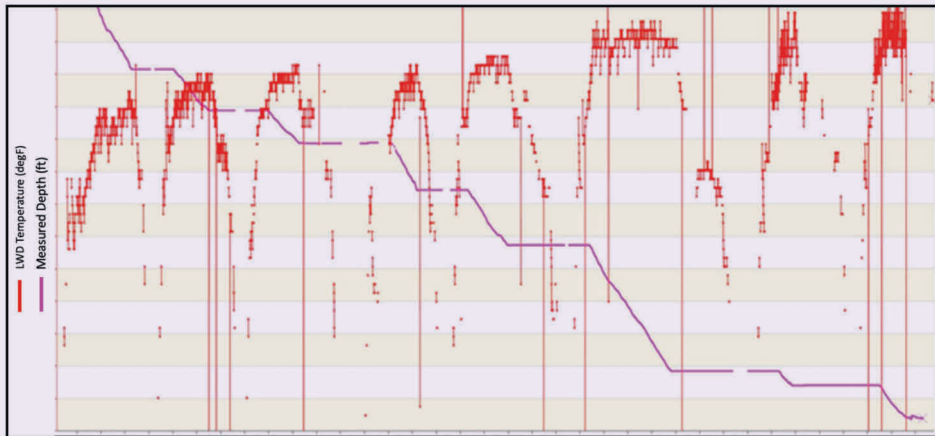
severity. Also, significant directional drilling had to be done while drilling the lateral to steer it out of the cap rock and into the reservoir, Fig. 5.

Caliper logs were run in the lateral after drilling to TD and they revealed that the hole sections drilled across the reservoir cap rock was significantly overgauged due to formation break outs and hole instability (see column 9 of Fig. 6). Due to this overgauged hole and the wellbore tortuosity, deploying a mechanical packer or swellable packer MSF completion in this well was not feasible since the MSF assembly would have required some aggressive rotation and "working" to get to bottom. This would have caused significant damage to these elastomer packers.

Reservoir Temperatures

While drilling the laterals in the wells, the actual dynamic downhole temperature was recorded by the logging while drilling (LWD) tools. These LWD measurements from the wells showed temperatures ranging from 310 °F to 328 °F, Fig. 7. The wireline

Fig. 8 *The wireline temperature logs confirming the high downhole static temperature.*
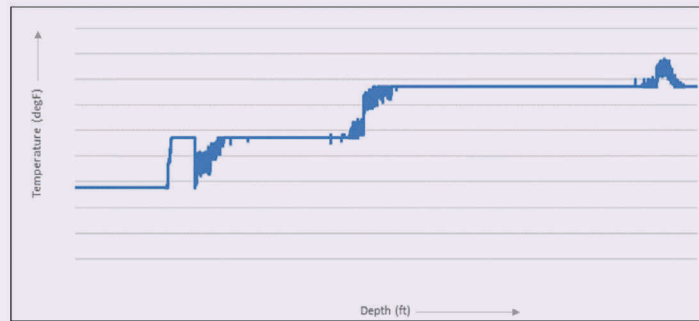
Fig. 9 *The drag chart for the MSF assembly in Well-A as it was RIH.*
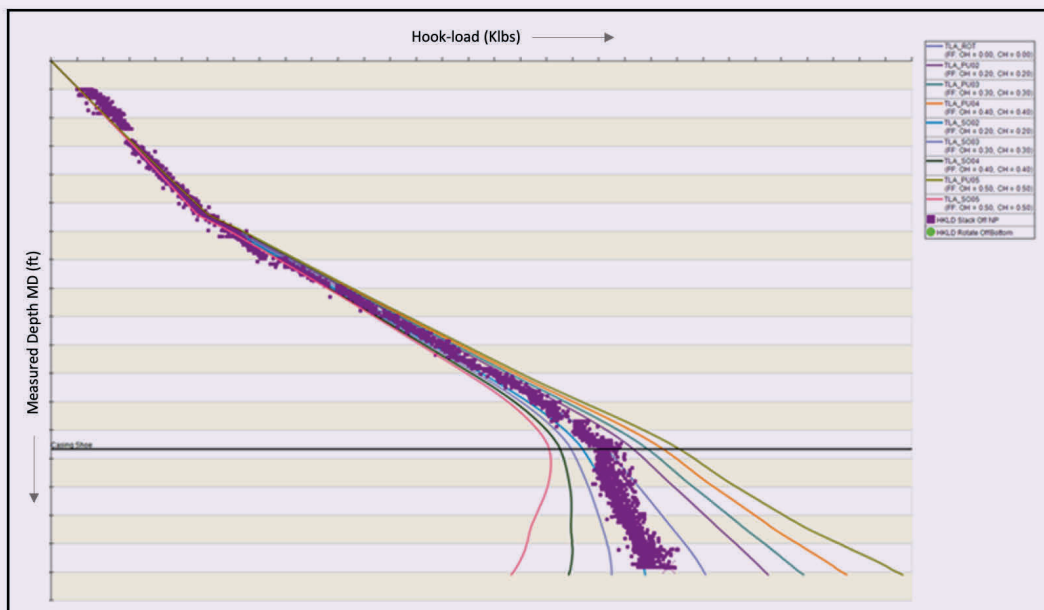
logs, which were subsequently run in these laterals, recorded downhole static temperature ranging from 316 °F to 320 °F, Fig. 8, further confirming the high reservoir temperatures recorded by the LWD. These temperatures were also detrimental to the elastomer packers and would have jeopardized their integrity if deployed in these wells.

Well-A: In Well-A, a 4,400 ft, 5⅞" horizontal lateral section was drilled in the minimum stress direction across the reservoir. As mentioned earlier, the shallower section of the lateral was significantly enlarged due to hole instability issues across the cap rock. Also, several tight spots were encountered while tripping out of hole and a stuck pipe incident occurred, which resulted in the severing and abandoning of the drilling bottom-hole assembly (BHA) in the lower section of the lateral.

After abandoning the BHA, a clean out trip was performed in the remaining open hole with a packed BHA to simulate the 4½" MSF completion run. This run also encountered multiple tight spots, which confirmed the lateral's harsh wellbore condition. It also confirmed that the MSF assembly could not be run to its setting depth without significant working and rotation. Caliper logs also showed several overgauged IDs of up to 6½" along the lateral wellbore.

These conditions were well beyond the capacities of both the mechanical elastomer packers and the swellable packers. Furthermore, the inherent stiffness and lesser pre-setting OD of the expandable packer meant they had a lesser risk of buckling while being deployed. In the end, the choice was made to use the expandable steel packers in the MSF assembly. A four-stage MSF assembly with seven expendable steel packers was deployed and successfully set at the

Fig. 10 *Well-B inclination, azimuth, DLS, and tortuosity charts for the 5⅞" motherbore (L-0) and sidetrack lateral (L-1).*

desired setting depth.

Figure 9 shows the drag chart for the MSF assembly as it was RIH. The expandable packer MSF assembly ran smoothly across the lateral to its setting depth with an average frictional factor of 0.2.

Well-B: In Well-B, a 4,600 ft, 5⅞" horizontal lateral section was drilled, also in the minimum stress direction across the reservoir. To keep the lateral within the developed sections of the reservoir, a lot of geo-steering had to be done while drilling the wellbore. Unfortunately, this resulted in multiple micro-doglegs in the lateral, Fig. 10.

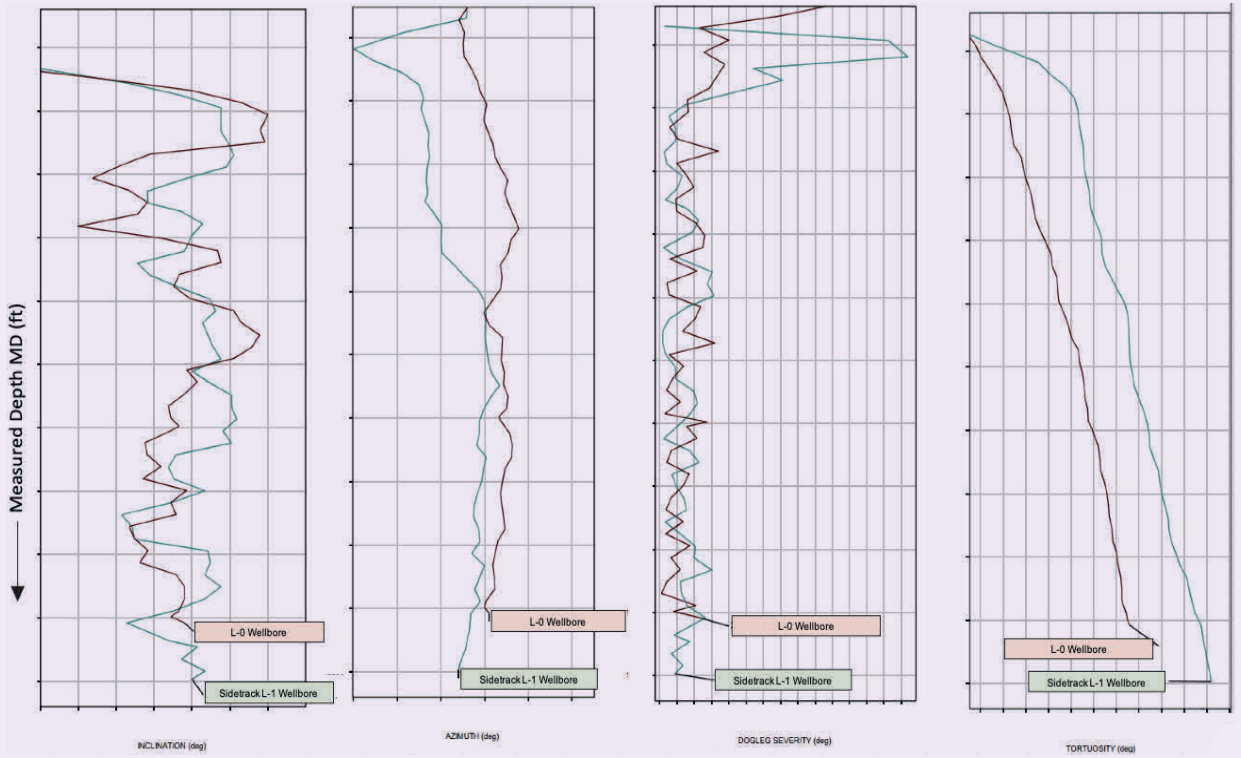An MSF completion string with swellable packers was deployed in the lateral and became mechanically stuck while RIH. This led to the severing and abandoning of the stuck MSF assembly as well as a sidetrack to re-drill the entire 5⅞" lateral section. The resulting high dogleg at the sidetrack initiation point extended for 200 ft with a maximum value of 7°/100 ft. Also, the inclination and azimuthal variations in the sidetrack lateral, L-1, and ultimately its overall tortuosity, was considerably higher when compared with the motherbore, lateral L-0. This was due to the difficulty of staying within the "sweet spots" of the reservoir while avoiding collision with the motherbore lateral containing the abandoned MSF assembly.

With such DLS, which exceeded the maximum DLS limits of the mechanical and swellable packers' capacities, the only option was to deploy the expandable

Fig. 11 *The actual trajectory of Well-C.*
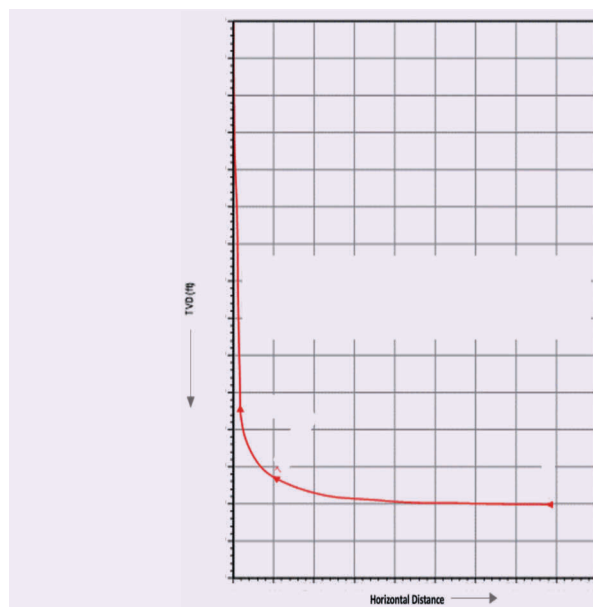
packers in the MSF. Therefore, in Well-B, the MSF assembly with expendable steel packers was deployed and successfully set at the desired setting depth in the more tortuous lateral than the one in which the

Fig. 12 *The caliper log of Well-D showing the washouts' ID ranged from 6.3" to 13.3" along the lateral.*
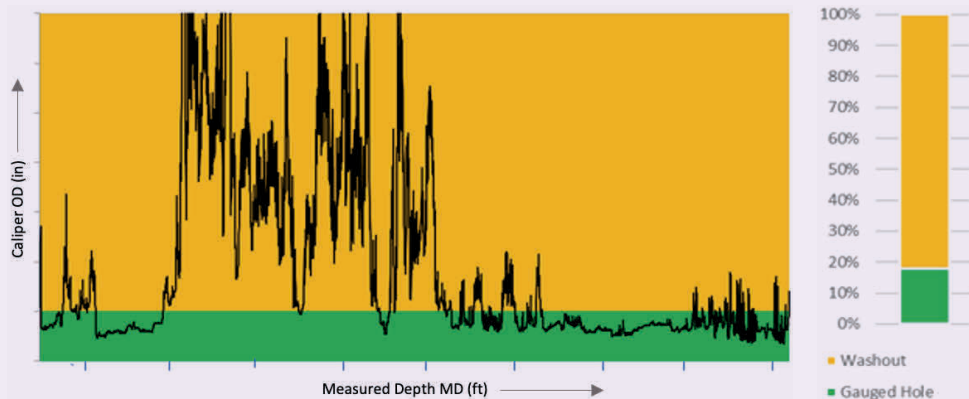
swellable packers became stuck.

Well-C: Well-C was drilled to a TD of 19,460 ft measured depth (MD) with a lateral length of over 7,000 ft. Despite having a gauge wellbore throughout most of the lateral sand, minimum geosteering was done while drilling the lateral, Fig. 11, and there was still a concern about the amount of drag that would be generated, since the long lateral would require more packers in its proposed MSF completion.

The 7,000 ft lateral required seven stages in its MSF completion, which in turn required 16 mechanical packers, with two packers between each stage. This challenge was managed with the expandable packers in two ways. First, due to their superior sealing capacity over the mechanical packers, fewer expandable packers were required for zonal isolation between stages. In the end, only eight packers were required in the MSF completion, with only one between each stage. Second, due to the smaller pre-setting OD of the expandable packers, the frictional factor was further reduced.

Therefore, in this well, the second MSF completion with eight expandable steel packers was successfully deployed and set at the well's TD of 19,460 ft MD without any issues.

Well-D: In Well-D, a 4,800 ft horizontal lateral was drilled across the reservoir. Although, due to the heterogeneity of the reservoir formation, there was a variation in formation competency and this resulted in washouts in over 80% of the lateral wellbore. The washouts' ID ranged from 6.3" to 13.3" along the lateral, Fig. 12.

Of the three packer types, only the expandable packers had the tolerance for such large hole diameters, as per sealing capacity (up to 6.6 ft, Table 1). They were therefore selected for the MSF completion and deployed successfully. Also, the subsequent fracturing operations were done successfully and there was total zonal isolation between each stage.

Well-E: Well-E was drilled to a TD of 17,150 ft with a 3,240 ft lateral across the reservoir. There was also substantial geosteering across the lateral, which led to a high tortuosity in the lateral, Fig. 13. As expected, several obstructions were encountered while running the MSF completion assembly through the lateral. For a mechanical packer or swellable packer MSF assembly, the only option when encountering obstructions would be to retrieve the MSF assembly from the hole and perform a reaming trip to condition the wellbore and clear the obstructions.

Consequently, since it was the expandable packers that were deployed, when the obstructions were encountered, the MSF completion could be rotated with additional slack off to pass through. In this particular well, the obstruction was encountered about 1,200 ft above the required setting depth, and the packer was rotated and worked past all the obstructions all the

Fig. 13 *The inclination chart of Well-E showing tortuosity where obstructions were encountered.*
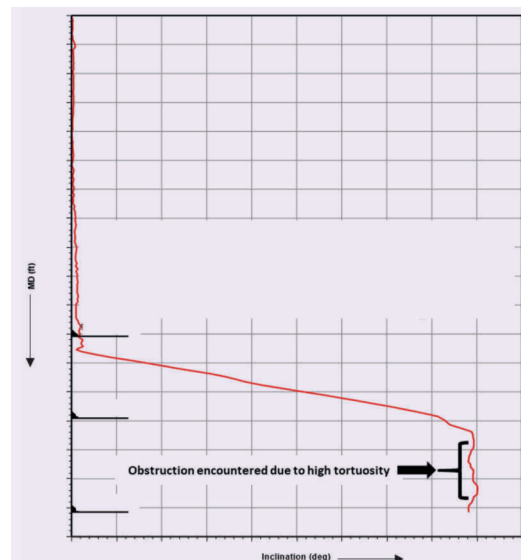
Fig. 14 *The torque and drag charts of Well-E showing a hook load (a), and surface torque (b) while running the MSF completion in an open hole with rotation to pass obstructions.*

(a)

(b)
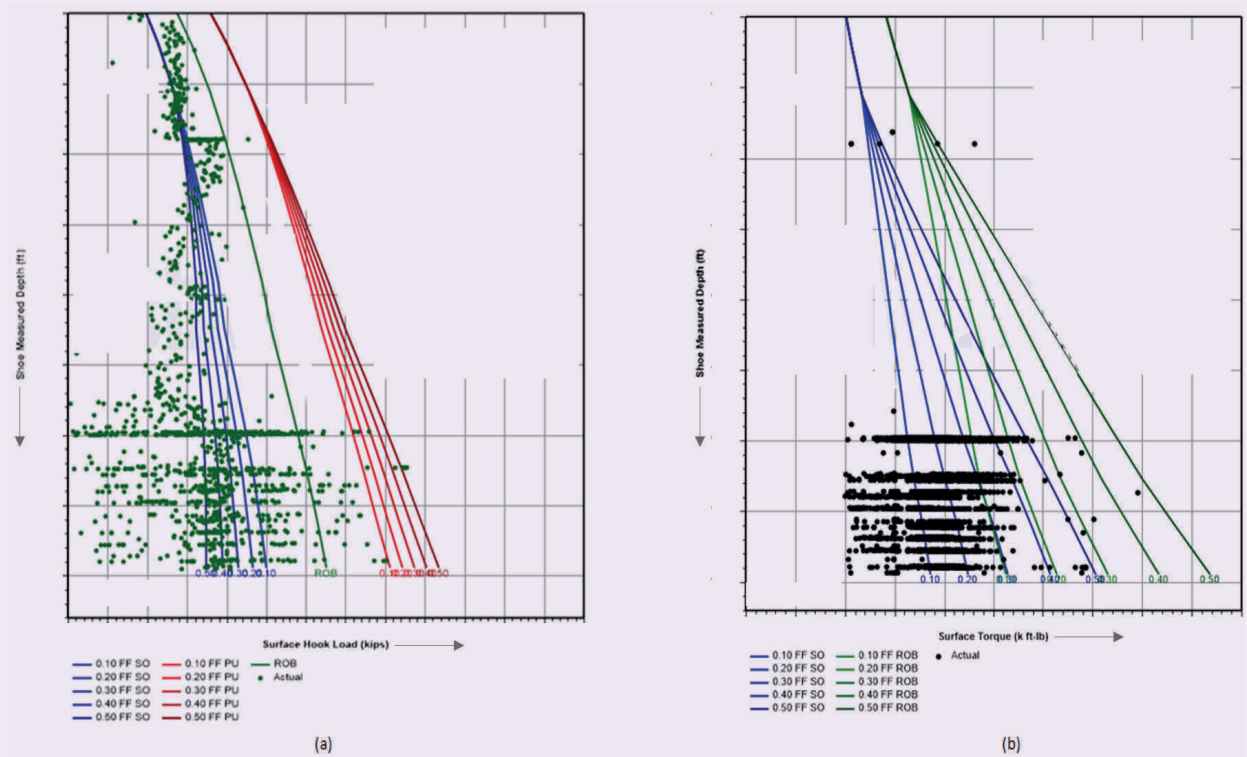
way down to the setting depth without damaging any of the packers in the MSF completion.

Figure 14a shows the torque and drag charts of Well-E showing a hook load, and Fig. 14b shows surface torque while running the MSF completion in an open hole with rotation to pass obstructions. The assembly was subjected to torque and drag forces, which were above the maximum expected values from torque and drag simulations, considering a maximum frictional factor of 0.5.

Note the fact that even with these harsh deployment conditions, the expandable packers were not damaged and were expanded successfully. The subsequent fracturing operations were also successful and there was total zonal isolation between each stage, further confirming the packers' integrity.

Conclusions

The use of the expandable packers has greatly enhanced the MSF completion deployment operations in the field of interest. Considering the complex and challenging wellbore conditions encountered in the wells discussed in this article, such as but not limited to excessive hole enlargement, high wellbore dogleg and tortuosity, and high wellbore temperature, the expandable steel packers have proven to be clearly more advantageous than both the mechanical packers and the swellable packers, mainly due to their robustness and resistance to damage.

References

1. Purusharthy, N.K., Nugraha, I., Hassan, Z. and Wood, K.: "Unique Open Hole Metal Expandable Annular Sealing Systems in High-Pressure Multistage Fracturing Completion," SPE paper 203354, presented at the Abu Dhabi International Petroleum Exhibition and Conference, Abu Dhabi, UAE, November 9-12, 2020.

2. Seale R.: "Open Hole Completion System Enables Multistage Fracturing and Stimulation along Horizontal Wellbores," *Drilling Contractor*, July-August 2007, pp. 112-114.

3. DeBruijn, G., Skeates, C., Greenaway, R., Harrison, D., et al.: "High-Pressure, High Temperature Technologies," *Oilfield Review Journal,* Vol. 20, Issue 3, Autumn 2008, pp. 46-60.

4. Arias, R.E., Guizada, P., Gaby, M. and Riou, Y.: "First Worldwide Application of Metal Expandable Fracture Packers to Enhance Integrity and Reduce Deployment Issues while Utilizing Open Hole MSAF Completions," SPE paper 201647, presented at the SPE Annual Technical Conference and Exhibition, Virtual, October 5-7, 2020.

About the Authors

Ebikebena M. Ombe

M.S. in Offshore and Ocean Technology (Subsea Engineering Option), Cranfield University

Ebikebena M. Ombe is a Drilling Engineer with 16 years of oil and gas drilling industry experience. He works with Saudi Aramco's Gas Drilling Engineering Department, where he is responsible for the design, drilling and completion of gas development wells for Saudi Aramco.

Before joining Saudi Aramco in 2014, Ebikebena worked as a Well Engineer for Shell. While at Shell, he worked with both the front end well design group and the well delivery department, and was involved with the design

and construction phases of numerous oil and gas drilling and workover projects. Ebikebena also worked as the regional wells directional survey focal point for Shell's Sub-Saharan Africa drilling operations.

He received his B.S. degree in Metallurgical and Materials Engineering from the Obafemi Awolowo University, Ile-Ife, Nigeria, and his M.S. degree in Offshore and Ocean Technology (Subsea Engineering Option) from Cranfield University, Bedford, U.K.

Ernesto S. Gomez

B.S. in Petroleum Engineering, University Central de Venezuela

Ernesto S. Gomez is a Drilling Engineer working in Saudi Aramco's Gas Drilling Engineering Department. He has extensive drilling experience in both onshore and offshore deep gas drilling. Ernesto's experience includes extended reach directional drilling in heavy oil wells, cost control and budget analysis, oil and gas well design, generating of best drilling practices guides, on-site rig supervision, end-of-well reports and drilling operations logistics.

He has been in the oil and gas industry for over 22 years. Before joining Saudi Aramco in 2008, Ernesto gained his experience working in onshore extended directional drilling campaigns in southeast Venezuela, where he worked as an on-site Drilling Supervisor for delineation and stratigraphic wells.

Ernesto received his B.S. degree in Petroleum Engineering from the University Central de Venezuela, Caracas, Venezuela.

Aldia Syamsudhuha

B.S. in Petroleum Engineering, Bandung Institute of Technology

Aldia Syamsudhuha is a Well Engineer with the Schlumberger Integrated Well Construction team in the Middle East, where he supports the Onshore Gas Drilling project in Saudi Aramco. Aldia has 7 years of professional experience in the oil and gas drilling industry. He has gained significant drilling engineering experience from his work across various drilling projects from around the world, including oil, gas, and geothermal drilling engineering and operations support.

Aldia is also involved with the design and construction of vertical, deviated, and horizontal wells and high-pressure, high temperature wells as well as workover and completion planning and design, field supervision for drilling and completion operations, and integrated project management.

He received his B.S. degree in Petroleum Engineering from the Bandung Institute of Technology, Bandung, Indonesia.

Abdullah M. Alkwiter

B.S. in Engineering, Surrey University

Abdullah M. Alkwiter is a Completions Engineer with eight years of experience. He started his career with Schlumberger in 2013 as a Field Engineer for Sand Management Tools/Open Hole completions, then crossed over to liner hangers, upper completions, and smart completions. Following his field experience and due to his notable achievements, Abdullah was promoted to a line management position, where he supervised the sand management field population ensuring excellent product and service delivery.

Abdullah has also worked as a Technical Completions Engineer. Currently, he is working as a Completion Account Lead with the Schlumberger Completions Group, where he provides completion technical solutions, design evaluations, completion account management support, and client relations support.

Abdullah also coaches and mentors trainee engineers, both within and outside of Schlumberger.

He received his B.S. degree in Engineering from the University of Surrey, Guildford, U.K.

Offshore Implementation of Temperature Microchip under Critical Well Conditions

Dr. Bodong Li, Dr. Vahid Dokhani, Dr. Chinthaka P. Gooneratne, Dr. Guodong Zhan, Timothy E. Moellendick and Zhaorui Shi

Abstract /

Drilling microchips are millimeter size sensing devices, capable of measuring in situ downhole temperatures, and at the same time, withstanding harsh downhole conditions. In this work, 140 microchips were dropped from the drillpipe during the connections. The devices travel through the bottom-hole assembly (BHA), drill bit, annulus, and are eventually recovered at the shale shaker. A total of 80 microchips were recovered at the shaker, which resulted in a physical recovery rate of 57%.

The microchip recorded the dynamic temperature profile of the entire wellbore, including a long open hole section, only a few hours before the well turned into a total loss. The data downloaded from the microchip shows an excellent consistency throughout the three tests. The measured dynamic bottom-hole temperature provides a correction of 10 °F to the best practice of the industry in terms of downhole thermal simulation, offering valuable measured input for the optimization of thermal activated lost circulation materials (LCMs) or cementing job.

To the best of our knowledge, it is the industry's first successful attempt in logging an open hole section in a high loss zone using drilling microchip-like technologies. The microchip recorded the dynamic temperature profile of a long open hole only a few hours before the well turned into a total loss. Due to the lack of industrial solutions for downhole temperature measurement under such conditions, the microchip technology showed unique advantage for critical applications, especially in operations with highly valued assets.

Introduction

Severe loss circulation is one of the major challenges in well control. When drilling through severe loss zones, conventional tools such as measurement while drilling (MWD) and/or logging while drilling (LWD) are not recommended, due to frequent pumping of lost circulation materials (LCMs), leaving drilling with limited access to direct downhole measurement for critical decision making and optimization. Drilling microchip technology was developed as an alternative logging solution to provide valuable downhole measurements at comparably low-cost while introducing minimum intervention to drilling operations. It is therefore considered as an ideal solution for wells with critical drilling conditions such as lost circulation.

Drilling microchips are small-sized sensor devices, consisting of an on-chip battery, microprocessor, memory, sensors, and a communication module all encapsulated in a spherical shell with a diameter of ¼" to ½"[1]. The microchips are manufactured with materials of high temperature strengths to survive the extreme temperature and pressures encountered when traveling through the entire wellbore.

During the drilling operations, microchips are dropped from the top of the drillpipe, and carried by the mudflow downwards inside the drillpipe. After reaching the bottom-hole assembly (BHA), the mud pushes the microchips through the bit nozzles and carries them back to the surface. Throughout the entire deployment process, the logging measurements are conducted sequentially with a time interval and the data is saved in the memory of the microchip, which can later be downloaded.

The depth information of each measurement point is calibrated by the time stamp of the recorded data and the well conditions such as the mud fluid rate. In this way, a drilling microchip is able to log the temperature distribution of the entire wellbore with minimum intervention to drilling operations. Since 2012, research and development has been focused on improving the performance and reliability of microchips. Recently, microchips with a bullet shape were introduced to provide different mechanical strength and density[2].

Shi et al. (2015)[3] presented the results of deploying drilling microchips in a well with a 13,800 ft vertical depth and a static bottom-hole temperature of 305 °F (152 °C). The measured temperature data for two microchips shows very good consistency, however, due to battery power issue, the measured data in the annulus is incomplete by a few minutes. The authors converted microchip data from time-scale to depth-scale considering a time marching method, which calculates the distance that the microchip traveled using the net velocity of the microchip, i.e., relative slip velocity of microchips with respect to average drilling fluid velocity. The authors employed a semi-analytical model[4] to predict the temperature profile during microchip travel. Comparing

the model prediction and microchip data indicates a good agreement in the drillpipe but a significant discrepancy in the annular space.

Li et al. (2017)[5] reported the first complete temperature logging of an onshore well using a second generation drilling microchip with optimized battery performance and reliability. The depth information for each microchip can be estimated from the time stamp of the recorded data and flow rate. Although consistent data measurements for the entire wellbore were achieved by the microchips, a significant difference between the calculated and measured traveltime in the annulus is realized. The authors attributed the extra time to the presence of drill cuttings, which can adversely affect the upward movement of the microchips.

Dokhani et al. (2016)[6] developed a transient heat wellbore simulator to calculate the wellbore pressure and temperature during drilling mud circulation and shut-in conditions for a generalized well profile, i.e., an inclined offshore well. The simulator considers various operating parameters such as mud loss and the pump rate schedule. Li et al. (2020)[7] followed the method of Dokhani et al. (2016)[6] for the prediction of the temperature profile during wellbore circulation. Multiple sets of field data measured by drilling microchips are used to validate the model. Temperature distribution vs. depth was obtained from the time series data, achieving a same format of well logging with mainstream logging techniques.

In this work, a systematic approach was carried out to demonstrate the value of a drilling microchip for temperature logging in an offshore well with critical downhole conditions. Due to the limited means of logging techniques in such wells, the measured data from the drilling microchip is considered as valuable information for risk mitigation. This article includes a theoretical basis on depth conversion for microchip data processing, an overview of an offshore field test, analysis on raw data from the field test, and a comparison of a converted microchip temperature log with a commercial drilling fluids simulator.

Theoretical Basis on the Depth Conversion from Time Series Data

The temperature measurement from the drilling microchips need to be processed since the measurements are recorded based on a time-scale. The data should be converted into temperature vs. depth to obtain a temperature profile in the wellbore and compare the results with model predictions or other logging techniques. A drilling microchip can be treated as a spherical particle, which is conveyed through drilling fluid along the well path, Fig. 1.

If the density of the microchip is higher than the drilling fluid, the microchip's travel velocity in the drillpipe is higher than the fluid velocity due to slip velocity (settling). In contrast, the microchips advance toward the surface in annular space at a rate, which is lower than the fluid velocity due to slip velocity. The slip velocity of a microchip can be calculated in

the same manner as drill cuttings using the physical properties of a microchip and rheological properties of drilling fluid. There are several methods in the literature proposed for calculation of slip velocity[8-10]. It can be initially postulated that:

$$v_{\text{tracer}} = \bar{v}_f \pm v_{\text{slip}}$$

<div align="right">1</div>

where $\bar{v}_f$ and v_{slip} represent the average fluid velocity and microchip slip velocity, respectively. The positive sign is used for flowing within the drillpipe and the negative sign is used for traveling in the annular space. The average fluid velocity in each interval can then be obtained knowing the pump rate and wellbore configurations.

From previous analysis[5-7], it was found that assuming an average fluid velocity for microchips may not be a correct assumption. In fact, it can be postulated that the microchips most likely travel near the center of the flow conduit. Therefore, the maximum fluid velocity shall be a better choice for microchip tracking. According to Chhabra and Richardson (1999)[11], the maximum fluid velocity can be expressed in terms of average fluid velocity for laminar flow of power-law fluids in a pipe as:

$$\frac{v_{\text{max}}}{\bar{v}_p} = \left(\frac{3n+1}{n+1}\right)$$

<div align="right">2</div>

where $\bar{v}_p$ is the average fluid velocity in a pipe and n is the flow behavior index. The laminar flow of the power-law fluid in an annular space can be approximated treating the annulus as a narrow slot. Subsequently, we can obtain the flowing expression for the maximum fluid velocity in terms of average fluid velocity for power-law fluids in an annulus:

$$\frac{v_{\text{max}}}{\bar{v}_f} = \left(\frac{2n+1}{n+1}\right)$$

<div align="right">3</div>

Nevertheless, such formulations for turbulent flow conditions may not be achieved. For Newtonian fluids,

Fig. 1 *An analysis of a drilling microchip's velocity in the drilling system.*
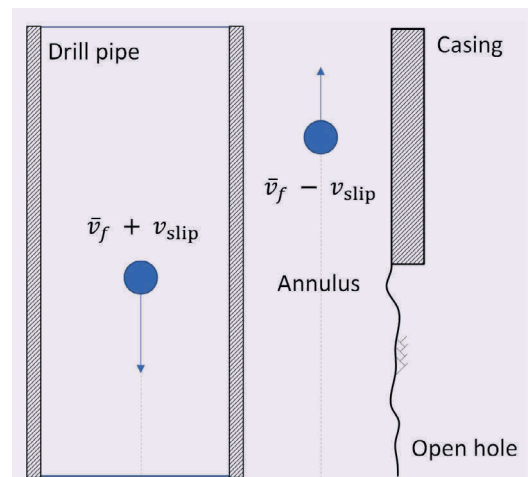
Bird et al. (2002)[12] suggested that a rough approximation for a given range of Reynolds number is:

$$\frac{v_{\max}}{\bar{v}_f} = \left(\frac{2n+1}{n+1}\right)$$

For a laminar flow in a pipe, the velocity profile is considered parabolic. Although, for a turbulent flow the velocity profile is logarithmic, meaning that far away from a wall, the velocity profile is independent of wall friction and becomes relatively flat. The experimental results of Nouri et al. (1994)[13] indicate that for non-Newtonian fluids, the ratio of maximum velocity to average fluid velocity in the annulus can range from 1.2 to 1.4 for a Reynolds number less than 10^4. Therefore, a multiplier of 1.25 was assumed to convert the average fluid velocity to maximum fluid velocity under turbulent conditions for both pipe and annular flow.

Subsequently, the multipliers presented for laminar flow, Eqns. 2 and 3, shall be regarded as an initial wise guess. The presence of a parabolic velocity profile under laminar flow condition indicates that any deviation from the center of the flow conduit has an impact on the magnitude of axial local fluid velocity in which the tracer travels with. In addition, with increasing drillstring eccentricity, the local maximum velocity in the wide and narrow sections of the annulus can be significantly different[14].

As a result, the multiplier of the laminar flow condition is considered as a variable to account for all uncertainties often found during the upward flow of tracers in the annulus, e.g., hindering effects of cuttings, deviation of tracer from conduit center, tracer slippage, drillstring eccentricity, etc. In fact, this modification is applied to any interval that is under laminar flow conditions. As a result, an iterative algorithm is designed to calibrate the predicted arrival time of the tracer with the actual arrival time. The algorithm employs the secant method, which is initialized with the wise guesses previously noted.
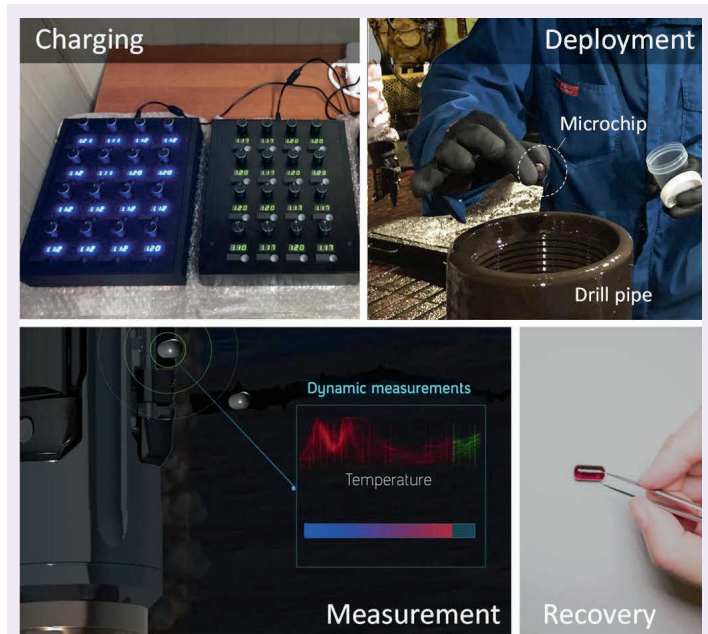
Field Test

Operational Workflow

The deployment of the drilling microchip consists of four main steps, Fig. 2. First, the microchips to be used are charged in a charging dock at the rig site. Due to the small size and limited battery capacity of the microchip, the device needs to be charged right before the deployment to maximize its endurance under high-pressure, high temperature downhole conditions.

When the microchips are fully charged, they are initiated and ready to be deployed. At this time, the microchips are in recording mode and are kept in the charging dock for power conservation. After the initialization, when the drilling BHA reaches the deployment depth, the crew collects the microchips from the charging dock and bring them to the rig floor. At the rig floor, the drillpipe is disconnected at a connection joint. This is the time when the microchips are dropped into the drilling fluid from the open end of the drillpipe. Due to the microchips being buoyant neutral compared to the drilling fluid, extra attention

has to be made to ensure no microchips escape from the drillpipe with the outflow of the drilling fluid during the pipe makeup.

The microchips are dropped in batches each time, as it is known that a percentage of the microchips will be lost or damaged throughout the run. A few barrels of high viscosity pill are pumped behind each batch to ensure a good sweep in the drillpipe and annulus to improve the recovery rate of the microchips. After deployment, the microchips carried by the drilling fluid start to take measurements at different positions of the drilling system from the inner drillpipe, BHA, drill bit, to open hole, cased open, and flow line, etc., until they are eventually recovered at the shale shaker.

During the third step, when the microchips are taking downhole measurements, it is important to closely monitor the drilling parameters such as bit depth, revolutions per minute, pump flow rate, etc., to gain perspectives on how and when the microchips pass through each downhole section to facilitate the last step — recovery.

For recovery, the microchips are collected from the shale shaker at the estimated time, cleaned, and connected to a computer for data download. The entire process from deployment to generating a logging report only takes 3 to 4 hours at the rig site; significant less effort and time-consuming when compared with conventional LWD or wireline logging techniques.

Field Test Procedure

The test well is an offshore well drilled to a total depth of 11,011 ft. Before the deployment, the well experienced a total loss; the crew managed to successfully cure the

losses, then conducted a pressure test and circulated near the casing shoe to condition the well. As introduced earlier, due to the high risk of having losses, the well was drilled by a rotary BHA to minimize downhole components with a restricted flow path such as MWD for de-risking the operations.

A drill bit with 22/32" nozzles were used for the easy pumping of the LCM. A PBL sub (a downhole device for opening/closing a port for delivering large particles) is also included in the BHA for the same reason of LCM deployment. Two full-gauge roller reamers without junk slots were installed near the bit. Three rounds of microchip field tests were conducted in this well at different stages of operations and under different well conditions. Table 1 is a summary of the well information for the three tests.

Test 1

During test 1, the bit was at 9,375 ft above the casing shoe. Drilling microchips of three different sizes were deployed: 9 mm, 10 mm, and 12 mm. There were 38 temperature microchips deployed in four batches while the PBL sub was in a closed state. Five were recovered at the estimated time, and 21 more temperature microchips were recovered with significant time delays after the PBL sub was opened.

Test 2

During test 2, the bit was at 9,375 ft above the casing shoe. Drilling microchips of three different sizes were deployed: 9 mm, 10 mm, and 12 mm. All 42 temperature microchips were deployed in one batch with the PBL in an open state. Then, 30 microchips were recovered with the majority arriving at the estimated time. Only a small number of microchips were recovered at a delayed time, possibly due to the restrictions at the PBL sub.

Test 3

After the first two tests at the casing shoe, the operator washed down to the bottom-hole at 11,011 ft when the third test was conducted. Drilling microchips of three different sizes were deployed: 9 mm, 10 mm, and 12 mm. A total of 60 temperature microchips were deployed in two batches while drilling with the PBL in a closed state. Then, 24 microchips were recovered at the estimated time. Five hours after the recovery of the last microchip, the well went into total lost circulation condition.

Results and Analysis

Recorded Data from the Drilling Microchip

Figures 3a, 3b, and 3c are the recorded temperature data from the drilling microchips deployed in tests 1, 2, and 3. The measured temperature profiles follow the similar trends reported previously[2, 5]. Different stages and corresponding positions of the drilling microchips throughout the tests can be identified easily.

Figure 3c shows the microchips experience a sudden increase of temperature as they are dropped into the drilling fluid, which has a surface temperature higher than the environmental temperature. As the microchip travels down along the drillpipe, the temperature continues to raise as a result of drilling fluid following the geothermal gradient, toward thermal equilibrium. After reaching a peak value, the temperature starts to decrease as the microchip travels upwards inside the annulus.

From the time domain data, it can be observed that the temperature curve has a much gradual decline than the raising part due to the difference of the fluid flow speed as a result of a larger cross-sectional area of the annulus than that of the drillpipe. Sudden drops of the temperature down to the environmental temperature are the indication that the microchips separated from the drilling fluid at the shale shaker.

Highly consistent measurements were obtained for the microchips that have gone through similar travel paths. Diverting trends from the same tests often

Table 1 *A summary of the well conditions for the three drilling microchip field tests.*

Parameter	Test 1	Test 2	Test 3
Total well depth	11,011 ft	11,011 ft	11,011 ft
Bit depth	9,375 ft	9,375 ft	11,011 ft
Drillpipe ID/OD	4.67"/5½"	4.67"/5½"	4.67"/5½"
Last casing size and depth	13⅜" at 9,739 ft	13⅜" at 9,739 ft	13⅜" at 9,739 ft
Open hole diameter	12¼"	12¼"	12¼"
Geothermal gradient	0.017 °F/ft	0.017 °F/ft	0.017 °F/ft
Mud weight	127 pcf	127 pcf	127 pcf
Viscosity (PV/YP)	39/29	39/29	39/29
Mud type	WBM	WBM	WBM
Pump rate	350 gpm	400 gpm	500 gpm

indicate incidents during the test. In Fig. 3a, the result clearly shows that two microchips are recovered first, while the rest of the microchips spend an extra 50 to 110 minutes in the well, due to the obstruction from the PBL sub.

In Fig. 3b, two "lost" microchips are found hours after the majority of the batch, which could be caused by being stuck somewhere inside the circulation system. In general, when diverting trends are found in one test, the shorter curves with good consistency are considered as data with better accuracy.

From the result, it was also found that test 3 has a lower physical and data recovery rate compared with the first two tests. It is believed that a greater bit

Fig. 3 *The recorded temperature data from the drilling microchips deployed in test 1 (a), test 2 (b), and test 3 (c).*
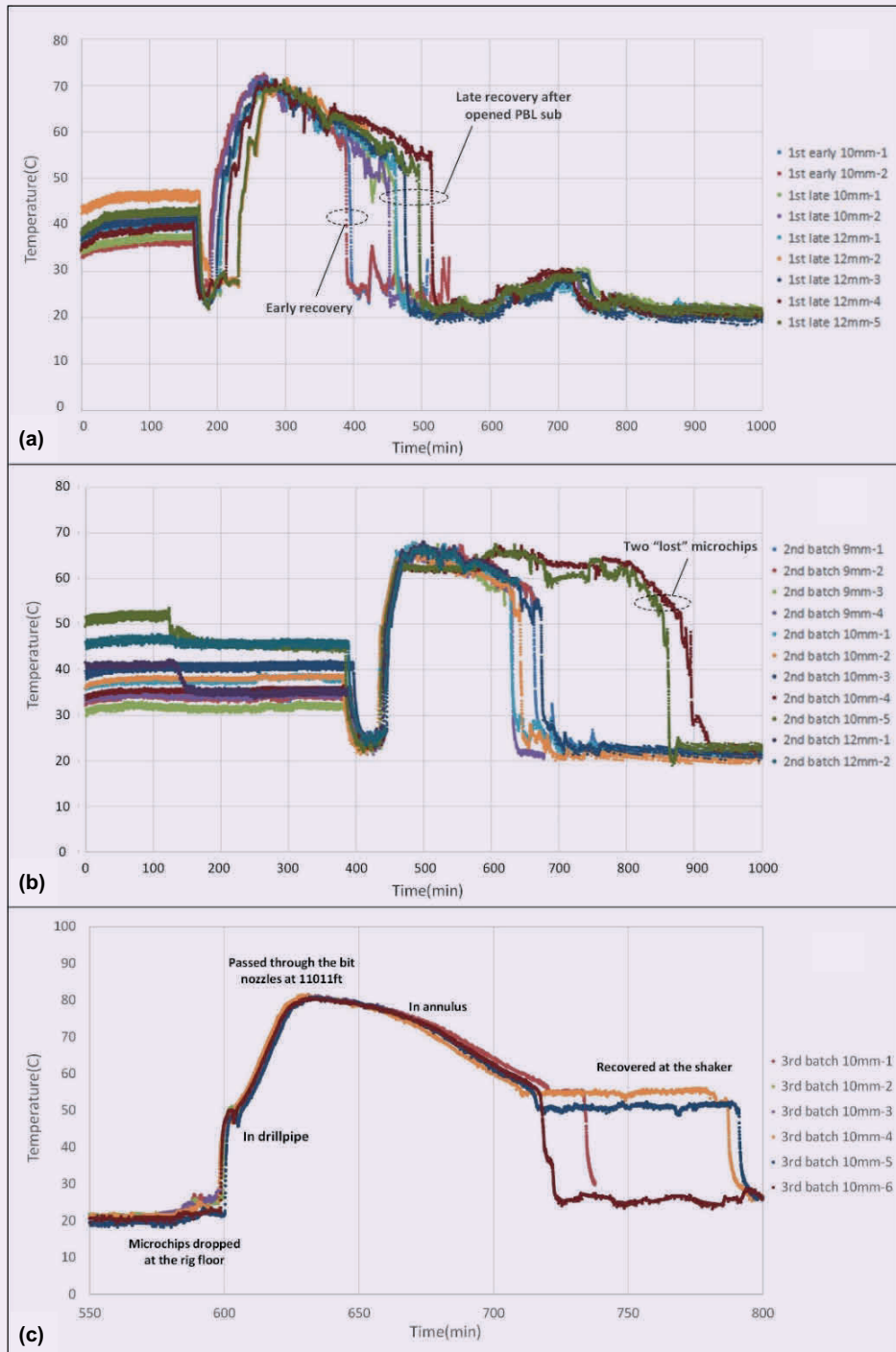
depth, along with the drilling condition and closed PBL sub, are the factors behind a lower recovery rate as they introduce additional downhole complexity to the system. Theoretically, for the drilling microchips to deliver reliable results, a minimum of two sets of highly consistent data are needed. By this standard, the result from test 3 is considered a good result.

Temperature vs. Depth Log

To receive a temperature vs. depth log, the pump rate schedule is plotted along the recorded temperature curves for test 3, Fig. 4a. Two sets of temperature data with minimum discrepancies are used for the analysis.

By implementing the microchip tracking model introduced earlier, a temperature vs. depth log is obtained, Fig. 4b. The temperature log contains two parts, with the left part being the temperature distribution inside the drillpipe and right part being the log in the annulus. The maximum dynamic temperature is observed in the annulus at the 9,500 ft depth. This is a unique and clear way of demonstrating downhole dynamic temperature

Fig. 5 *The measured temperature profile from the drilling microchips in comparison with a simulation from a commercial drilling fluid simulator.*

Fig. 4 *(a) The measured temperature data of the drilling microchips from test 3 along with pump rate vs. time; (b) The temperature vs. depth profiles converted from the drilling microchip measurement from test 3.*
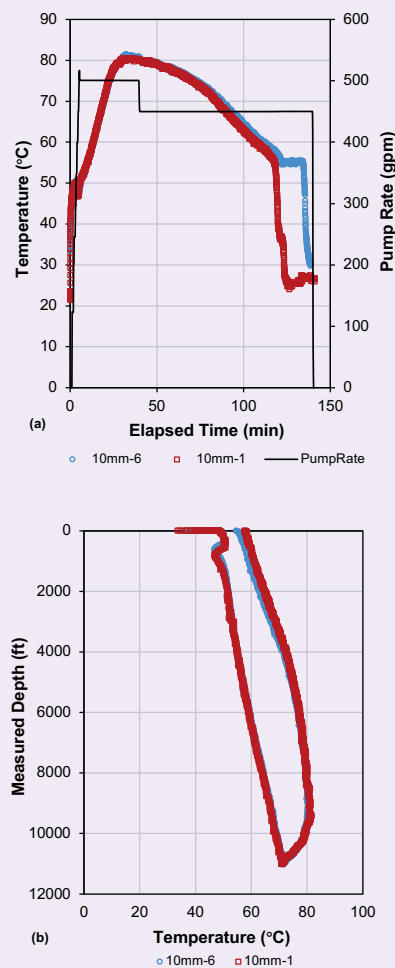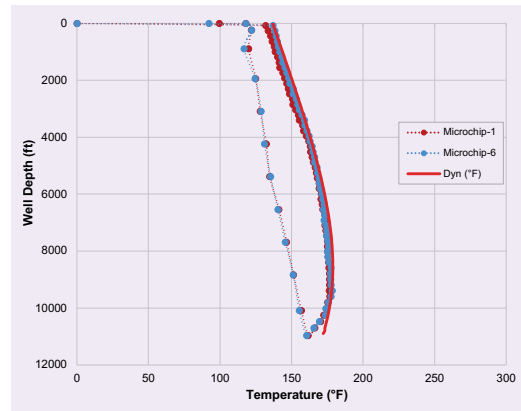

distribution inside and outside of the drillpipe.

To further verify the measured downhole temperature distribution, the temperature vs. depth log from the microchip is plotted alongside the result from a commercial drilling fluid simulation software, Fig. 5. When comparing with the simulated dynamic temperature distribution, the measured microchip temperature log is in very good accordance with the simulation throughout the majority of the well until reaching 10,000 ft. From 10,000 ft, the discrepancy starts to develop down to the bottom-hole with a maximum deviation of 10 °F at 10,011 ft. The discrepancy of the simulated temperature near the bottom of the well against the measured result could come from the change of the boundary conditions introduced by the BHA and drilling activities.

Conclusions

This article provides a systematic approach on the implementation of drilling microchips for temperature logging in an offshore well. Details of the three field tests using 140 temperature microchips in a critical offshore well were presented to demonstrate the operational workflow of this unique downhole technology in a real world environment. In addition to giving insights on the process for data gathering, the method for data interpretation is also provided to convert the time series data into depth data. The converted temperature vs. depth log is compared with a commercial drilling fluid simulator for the validation of the technology.

To our best knowledge, it is the industry's first successful attempt in logging an open hole section in a high loss zone using alike drilling microchip technologies. The microchip recorded the dynamic temperature profile of a long open hole only a few hours before the well turned into a total loss. Due to the lack of industrial solutions for downhole temperature measurement under such conditions, the microchip technology showed a unique advantage for critical applications, especially in operations with highly valued assets.

Compared with simulated temperature distributions under various assumptions, the drilling microchip offers a direct and promising measurement to complement the existing industrial practices for cement and LCM design and optimization.

Acknowledgments

References

1. Yu, M., He, S., Chen, Y., Takach, N., et al.: "A Distributed Microchip System for Subsurface Measurement," SPE paper 159583, presented at the SPE Annual Technical Conference and Exhibition, San Antonio, Texas, October 8-10, 2012.

2. Li, B., Gooneratne, C.P., Bassam, M.K. and Zhan, G.: "Measurement of Temperature in Deep Reservoir Zones by Mobile Sensor Devices," SPE paper 192909, presented at the Abu Dhabi International Petroleum Exhibition and Conference, Abu Dhabi, UAE, November 12-15, 2018.

3. Shi, Z., Chen, Y., Yu, M., Zhou, S., et al.: "Development and Field Evaluation of a Distributed Microchip Downhole Measurement System," SPE paper 173435, presented at the SPE Digital Energy Conference and Exhibition, The Woodlands, Texas, March 3-5, 2015.

4. Kabir, C.S., Hasan, A.R., Kouba, G.E. and Ameen, M.: "Determining Circulating Fluid Temperature in Drilling, Workover, and Well Control Operations," *SPE Drilling & Completion*, Vol. 11, Issue 2, June 1996, pp. 74-79.

5. Li, B., Gooneratne, C.P., Badran, M.S. and Shi, Z.: "Implementation of a Drilling Microchip for Downhole Data Acquisition," SPE paper 186550, presented at the SPE/IATMI Asia Pacific Oil and Gas Conference and Exhibition, Jakarta, Indonesia, October 17-19, 2017.

6. Dokhani, V., Ma, Y. and Yu, M.: "Determination of Equivalent Circulating Density of Drilling Fluids in Deepwater Drilling, *Journal of Natural Gas Science and Engineering*, Vol. 34, August 2016, pp. 1096-1105.

7. Li, B., Dokhani, V., Zhan, G.D. and Sehsah, O.: "Evaluating Distribution of Circulating Temperature in Wellbores Using Drilling Microchips," SPE paper 203170, presented at the Abu Dhabi International Petroleum Exhibition and Conference, Abu Dhabi, UAE, November 9-12, 2020.

8. Chien, S-F.: "Annular Velocity for Rotary Drilling Operations," *International Journal of Rock Mechanics and Mining Sciences & Geomechanics Abstracts*, Vol. 9, Issue 3, May 1972, pp. 403-416.

9. Bourgoyne Jr., A.T., Millheim, K.K., Chenevert, M.E. and Young Jr., F.S.: *Applied Drilling Engineering*, Richardson, TX: Society of Petroleum Engineers, 1990, 512 p.

10. Chien, S-F.: "Settling Velocity of Irregularly Shaped Particles," *SPE Drilling & Completion*, Vol. 9, Issue 4, December 1994, pp. 281-289.

11. Chhabra, R.P. and Richardson, J.F.: *Non-Newtonian Flow in the Process Industries: Fundamentals and Engineering Applications*, Butterworth-Heinemann: Oxford, U.K., 1999, 436 p.

12. Bird, R.B., Stewart, W.E. and Lightfoot, E.N.: *Transport Phenomena*, 2nd edition, John Wiley & Sons Inc., 2006, 905 p.

13. Nouri, J.M., Umur, H. and Whitelaw, J.H.: "Flow of Newtonian and non-Newtonian Fluids in Concentric and Eccentric Annuli," *Journal of Fluid Mechanics*, Vol. 253, August 1993, pp. 617-641.

14. Dokhani, V., Ma, Y., Li, Z., Geng, T., et al.: "Effects of Drill String Eccentricity on Frictional Pressure Losses in Annuli," *Journal of Petroleum Science and Engineering*, Vol. 187, April 2020.

About the Authors

Dr. Bodong Li

Ph.D. in Electrical Engineering, King Abdullah University of Science and Technology

Dr. Bodong Li joined Saudi Aramco in 2015. He is the Technology Leader on Internet-of-Things and Robotics at Saudi Aramco's Upstream Advanced Research Center. Bodong is also a member of the Drilling Technology Division focusing on research and development of advanced drilling tools.

He has 12 granted U.S. patents, and has authored and coauthored numerous articles published in scientific journals and conference papers covering the areas of sensing and downhole technologies.

Bodong is an active member of the Society of Petroleum Engineers (SPE) and the Institute of Electrical and Electronics Engineers.

He received the Discovery Scholarship and Fellowship from King Abdullah University of Science and Technology (KAUST).

Bodong received his M.S. degree in Mechanical Engineering and his Ph.D. degree in Electrical Engineering, both from KAUST, Thuwal, Saudi Arabia.

Dr. Vahid Dokhani

Ph.D. in Petroleum Engineering, University of Tulsa

Dr. Vahid Dokhani joined YU Technologies Inc., in 2015 and is currently a Chief Technology Specialist for the company in Tulsa, Oklahoma. Previously, he worked for 6 years as a Production Engineer for the National Iranian Oil Company.

Vahid's research interests include wellbore stability, drilling hydraulics, and drilling simulation.

He is the author of more than 20 technical papers and one book chapter. Vahid is a member of the Society of Petroleum Engineers (SPE), and the recipient of the 2014 SPE Nico van Wingen Award. He is also a reviewer for several international petroleum journals.

Vahid received his B.S. degree in Petroleum Engineering from the Petroleum University of Technology, Ahvaz, Iran. He received his M.S. and Ph.D. degrees in Petroleum Engineering from University of Tulsa, Tulsa, OK.

Dr. Chinthaka P. Gooneratne

Ph.D. in Electrical Engineering, Kanazawa University

Dr. Chinthaka P. Gooneratne is the Technical Leader for Sensors and Instrumentation (S&I) and Internet-of-Things (IoT) in the Drilling Technology Division at Saudi Aramco's Exploration and Petroleum Engineering Center – Advanced Research Center (EXPEC ARC). He is the Principal Architect of the multiple award-winning Drilling at the Edge (DATE) program, a major technology initiative at Saudi Aramco, where the people, algorithms, data, machines and processes coexisting on a drilling rig are coordinated at the edge to allow real-time information to accelerate decision making and optimize operations.

Chinthaka has over 10 years of experience in creating, leading, and managing programs designed to commercialize innovative S&I systems and developing emerging markets, such as micro-electromechanical system actuators and IoT edge platforms, that utilize advanced S&I.

He is the author of 50 filed/published/granted U.S. patents, 40 peer-reviewed journal papers, one book, five book chapters, and 45 conference papers.

In 2006, Chinthaka received the Monbukagakusho Scholarship from the Government of Japan.

He is a senior member of the Institute of Electrical and Electronics Engineers (IEEE) (USA), a Fellow of the Institution of Engineering and Technology (IET) (U.K.), and a member of the Society of Petroleum Engineers (SPE). Chinthaka is the recipient of the 2020 Drilling Engineering Award for the Middle East and North Africa region in recognition of work to develop new sensors and IoT platforms for digital transformations of the drilling industry.

He received his Ph.D. degree in Electrical Engineering from Kanazawa University, Kanazawa, Japan, in 2009, where he was the recipient of the President's Award for Outstanding Doctoral Research.

Dr. Guodong "David" Zhan

Ph.D. in Metallurgical Engineering, Huazhong University of Science and Technology

Dr. Guodong "David" Zhan is a Science Specialist and the Team Leader of the Advanced Drilling Tools team in the Drilling Technology Division at Saudi Aramco's Exploration and Petroleum Engineering Center – Advanced Research Center (EXPEC ARC). David is a world-renowned materials scientist and expert in advanced drilling tools/technology. He has over 29 years of experience in industrial R&D and managerial positions, including positions as Chief Engineer and R&D Manager at top oil/gas and semiconductor global companies, such as Schlumberger, NOV, and Applied Materials.

Additionally, David has held academic positions at the University of London and the University of Colorado at Boulder, and staff scientist positions at the Japan National Institute for Materials Science.

He is an active member of the Society of Petroleum Engineers (SPE) where he serves on several conferences such as the SPE International Petroleum Technology Conference and the Asia Pacific Drilling Technology Conference/International Association of Drilling Contractors as co-chair and technical committee member. David is also serving as an editorial board member and reviewer for a number of international scientific journals published by The Minerals, Metals and Materials Society and the Material Research Society.

He has won several prestigious international industry and academic awards, e.g., the World Oil Award and the E&P Hart Energy Award.

David has published 96 peer-reviewed articles in journals such as *Nature Materials* and *Nature Scientific Reports,* 105 conference proceedings, and has more than 120 filed/published/granted U.S. patents, with an H-index of 37.

In 1994, he received his Ph.D. in Metallurgical Engineering from Huazhong University of Science and Technology, Wuhan, China, and completed a postdoctoral fellowship in Nanomaterials and Nanotechnology at the University of California at Davis.

Timothy E. Moellendick

B.S. in Petroleum Engineering, Marietta College

Timothy E. Moellendick is the Chief Technologist for the Drilling Technology Division at Saudi Aramco's Exploration and Petroleum Engineering Center – Advanced Research Center (EXPEC ARC). Timothy is considered the industry expert in casing and liner drilling applications and engineering.

In his previous role as Director of Technology for Schlumberger, he was responsible for growing the technical and operational knowledge base used to develop, plan, and execute this technology worldwide. Timothy has also held drilling operations and engineering positions, including Senior Drilling Engineer, Drilling Manager for North America, Senior Field Engineer/Directional Driller and Operations Coordinator for the Gulf Coast of Mexico.

With more than 25 years of oil and gas industry experience, he leads a team of world-class researchers in developing the next generation of drilling technology required by Saudi Aramco's Drilling and Workover stakeholders.

In 1996, Timothy received his B.S. degree in Petroleum Engineering from Marietta College, Marietta, OH.

Zhaorui Shi

M.S. in Petroleum Engineering, University of Tulsa

Zhaorui Shi currently works as a Technology Specialist and Manager in YU Technologies Inc. He is the major developer and contributor of the drilling microchip technology, which was selected as a finalist of the World Oil Best Drilling Technology.

Zhaorui's research interests include downhole electronics, measurement tools, and downhole communication.

He is a member of the Society of Petroleum Engineers (SPE) and the Society of Photo-Optical Instrumentation Engineers (SPIE).

Zhaorui received two M.S. degrees, the first in Electrical Engineering, and the second in Petroleum Engineering, both from the University of Tulsa, Tulsa, OK.

Enhanced Experimental Carbon Dioxide Sweep Using Surface Coated Silica Nanoparticles as a Foaming Agent

Ahmad M. Alfakher and Dr. David A. DiCarlo

Abstract /

Solvent flooding is a well-established method of enhanced oil recovery (EOR), with carbon dioxide (CO_2) being the most-often used solvent. As CO_2 is both less viscous and less dense than the fluids it displaces, the displacement suffers from poor sweep efficiency caused by an unfavorable mobility ratio and an unfavorable gravity number. Creating in situ CO_2 foam improves the sweep efficiency of CO_2 floods. Another application is the injection of CO_2 foam into saline aquifers for carbon capture and storage (CCS).

The goal of the coreflood experiments in this article was to study the effectiveness of surface coated silica nanoparticles as an in situ CO_2 foaming agent. In each experiment, the pressure drop was measured across five separate sections in the core, as well as along the whole core. In addition, the saturation distribution in the core was calculated periodically using computed tomography (CT) scanning measurements. The experiments consisted of vertical corefloods where liquid CO_2 displaced brine from the top to the bottom of the core.

A flood with surface coated silica nanoparticles suspended in the brine is performed in the same core and at the same conditions to a flood with no nanoparticles, and results from these floods are compared. In these experiments, breakthrough occurred 45% later with foamed CO_2, and the final CO_2 saturation was also 45% greater than with the unfoamed CO_2.

The study shows how nanoparticles stabilize the CO_2 front. The results provide quantitative information on, as well as a graphical representation of, the behavior of the CO_2 foam front as it advances through the core. This data can be used to upscale the behavior observed and properties calculated from the core-scale to the reservoir-scale to improve field applications of CO_2 flooding.

Introduction

Carbon dioxide (CO_2) flooding is the most used solvent in enhanced oil recovery (EOR), which can increase recovery by up to 15%[1]. Another application of CO_2 injection is into brine aquifers for the purpose of carbon storage, and is the only carbon storage method that has been implemented on a commercial scale.

One of the problems facing expanded use of CO_2 EOR is CO_2 availability. In EOR applications, CO_2 is permanently stored in the reservoir as it displaces oil. It is therefore an effective method of carbon storage that also generates revenue, which could offset the cost of carbon capture. When the field is to be abandoned, excess CO_2 can either be stored in the reservoir itself or in a deeper saline aquifer[2].

One of the most important parameters in fluid displacement is the endpoint mobility ratio, which is the fluid mobility evaluated at the endpoint of the relative permeability curve for that fluid, written as:

$$M^o = \frac{\lambda_1^o}{\lambda_2^o} = \frac{k_{r1}^o/\mu_1}{k_{r2}^o/\mu_2} \qquad \text{1}$$

A mobility ratio greater than 1 indicates that the displacing fluid is more mobile than the resident fluid, which favors a non-stable flood and leads to viscous fingering. A mobility ratio less than 1 indicates that the displacing fluid is less mobile than the resident fluid, which favors a stable flood and inhibits viscous fingering. As the mobility of CO_2 is much greater than that of brine, CO_2 floods suffer from viscous fingering, and consequently, low sweep efficiencies.

Another important aspect affecting sweep efficiency is the buoyancy effects, caused by density differences. CO_2 is a supercritical fluid at reservoir conditions, and more than many other solvents, behaves like a liquid as it has a relatively high density. The gravity number is the ratio of gravity to viscous forces and is used to evaluate the extent to which fluids will move because of buoyancy effects[1]:

$$N_g^o = \frac{k k_{r2}^o \Delta \rho g}{\mu_2 u} \qquad \text{2}$$

Multiple injection strategies have been devised and tested to overcome the challenges and disadvantages of CO_2 flooding. These include creating a foam or alternating the injection between CO_2 and another liquid[5].

Foam stabilization using solid particles and no surfactants was previously studied and demonstrated[4], and ex-situ CO_2 foam was previously generated and observed with the use of surfactants, nanoparticles, or both as stabilizing agents[5]. As in situ CO_2 foam generation cannot be directly observed in porous media, it has been inferred from effects expected from and associated with foams and emulsions[6].

The method by which CO_2 changes from a continuous phase to disconnected bubbles or droplets in a water-wet medium is called Roof snap-off, and results from the capillary forces associated with forcing the CO_2 through the constrictions of a pore throat[7]. The application and importance of Roof snap-off on the creation of in situ foam has been demonstrated both thorough modeling by Rossen (1999)[8] and Deng et al. (2013)[9], and in experiments by Gauglitz et al. (2002)[10]. One method of preventing bubbles from coalescing and thereby creating CO_2 foam is through injecting it into a core saturated with a surfactant solution. This has been shown to greatly reduce the CO_2 mobility for multiple pore volumes (PVs) of injection after breakthrough[11]. CO_2 foams stabilized by surfactants are, however, not stable in harsh reservoir conditions of high temperature and salinity[12].

Flooding a core initially saturated with nanoparticle brine with liquid CO_2 has been shown to increase sweep efficiency using computed tomography (CT) scans[13]. Foaming CO_2 has been shown to decrease its mobility by causing a significant portion of the gas to be stationary or trapped[14]. Others have shown that saturating a core with nanoparticle brine improves the sweep of CO_2 in a buoyancy-driven flow[15], in water-wet as well as oil-wet pores[16], and increased CO_2 trapping was studied in both drainage and subsequent imbibition[17].

Experimental Equipment, Setup and Procedures

The core is a Berea sandstone that is 2.8" in diameter and 24" in length. The core holder has multiple pressure taps that allow for measuring pressure drops along multiple sections of the core. X-ray CT scanning was used to obtain the saturation data. The scanner is a Picker medical scanner, outfitted for petrophysical use. The brine used was 2% sodium chloride by weight. The nanoparticles used are Nissan Chemical America Corporation EOR 5XS-V4.2, mixed to a solution of 2% nanoparticles and 2% sodium chloride by weight.

One PV of brine was pumped to flush the core and measure base permeability. The first CO_2 flood was conducted to acquire a baseline. The core was re-saturated with brine and a second CO_2 flood was conducted and compared to the previous flood to show repeatability. The core was saturated with nanoparticle brine by pumping at least 1 PV of nanoparticle brine through the core and another CO_2 flood was conducted. The CT scanner was used to take 59 slices that are each 10 millimeters thick.

Experimental Results

A brine flood was conducted prior to each CO_2 flood. In the case of CO_2 floods with nanoparticles, the brine flood was conducted with nanoparticle brine. The brine floods that contain nanoparticles exhibit the same pressure drops as the brine floods that do not contain nanoparticles, showing the nanoparticles have no effect on brine mobility.

Figure 1 shows the CO_2 saturation vs. position along the core for a CO_2 flood without nanoparticles. Each line was taken at a different dimensionless time (PVs pumped). The front moves from lower to greater slice number.

It can be seen in the graph that the flood front moves as a shock where the CO_2 saturation changes from zero to 0.24 in the span of 10 slices (0.1 meters or 0.16

Fig. 1 *The CO_2 saturation vs. position along the core for a CO_2 flood without nanoparticles.*
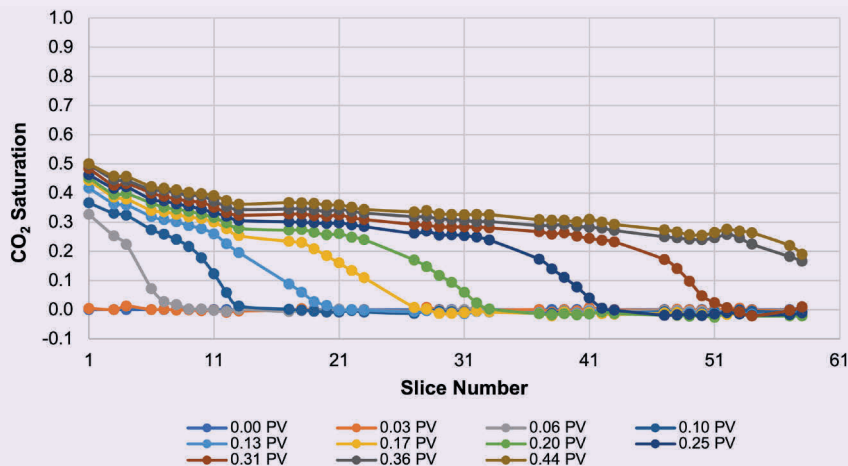
of the core's length), and that the shock is followed by a rarefaction wave. Unlike a typical Buckley-Leverett solution to an immiscible displacement where the inlet saturation is constant, the saturation at the inlet in these experiments was found to be increasing with time. An edge effect was seen at the outlet of the core, where saturations are slightly greater than would be expected from the trend. Breakthrough occurred when the shock reached the outlet, which from the graph is between 0.31 PV and 0.36 PVs pumped.

Figure 2 shows CO_2 saturation vs. position along the core for a CO_2 flood with nanoparticles. It was seen that the CO_2 front has a sharper shock in the presence of nanoparticles and goes to a greater saturation. The saturation change in the shock is from zero to 0.46, as opposed to 0.26 in the flood without nanoparticles. The shock's saturation change also occurs in the span of five slices (0.05 meters or 0.08 of the core's length), which is half the value in the flood with no nanoparticles.

Rarefaction is also present with nanoparticles, as the saturation behind the shock increases from 0.46 to 0.76. Breakthrough can be inferred from the location and movement of the shock in dimensionless time, which from the graph is between 0.46 PV and 0.51 PVs pumped. Therefore, 0.1 PV to 0.2 PVs, or 28% to 56% delayed breakthrough. Like the previous flood, the CO_2 saturation at the inlet also increases with time in this flood.

After the nanoparticle CO_2 flood, the core was flushed with 4.4 PVs of brine with no nanoparticles before conducting the next CO_2 flood. The results in this flood are similar to the flood without nanoparticles. The flood front moves as a shock where the CO_2 saturation changes from zero to 0.3 in the length of 10 slices (0.1 meters or 0.16 of the core's length), and the shock is followed by a rarefaction wave. Breakthrough occurred when the shock reached the outlet, which

from the graph, is briefly after 0.36 PVs pumped.

Discussion

Saturating the core with nanoparticle brine before flooding it with CO_2 was observed to cause the following effects:

- At the same flow rate, the CO_2 front moved slower through the core in the nanoparticle case, Fig. 3.
- The final CO_2 saturation in the core was greater by 45% in the nanoparticle case, Fig. 4.
- Breakthrough in the nanoparticle case was delayed by 45%.

The greater CO_2 saturation achieved in the nanoparticle case compared to the base case and the slower breakthrough time are consistent with results from multiple previous studies, as highlighted earlier. These effects have been interpreted to indicate the formation of an in situ CO_2/brine foam or emulsion stabilized by nanoparticles during the flood.

The new measurement of pressure drops across separate segments of the core adds some insight and further evidence to the foam or emulsion hypothesis; foams have much lower mobilities and greater pressure drops than separate fluid phases, as observed. This lower mobility helps stabilize the CO_2 flood and thereby results in a greater CO_2 saturation and improved brine displacement.

One of the major questions investigated by these experiments, besides measuring the mobility decrease, is whether that mobility decrease changes with time. More particularly, the investigation into whether the increase in CO_2 saturation at the inlet would cause the CO_2 foam to break. In these experiments, it was observed that the CO_2 foam does not break for the entire duration of the flood, which is after flooding with 4 PV to 6 PVs and reaching an average CO_2 saturation of 0.65.

Fig. 2 *The CO_2 saturation vs. position along the core for a CO_2 flood with nanoparticles.*
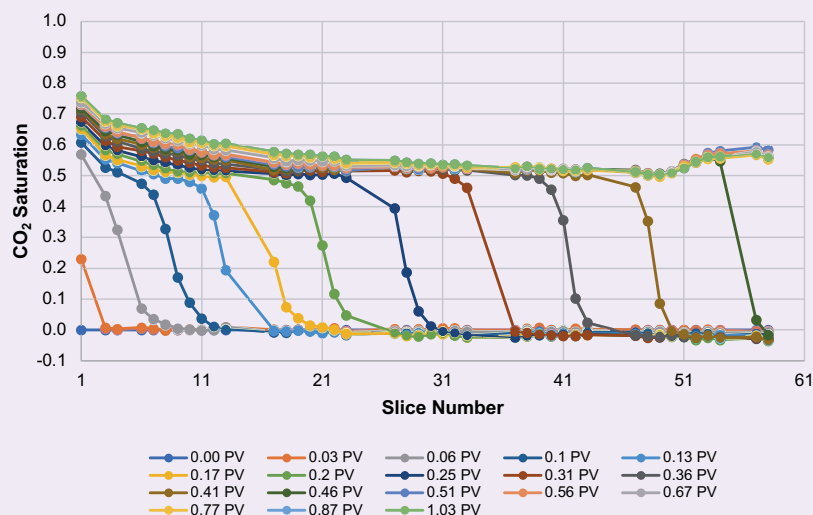
Fig. 3 *A comparison of the CO_2 saturation profile at 0.20 PVs pumped of CO_2 floods with and without nanoparticles.*
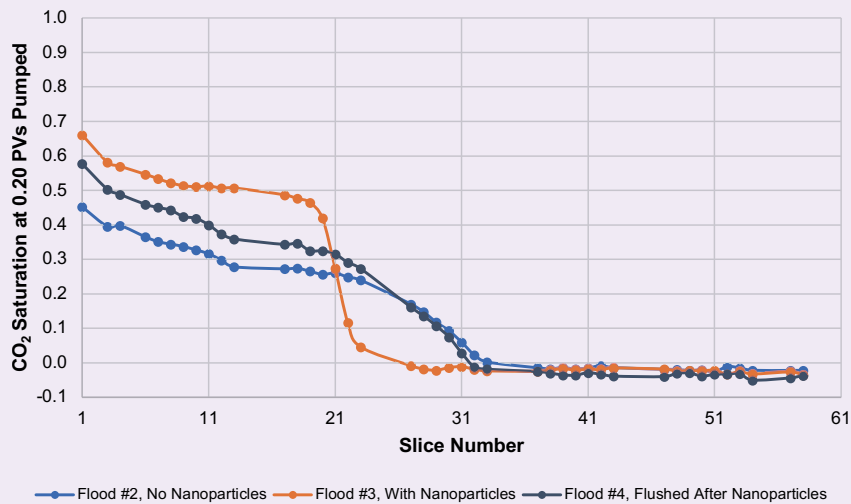
Fig. 4 *The final saturation profile comparison of floods with and without nanoparticles.*
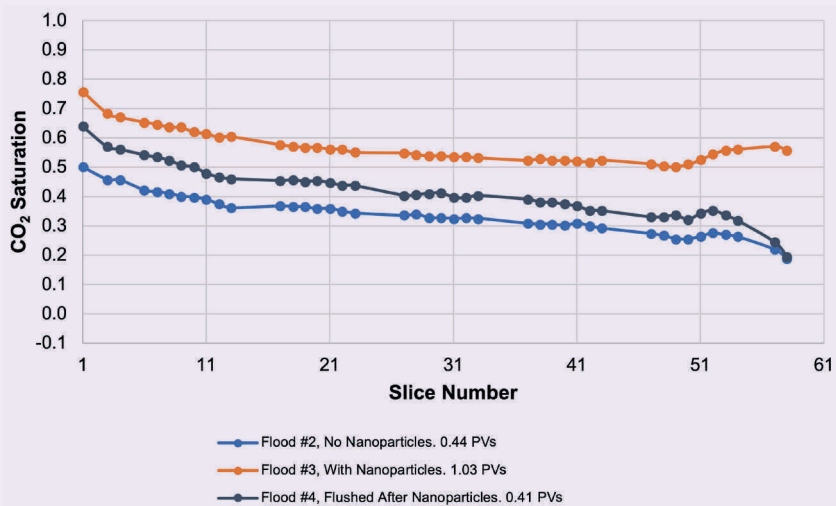
Figure 5 is the average CO_2 saturation in the core vs. PVs pumped, with the data point closest to breakthrough made larger for emphasis. Before breakthrough, all lines overlap and are straight with a slope of 1. Shortly after breakthrough, the saturation is in the core plateaus, indicating no additional brine is being displaced by the CO_2. The point at which breakthrough occurs, and the value of average CO_2 saturation at that point is equal between the flood before and the flood after nanoparticles. The flood with nanoparticles in comparison has a delayed breakthrough and a greater final saturation.

Figure 6 through Fig. 8 shows the CO_2 saturation in the core at different dimensionless times. The top slice in these images is at the top of the core, which

is at the inlet. The bottom slice is at the bottom of the core, which is at the outlet. The two slices in the middle are picked so that the distance between each slice and the next is almost constant.

The figures show that a preferential flow path exists for the CO_2 in both the flood before nanoparticles, and the flood after the core is flushed with non-nanoparticle brine following the nanoparticle brine flood. Since the preferential flow path is at the same location for both floods, it is likely to be initiated by heterogeneity in the core and propagated by viscous fingering. The flood with nanoparticles is closer to piston-like compared to the others, and the effect of the preferential flow path is greatly dampened. This suggests the nanoparticles suppress the effects of heterogeneity and viscous

Fig. 5 *The average CO$_2$ saturation vs. PVs pumped.*
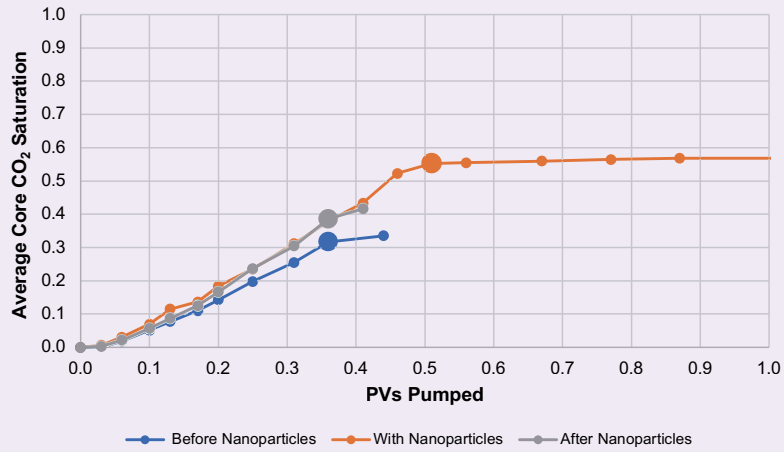
Fig. 6 *The saturations without nanoparticles at 0.03, 0.06, 0.13, 0.17, 0.20, 0.25, 0.31, 0.36, and 0.44 PVs pumped, respectively, starting from top left.*
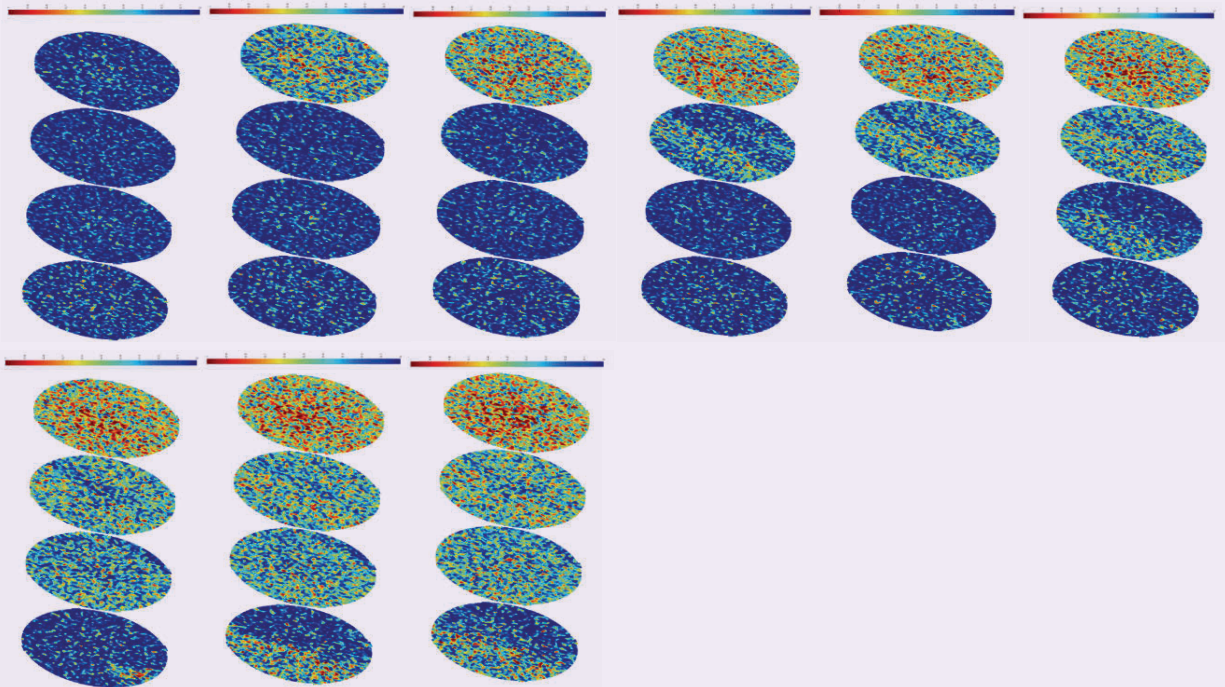
fingering and help stabilize the flow.

Conclusions

This study evaluated the use of brine with suspended surface coated nanoparticles as a means of improving the sweep efficiency of CO$_2$ floods. In each flood, the core was scanned periodically with a CT scanner, which was used to calculate the CO$_2$ saturations.

In the CO$_2$ floods with nanoparticles, it was observed that breakthrough was delayed by 45%. This delay in breakthrough was measured through pressure drop data, CT scanner saturation data, and visual inspection of breakthrough time. The CO$_2$ saturation front was observed to be sharper in the flood with nanoparticles. The saturation front also went to a greater CO$_2$ saturation in the nanoparticle case: a jump from zero to 0.46 in the nanoparticle case as opposed to a jump from zero to 0.26 in the control case.

Fig. 7 *The saturations with nanoparticles at 0.03, 0.06, 0.10, 0.13, 0.17, 0.20, 0.25, 0.31, 0.36, 0.41, 0.46, 0.51, 0.56, 0.67, 0.77, 0.87, and 1.03 PVs pumped, respectively, starting from top left.*
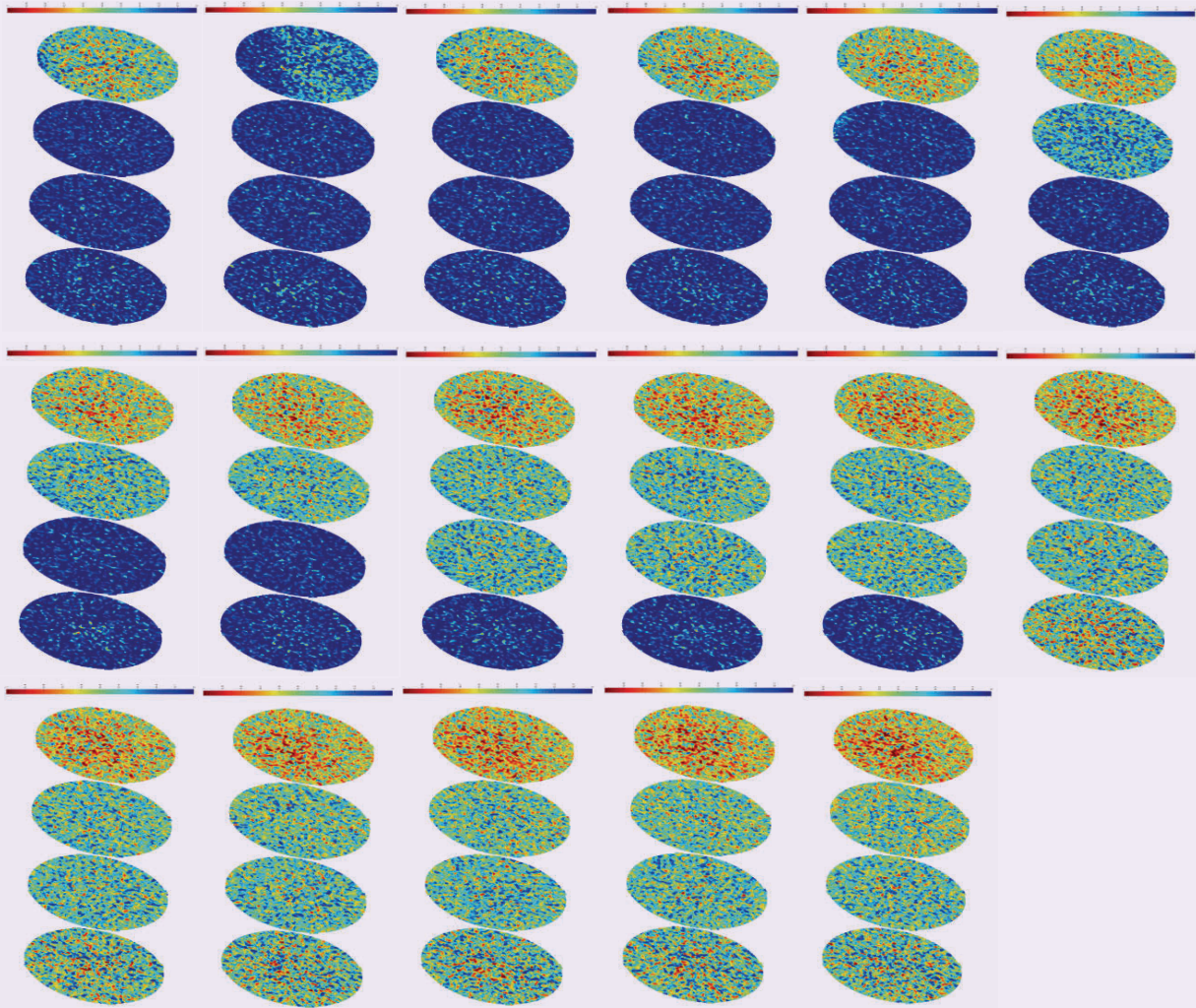
The saturation profile along the core consisted of a shock followed by a rarefaction wave, mostly like a typical Buckley-Leverett solution of an immiscible displacement. Unlike a typical Buckley-Leverett displacement, the CO_2 saturation at the inlet in this study was measured to not be constant with time but to increase with time.

Consistent with previous work, these effects are interpreted to indicate in situ formation of CO_2/brine foam. This is supported by visually observing a foam-like effluent in the nanoparticle case.

After the core was flushed with over 4 PVs of brine, the subsequent CO_2 flood was similar to that before the introduction of nanoparticles. This indicates these effects are reversible, and that nanoparticles do not permanently adsorb to the rock.

The visual representation CT saturation data shows a preferential path for the CO_2. Since these experiments are conducted vertically, this cannot be explained by buoyancy effects, and is interpreted to be caused by rock heterogeneity. This is supported by the observation that the preferential flow path was at the same location in both the flood before nanoparticles and the flood after the core was flushed with brine. In the nanoparticle flood, this preferential flow path is suppressed, and the CO_2 front looks much more spread through the entire cross-section. This is a direct observation of nanoparticles improving the sweep in CO_2 injection.

Acknowledgments

References

1. Lake, L.W., Johns, R.T., Rossen, W.R. and Pope, G.A.: *Fundamentals of Enhanced Oil Recovery*, Richardson, TX: Society of Petroleum Engineers, 2014, 496 p.

2. Hill, B., Hovorka, S. and Melzer, S.: "Geologica Carbon

Fig. 8 *The saturations after brine flush post-nanoparticles at 0.03, 0.06, 0.10, 0.13, 0.17, 0.20, 0.25, 0.31, 0.36, and 0.41 PVs pumped, respectively, starting from top left.*

Storage through Enhanced Oil Recovery," *Energy Procedia*, Vol. 37, 2013, pp. 6808-6830.
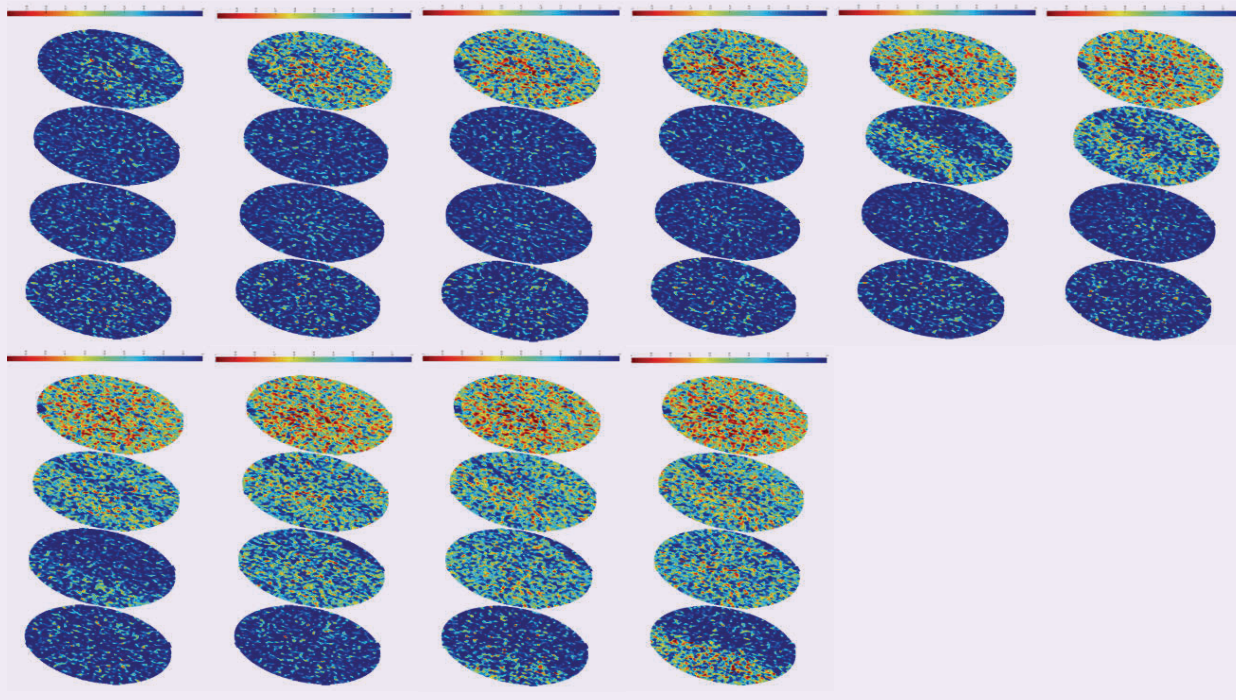
3. Shan, D. and Rossen, W.R.: "Optimal Injection Strategies for Foam IOR," *SPE Journal*, Vol. 9, Issue 2, June 2004, pp. 132-150.

4. Aveyard, R., Binks, B.P. and Clint, J.H.: "Emulsions Stabilized Solely by Collodial Particles," *Advances in Colloid and Interface Science*, Vols. 100-102, February 2003, pp. 503-546.

5. Emrani, A.S. and Nasr-El-Din, H.A.: "Stabilizing CO_2 Foam Using Nanoparticles," SPE paper 174254, presented at the SPE European Formation Damage Conference and Exhibition, Budapest, Hungary, June 3-5, 2015.

6. Aminzadeh, B., DiCarlo, D.A., Roberts, M., Chung, D.H., et al.: "Effect of Spontaneous Formation of Nanoparticle Stabilized Emulsion on the Stability of a Displacement," SPE paper 154248, presented at the SPE Improved Oil Recovery Symposium, Tulsa, Oklahoma, April 14-18, 2012.

7. Roof, J.G.: "Snap-Off of Oil Droplets in Water-Wet Pores," *SPE Journal*, Vol. 10, Issue 1, March 1970, pp. 85-90.

8. Rossen, W.R.: "Foam Generation at Layer Boundaries," *SPE Journal*, Vol. 4, Issue 4, December 1999, pp. 409-412.

9. Deng, W., Cardenas, M.B. and Bennett, P.C.: "Extended Roof Snap-Off for a Continuous Nonwetting Fluid and an Example Case for Supercritical CO_2," *Advances in Water Resources*, Vol. 64, January 2013, pp. 34-46.

10. Gauglitz, P.A., Friedmann, F., Kam, S.I. and Rossen, W.R.: "Foam Generation in Porous Media," SPE paper 75177, presented at the SPE/DOE Improved Oil

Recovery Symposium, Tulsa, Oklahoma, April 13-17, 2002.

11. Kovscek, A.R., Patzek, T.W. and Radke, C.J.: "Simulation of Foam Transport in Porous Media," SPE paper 26402, presented at the SPE Annual Technical Conference and Exhibition, Houston, Texas, October 3-6, 1993.

12. Rossen, W.R.: "Foam in Enhanced Oil Recovery," in Prud'homme, R.K. and Khan, S.A. (eds.) *Foams: Theory, Measurements, and Applications*, New York, NY: Marcel Dekker Inc., 1996, 610 p.

13. Aminzadeh, B., DiCarlo, D.A., Chung, D.H., Kianinejad, A., et al.: "Effect of Nanoparticles on Flow Alteration during CO_2 Injection," SPE paper 160052, presented at the SPE Annual Technical Conference and Exhibition, San Antonio, Texas, October 8-10, 2012.

14. Tang, G-Q. and Kovscek, A.R.: "Measurement and Theory of Gas Trapping in Porous Media during Steady-State Foam Flow," SPE paper 90142, presented at the SPE Annual Technical Conference and Exhibition, Houston, Texas, September 26-29, 2004.

15. Senthilnathan, S.: "Surface Coated Silica Nanoparticles for Conformance Control of Buoyancy-Driven CO_2 Flow," M.S. thesis, the University of Texas at Austin, August 2017.

16. Alghamdi, A.A.: "Experimental Evaluation of Nanoparticles Impact on Displacement Dynamics for Water-Wet and Oil-Wet Porous Media," M.S. thesis, the University of Texas at Austin, August 2015, 207 p.

17. Wung, R.M.: "Utilizing Surface Treated Nanoparticles for Enhanced Geologic Carbon Sequestration," M.S. thesis, the University of Texas at Austin, August 2015.

About the Authors

Ahmad M. Alfakher

M.S. in Petroleum Engineering,
The University of Texas at Austin

Ahmad M. Alfakher is a Petroleum Engineer in Saudi Aramco's Northern Area Production Engineering Department. He has over 10 years of work experience with Saudi Aramco in areas that include production engineering, reservoir management, workover engineering, and human resources, including various leadership positions.

Ahmad is currently working on a project to establish a training academy that serves all of the Northern Area Oil Operations.

In 2011, he received his B.S. degree, and in 2019 his M.S. degree, both in Petroleum Engineering, from the University of Texas at Austin, Austin, TX.

Dr. David A. DiCarlo

Ph.D. in Physics,
Cornell University

Dr. David A. DiCarlo is an Associate Professor in the Hildebrand Department of Petroleum and Geosystems Engineering in the Cockrell School of Engineering at the University of Texas at Austin, where he holds the George H. Fancher Centennial Teaching Fellowship in Petroleum Engineering.

David's research is focused on applying advanced experimental techniques to understanding fluid flow in hydrocarbon reservoirs. In particular, judicious use of computed tomography scanning provides in situ phase saturations, which can then be converted into permeabilities and relative permeabilities. These can be

obtained on a much shorter time scale and over a wider range of saturations then traditional steady-state methods. Topics relevant to enhanced oil recovery such as three-phase flow (water, oil, and gas), surfactant imbibition, compositional displacements, flow stability, and the effect of nanoparticles in porous media are studied using these methods.

In 1987, he received his B.S. degree in Physics from Case Western Reserve University, Cleveland, OH. In 1990, David received an M.S. degree in Physics and in 1994, he received his Ph.D. degree in Physics, both from Cornell University, Ithaca, NY.

Development and Testing an Electrical Drillstem Test Tool Conveyed by Coiled Tubing with a Real Time Control and Acquisition System

Michael A. Affleck, Monika Bakke Maimin and Falah A. Alosaimi

Abstract /

Some exploration well testing operations are executed by performing multiple runs in hole using slick line and coiled tubing (CT). A new technology has been developed that combines many of these operations, including contingency stimulation activities into one run.

The electrical drillstem test (e-DST) tool is an intelligent, surface controlled tool designed to be run on CT that allows exploration well testing operations, including stimulation, to be performed in one run. Existing operations involve rigging up slick line and CT in varying sequences depending on well conditions, such that the requirement for nitrogen lifting and acid stimulation through CT — as well as gauge setting and retrieving by slick line — can be established. In addition, to save substantial time, the new system is designed to optimize test quality through the display of real-time bottom-hole production logging data at the surface, allowing the early ending of poor tests or the extension of interesting ones. Selective stimulation of zones through repositioning of the e-DST tool on CT eliminates costly trips into the well and the requirement for pre-planning of flow test durations is removed. The innovative tool includes a cable head connector, upper flow port, packer element, slips anchor, shut-in valve, and real-time instrumentation and control with monitoring from the surface.

This article will introduce the major system components and review challenges associated with design, manufacture, and testing. A summary of the first trial test results, conclusions, and lessons learned will also be presented.

Introduction

Flow testing exploration wells can be performed by multiple methods, but typically, downhole pressures and temperatures in addition to surface parameters are recorded for all[1]. Most methods have a degree of complexity in common, with the expected operational timeline increasing as soon as multiple perforation intervals are tested and the availability of real time data transfer to the surface while testing is preferred[2]. Depending on stimulation requirements, often only known after the completion of initial flow testing, rigging up and rigging down coiled tubing (CT), slick line and electric wireline multiple times during a test is common and add significantly to the time and cost associated with collecting the well data[3]. In addition, operational costs can quickly accumulate when the drilling rig is still on location. This is sometimes required for plugging and abandonment operations post-testing.

In ideal circumstances, live results with excellent data quality allow real-time changes to the well testing program. Testing durations may be extended or shortened, and production zones with promising results may be identified as candidates for immediate stimulation, followed by re-testing, allowing early identification of effective stimulation methods. With the availability of real-time transmission of data to the surface, the new method provides a very efficient and opportunistic approach through tailoring the testing process to the observations made[4].

Developing and Qualification Testing of the New Tool

Prior to engaging in the new tool development process, the following major operational requirements were identified and confirmed:

- Introduce for the first time an exploration well testing process, which capitalizes heavily on the combined mechanical, hydraulic, and electrical capabilities of CT (with internal cable) and a flexible new tool.

- Reduce the number of different services required and their associated rig-up and rig-down times by maximizing the work scope performed with CT.

- Increase timely access to high quality data for rapid on-site decision making during well testing, by changing from memory-based gauges and time activated downhole shut-in tools to real-time control and real-time data transmission to the surface.

- Maximize operational efficiency during well testing by having real-time data transmission to the surface, allowing testing periods to be terminated early, or extended based on the actual reservoir response observed and recorded.

- Introduce on-demand, selective stimulation capability while the new tool and CT remain downhole, eliminating the need for tripping and tool string change out. The new tool's packer module should be able to provide isolation during the stimulation process if required.

- The system should allow multiple testing periods during one trip in hole when required at different depths. This is achievable by designing the system with packers, slips, and a shut-in valve module with multicycle capability.

- Increase the effectiveness of transferring the well from underbalance to overbalanced status or vice versa. This is achieved by either changing out fluids in the well or pumping nitrogen through the CT. Although the electrical drillstem test (e-DST) process is a live-well intervention process as such, perforating techniques, stimulation preferences or simply general pressure control requirements with the drilling rig still on location, or rig-less operations, may stipulate a variety of additional system functionality requirements.

- Reduce overall risk of stuck pipe or stuck tool occurrences during well testing by always having circulation available above the packer module. The operational value of this option should not be underestimated, as the retrieval process of conventional memory shut-in tools can be greatly complicated by circulated fluids not being as clean as desired, or the reservoir producing solids during the flow state.

Following multiple design iterations, two complete prototype tools were manufactured and module level function testing performed. In parallel, software development and testing of the graphical user interface progressed. Significant effort was applied to ensure that module testing was conducted in as realistic as possible downhole environment. Dedicated testing equipment had to be designed and manufactured, allowing the following tests to be conducted:

- Multicycle temperature and pressure cycling in liquid and gas environments.

- Force manipulation on the tool, verifying mechanical strength and specifications.

- Multiple "well testing" cycles, mirroring the expected downhole operations process. This included multiple setting and unsetting of packer and slips, as well as opening and closing of the shut-in valve under temperature and pressure.

- Verification of contingency options, such as emergency release of the slips and packer in case of loss of electrical signal or control from the surface and releasing of the bottom-hole assembly (BHA) from the CT in case of a stuck tool string.

- Multiple routine and stress testing of electrical downhole and surface components, as well as software.

Design, manufacture, and module testing was carried out in Algard, Norway. The photographs in Fig. 1 provide an impression of the qualification testing performed under simulated downhole conditions.

Following the qualification testing, but prior to the first field application, a system integrity test with the CT service company was performed. Focus was given to verifying all interfaces between the downhole tool and CT supplier equipment and processes. In particular, the verification of operating the new tool through the full length of cable (inside the CT) was thoroughly tested. Significant calibration was expected, required and performed, as the mono-conductor cable is used

Fig. 1 *An example of the full-scale e-DST qualification testing under simulated downhole conditions.*

for data communication, in addition to the tool power supply.

Specifications and Main Components of the e-DST Tool

Table 1 lists the most important specifications of the new tool.

Figure 2 and Table 2 give an overview of the complete e-DST tool string, the main components and module functions.

Exploration Well Testing Revisited — Description of the New Process

One of the objectives on the new tool development was the introduction of a new exploration well testing process, which capitalizes heavily on the combined mechanical, hydraulic, and electrical capabilities of the CT (with an internal cable) and the new tool. Consequently, several new opportunities exist to enhance the process, the most obvious being:

- The ability to test — at multiple depths — without the need to trip out of hole or have the completion pre-configured, e.g., nipple profiles at certain depths.
- The ability to stimulate on-demand as required following the analysis of the well test data, without the need to trip out of hole and change between different well services.
- Optimize the well test process by utilizing real-time information transmittal to the surface.
- The ability to circulate different fluids through the CT, adjusting the well status from overbalanced to underbalanced or vice versa, as and when required.

Figure 3 provides an overview of how the new tool may be used during well testing in an exploration well.

Conveyed on the CT, the e-DST tool may be positioned inside the casing or liner directly above the perforation interval, or inside the production tubing. The latter is typically true when the casing is larger than the 4½" production tubing suitable for setting the packer and slips.

When the packer is not set, flow from the well passes the tool externally in a conventional manner. Typically, this is the preferred condition when flowing an exploration well for the first time after perforating, giving verification of flow rates, pressures, and assessing the potential risk of solids production from the reservoir. The well returns are monitored at the surface. The tool is anchored into the casing or tubing by setting the slips and maintaining a positive overpull with the CT control at the surface. By setting the slips, the tool is secured against unintentional movement in the up hole direction, as soon as differential pressure across the packer is created. This also protects the CT itself against unwanted forces being transmitted from the tool.

With the packer module activated and the element sealed, two options exist, depending on the shut-in valve's position.

Option 1

The flow from the well enters the lower flow port below the packer, continues through the internal diameter of the tool and exits into the annulus at the upper flow port above the packer — as shown by the small red arrows in Fig. 3. The shut-in valve is in the open position for the flow to enter the lower flow port and the well's returns are monitored at the surface.

Option 2

With the shut-in valve in the closed position, the flow from the well cannot enter the lower flow ports, causing the pressure below the set packer to increase. This stage of the testing program is typically referred to as the shut-in period. As with all other downhole measurements acquired by the tool, the pressure buildup curve during the shut-in period is observed in real-time at the surface.

In both options, pumping fluids through the CT

Table 1 *The most important specifications of the e-DST tool.*

Parameter	Specification	Loading
Outer tool diameter	3.5″	0.5
To be set in liner/tubing	4.5″	10
Maximum downhole ambient temperature	302 °F (150 °C)	2.0
Maximum downhole ambient pressure	10,000 psi	2.5
Maximum packer differential pressure	7,500 psi from below during well testing	3.0
5,000 psi from above during stimulation	gpt	3 - 4
CT internal cable	Depending on length, 16 American wire gauge mono-conductor	0.6 - 0.9
H_2S, nitrogen, and acid compatibility	Yes, within standard precautions also related to CT	1 - 5
Tool string length	42 ft — standard configuration	5.0

Fig. 2 *The e-DST tool's main components.*
Table 2 *The e-DST tool's main components and their functional descriptions.*

Component	Functional Description
CT internal cable	Provides electrical communication, control and electrical power to/from the e-DST tool.
CT	Provides conveyance of the e-DST tool, as well as hydraulic supply of fluids and sheltering of the CT internal cable.
CT end connector	Physical connection between CT and e-DST tool.
Electrical termination sub	Houses electrical cable termination and interface to e-DST tool.
Dual flapper check valves	Downhole barrier against unwanted flow into the CT.
Disconnect sub	Ball operated. Provides contingency against stuck tool string (optional with burst disc).
Casing collar and perforations locator	Allows real-time depth control based on downhole installed completion items or perforation holes of sufficient size.
Tension compression sub	Provides real-time verification of push/pull exerted onto the e-DST tool.
External pressure and temperature sensor	Provides real-time verification of external pressure and temperature above the packer.
Contingency disconnect sub	Provides disconnect option in case of loss of "electric" control from surface, while packer is set. Ball operated.
Upper flow ports (outlet)	Exit point for fluids pumped through the CT from surface and well contents being "flowed" through the e-DST tool (entering at lower flow ports).
Packer	Electrically operated, multicycle packer. Bidirectional pressure holding capability.
Shut-in valve	Electrically operated, multicycle valve. Bidirectional pressure holding capability.
Lower flow ports (inlet)	Entry point for well contents when packer is set and shut-in valve in open position.
Bidirectional slips	Electrically operated, securing the e-DST against unwanted movement in either an up hole or downhole direction (one at the time). Protect the CT against forces resulting from differential pressures across the packer. Includes contingency slip release in case of loss of "electric" control from surface.
External pressure and temperature sensor	Provides real-time verification of external pressure and temperature below the packer.
Electrical bottom connections	For future contingency.

from the surface is possible as indicated by the blue arrows in Fig. 3. The pumped fluids exit the tool into the annulus through the upper flow ports above the packer. Typically, this option is used for either pumping nitrogen to assist the flow from the well or placing fluid (such as water) on top of the packer when differential pressure across the packer requires reduction during the shut-in period. The latter is an optional process feature that avoids the need to accept high differential pressures across the packer. This is especially useful in higher pressured wells. In addition, the ability to pump through the CT during flowing or shut-in periods is especially beneficial in wells containing hydrogen sulfide (H_2S), as corrosion inhibitors and/or H_2S scavengers can be applied periodically for protecting the CT string, BHA, and wellbore tubulars.

At the end of the shut-in period, fluid is pumped through the CT string and placed above the packer. This process equalizes any differential pressure across the packer, prior to opening the shut-in valve and packer. As the last step in the testing cycle, the slips are unset prior to positioning the tool at a different depth for additional testing/stimulation or pulling out of the hole.

It is important to understand that at no point does flow from the well enter the CT string. Dual non-return flapper check valves are located below the CT end connector.

Field Trial Results

With the in-house performance verification, qualification and system integrity testing with the CT service company completed, the tool was deployed for the first time in an exploration well in the Kingdom of Saudi Arabia.

The chosen trial well had multiple perforation intervals or zones, all requiring independent testing. The original program sequence requested a single flowing and shut-in period per zone. Nitrogen lift and the requirement for hydrochloric acid wash and/or

squeeze was a contingency if adequate flow proved unachievable.

Figures 4 and 5 give examples of the selected parameters acquired by the tool during the well testing operation.

Figure 4 displays Zone A data: Two flowing, as well as two shut-in periods with a stimulation activity in between. For the first time, a direct comparison of the well's response before and after stimulation is available in real-time, without having to pull out of hole to change to a different service or change the CT BHA.

During the second shut-in period, the pressure above the packer was reduced due to operational reasons, effectively increasing the differential pressure across the packer. Reassuringly for the critical test, the reservoir pressure below the packer remained unaffected, reaffirming system pressure integrity. With fluid circulation continuously available through the CT string during testing, the pressure above the packer was increased by placing fluid on top of the packer, effectively decreasing the differential pressure over the packer.

Taking advantage of the multi-setting capability of the packer, the slips and shut-in valve, the e-DST tool was positioned at multiple testing depths in response to data already obtained. This additional data is not shown.

In Figure 5, a different option for well testing Zone B is shown. Three flow periods are performed, but only the third one is immediately followed by shut-in to obtain the full pressure buildup curve. A downhole pressure buildup period, where circulation of nitrogen through the CT was stopped and the well remained open at the surface, follows the first and second flow periods. As a result, the fluid level in the well, monitored in real-time,

Fig. 3 *Visualization of the flow paths during the e-DST testing process.*
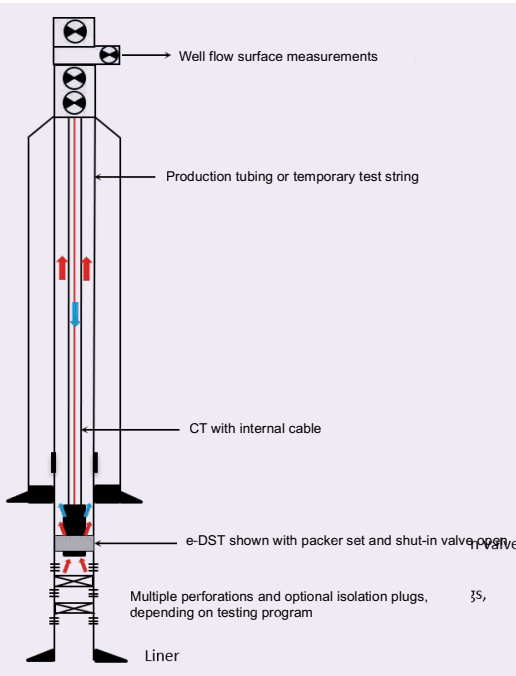
Fig. 4 *Zone A data: Selected downhole parameters acquired by the e-DST tool during well testing.*
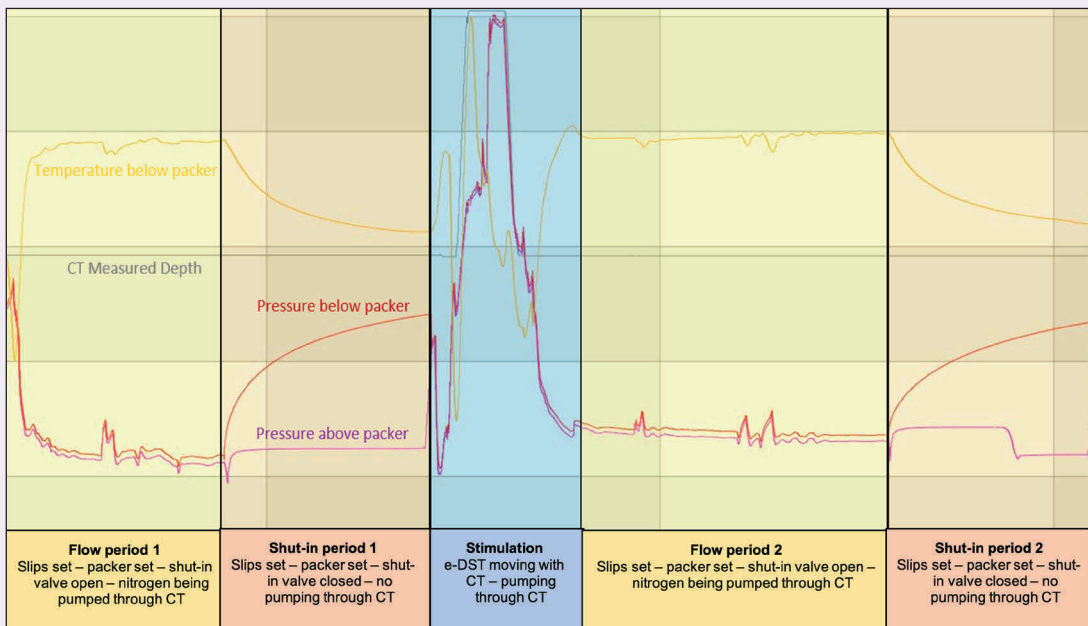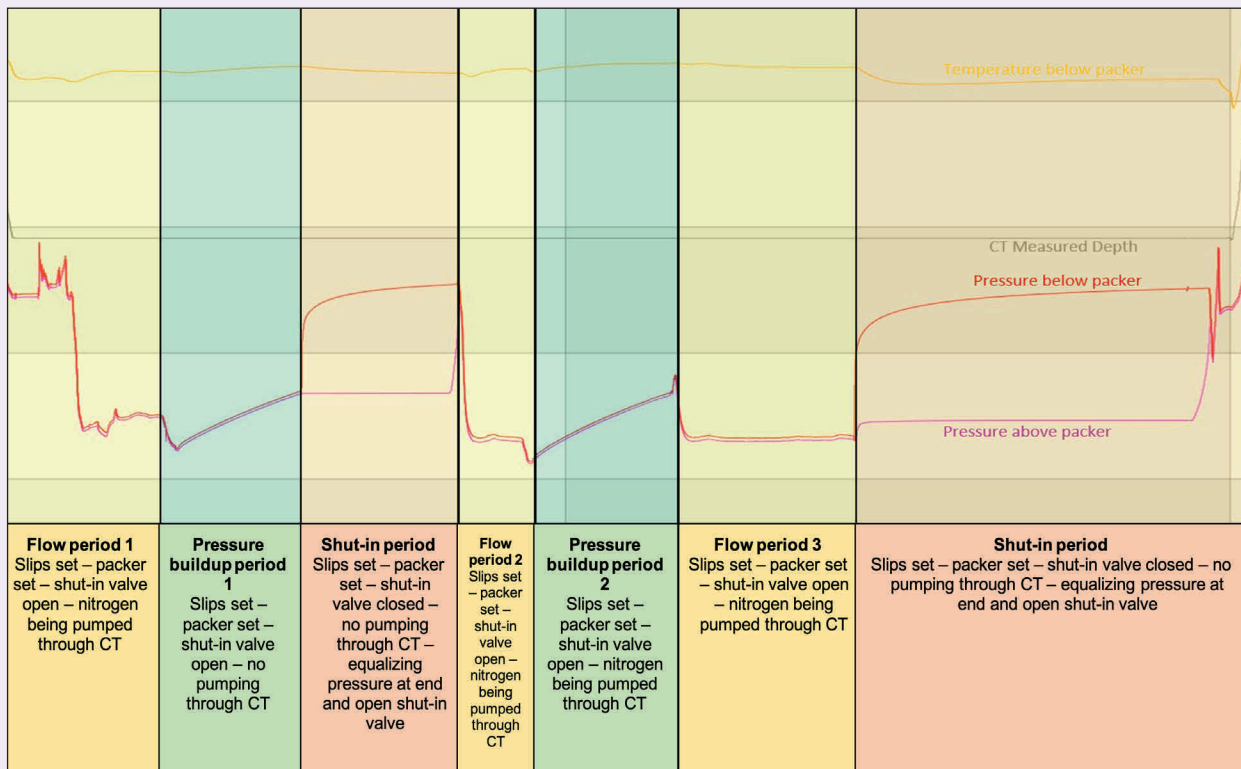
Fig. 5 *Zone B data: Selected downhole parameters acquired by the e-DST tool during well testing.*

Flow period 1 Slips set – packer set – shut-in valve open – nitrogen being pumped through CT	**Pressure buildup period 1** Slips set – packer set – shut-in valve open – no pumping through CT	**Shut-in period** Slips set – packer set – shut-in valve closed – no pumping through CT – equalizing pressure at end and open shut-in valve	**Flow period 2** Slips set – packer set – shut-in valve open – nitrogen being pumped through CT	**Pressure buildup period 2** Slips set – packer set – shut-in valve open – nitrogen being pumped through CT	**Flow period 3** Slips set – packer set – shut-in valve open – nitrogen being pumped through CT	**Shut-in period** Slips set – packer set – shut-in valve closed – no pumping through CT – equalizing pressure at end and open shut-in valve

increases. It is interesting to note that the two pressure buildup periods mark the lowest bottom-hole pressures recorded during the testing process, thereby maximizing the pressure range that is "built-up" by the reservoir. Having analyzed the initial shut-in data, two different duration pressure buildup tests were requested.

Compared to previous multi-zone well testing operations of this type, the scope of the field trial was significantly larger. Changes were made to the testing program based on the real-time downhole data obtained, as well as wanting to opportunistically explore the additional capabilities of the e-DST tool. In total, the two new tools deployed on the trial well recorded and transmitted high quality data on three zones of interest for over 230 hours.

Conclusions and Lessons Learned

A new e-DST tool, with a real-time control and acquisition system has been engineered, manufactured, workshop tested, and successfully in well field deployed. The tool, conveyed by CT with an internal electrical cable has shown significant benefits, resulting in a proven new process of well testing in Saudi Arabia. With downhole information available in real-time supplementing surface parameters, testing can be combined with stimulation, resulting in opportunistic and flexible programs. This is not a method obtainable with conventional technology and methods.

The key points are noted as:

- The development of the new e-DST tool was lengthy and complicated, but it proved immensely beneficial to invest in realistic and thorough qualification testing prior to application of the technology in the field.

- The combined benefits of the e-DST tool and conveyance on CT with an internal cable required a new type of thinking from operational personnel, as well as adjustment to the conventional well testing program.

- The multifunction/multi-setting capability of the tool modules, namely, packer, slips, and shut-in valve, allowed the completion of multiple tasks with one trip in hole. This maximized the use of valuable operation time and avoided having to switch back and forth between different well services.

- Adding ad hoc stimulation capability into the portfolio of quickly available options at the wellsite, followed by an immediate re-testing of the well (or single zone) represented a significant benefit.

- The field trial was completed successfully with a greater than normal scope of work. The operation demonstrated how changes could be implemented into the well testing program. For example, pressure buildup periods were effectively extended or

shortened based on real-time information.

- The project's objective to achieve superior data quality compared to a conventional well testing method was achieved.
- The project's objective to achieve a 30% time saving compared to a conventional well testing method was exceeded.

Acknowledgments

References

1. Barnum, R.S. and Vela, S.: "Testing Exploration Wells by Objectives," SPE paper 13184, presented at the SPE Annual Technical Conference and Exhibition, Houston, Texas, September 16-19, 1984.

2. Awara, A., Mansila, C. and Fink, K.: "Maximizing Cost Efficiencies through Real-Time Well Testing," SPE paper 164699, presented at the North Africa Technical Conference and Exhibition, Cairo, Egypt, April 15-17, 2013.

3. Dolciani, G., Tiwari, S., Adewuya, O., Mousa, A., et al.: "First Dual Zone Drillstem Test with Acoustic Telemetry Using Multiple Retrievable Packers for Single Trip Testing of Two Independent Reservoirs," SPE paper 181354, presented at the SPE Annual Technical Conference and Exhibition, Dubai, UAE, September 26-28, 2016.

4. Hoyer, C., Fried, S. and Sask, D.: "Test, Treat, Test System Using a Concentric Coiled Tubing/DST Package," paper 96-77, presented at the Annual Technical Meeting, Calgary, Alberta, Canada, June 9-11, 1996.

About the Authors

Michael A. Affleck

B.Eng. in Mechanical Engineering, University of Bath

Michael A. Affleck is a Research Consultant working in the Aramco Overseas Company (AOC) Drilling Technology Team of the Aberdeen Technology Office. He has 25 years of experience, which includes wireline logging, drilling rig systems design, managed pressure drilling and downhole robotics.

Michael started his career with the Institute Francais du Petrole working as a design engineer in Paris. He later joined Atlas Wireline and served as a Logging Engineer in many

locations, including the North Sea and Middle East. Following that, Michael joined Varco then Shell Technology Ventures as Regional Director for the MPD business @balance.

He is the author of several patents, journals articles and papers, and his R&D projects have been recognized by international award bodies.

Michael received his B.Eng. degree in Mechanical Engineering from the University of Bath, Bath, U.K.

Monika Bakke Malmin

Monika Bakke Malmin is the co-founder and CEO in Target Intervention, a technology company founded in 2012 that develops electric operated real-time coiled tubing downhole tools.

She has 18 years of experience in the oil and gas industry, mainly within well service operations and downhole tool technology

development. Monika's experience includes coiled tubing operations offshore in the North Sea for Maritime Well Services and BJ Services.

She worked for 5 years with product development and testing of downhole tools in Bakke Oil Tools and with technical sales in Weatherford.

Falah A. Alosaimi

B.Eng. in Chemical Engineering, Arizona State University

Falah A. Alosaimi is a Supervisor of in the Well Testing Operation Unit of Saudi Aramco's Reservoir Description and Simulation Department. He has 20 years of experience, which includes well intervention, wireline logging, drilling operation and reservoir characterization.

Falah started his career with Schlumberger working as a Field Engineer in Saudi Arabia and Kuwait. Later, he was assigned as a Desk Engineer in Chevron Kuwait, where he provided technical support for well evaluation and

completion design.

Following that, Falah joined Saudi Aramco as a Petrophysist to evaluate and interpret logs. Currently, he is assigned to lead the testing operation and evaluation unit for exploratory and delineation wells in Saudi Arabia.

Falah is the founder and initiator of several R&D projects have been recognized by international award bodies.

He received his B.Eng. degree in Chemical Engineering from Arizona State University, Tempe, AZ.

Have an article you would like to publish? Here are our guidelines.

These guidelines are designed to simplify and help standardize submissions. They need not be followed rigorously. If you have any questions, please call us.

Length

Average of 2,500-4,000 words, plus illustrations/photos and captions. Maximum length should be 5,000 words. Articles in excess will be shortened.

What to send

Send text in Microsoft Word format via email. Illustrations/photos should be clear and sharp. Editable files are requested for graphs, i.e., editable in Excel.

Procedure

Notification of acceptance is usually within three weeks after the submission deadline. The article will be edited for style and clarity and returned to the author for review. All articles are subject to the company's normal review. No paper can be published without a signature at the manager level or above.

Format

No single article need include all of the following parts. The type of article and subject covered will determine which parts to include.

Working Title
Lorem Ipsum here.

Abstract
Usually 150-300 words to summarize the main points.

Introduction
Different from the abstract in that it sets the stage for the content of the article, rather than telling the reader what it is about.

Main body
May incorporate subtitles, artwork, photos, etc.

Conclusion/Summary
Assessment of results or restatement of points in introduction.

Endnotes/References/Bibliography
Use only when essential. Use author/date citation method in the main body. Numbered footnotes or endnotes will be converted. Include complete publication information. Standard is *The Associated Press Stylebook*, 52nd ed. and *Wesbter's New World College Dictionary*, 5th ed.

Acknowledgments
Use to thank those who helped make the article possible.

Illustration/Tables/Photos and explanatory text

If the files are large, these can be submitted separately, due to email size limits. Initial submission may include copies of originals; however, publication will require the originals. When possible, submit original images. Color is preferable.

File Format

Illustration files with .EPS extensions work best. Other acceptable extensions are .TIFF/.JPEG/.PICT.

Permission(s) to reprint, if appropriate

Previously published articles are acceptable but can be published only with written permission from the copyright holder.

Author(s)/Contibutor(s)

Please include a brief biographical statement.

Submission/Acceptance Procedures

Papers are submitted on a competitive basis and are evaluated by an editorial review board comprised of various department managers and subject matter experts. Following initial selection, authors whose papers have been accepted for publication will be notified by email.

Papers submitted for a particular issue but not accepted for that issue may be carried forward as submissions for subsequent issues, unless the author specifically requests in writing that there be no further consideration.

Submit articles to:

Editor
The Saudi Aramco Journal of Technology
C-10B, Room AN-1080
North Admin Building #175
Dhahran 31311, Saudi Arabia
Tel: +966-013-876-0498
Email: *william.bradshaw.1@aramco.com.sa*

Submission deadlines

Issue	Paper submission deadline	Release date
Summer 2022	February 1, 2022	June 30, 2022
Fall 2022	May 10, 2022	September 30, 2022
Winter 2022	August 4, 2022	December 30, 2022
Spring 2023	November 7, 2023	March 31, 2023

There is more.

Deep Dielectric-Based Water Saturation in Freshwater and Mixed Salinity Environments

Dr. Ping Zhang, Dr. Wael Abdallah, Dr. Gong Li Wang and Dr. Shouxiang M. Ma

Abstract /　A low frequency, i.e., KHz, resistivity-based method for water saturation (S_w) evaluation is the desired method in the industry due to its deep depth of investigation (DOI) — up to 8 ft. The method becomes unreliable if the formation water is fresh or has mixed salinity (SAL_w). Dielectric permittivity and conductivity dispersion have been used to estimate the S_w and SAL_w. The current dielectric dispersion tools, however, have very shallow DOI due to their high measurement frequency up to GHz, which most likely confines the measurements within the near wellbore mud filtrate invaded zones.

A Safer Dual Functional Gas Hydrate Dissolver and Inhibitor to Replace Methanol

Dr. Mohammed A. Sayed, Dr. Rajesh K. Saini, Eyad A. Alali, Dr. Rajendra A. Kalgaonkar and Ahmed B. Al-Arnous

Abstract /　In the presence of free water and under certain conditions of temperature and pressure, low molecular weight gases, such as methane and ethane, present in the fluid stream flowing in pipelines, cause gas hydrate crystals to form. These gas hydrate crystals may accumulate and cause a partial or complete plugging of pipelines in the vertical or horizontal section.

Photoacoustic Nanotracers for Subsurface Applications: Opportunities and Challenges

Jesus M. Felix Servin, Hala A. AlSadeg and Dr. Amr I. Abdel-Fattah

Abstract /　Tracers are practical tools used to gather information about the subsurface fluid flow in hydrocarbon reservoirs. Typical interwell tracer tests involve injecting and producing tracers from multiple wells to evaluate important parameters such as connectivity, flow paths, fluid-fluid and fluid-rock interactions, and reservoir heterogeneity, among others. The use of nanotechnology enables the development of novel nanoparticle-based tracers to overcome many of the challenges faced by conventional tracers.

Establishing and Estimating Gas-Liquid Performance Characteristics of Multiphase Pumps

Dr. Chidirim E. Ejim

Abstract /　Multiphase electric submersible pumps (ESPs) are used to produce gas and liquid in wells with high gas content. These pumps are operated at different speeds, and designed to handle flows with various gas volume fractions (GVFs). This study uses gas-liquid dimensionless parameters to obtain and compare the performance of conventional multiphase pumps. Knowledge of such techniques is important for production engineers, field operators, and application engineers to ascertain pump performance for given gas-liquid operating conditions.

أرامكو السعودية
saudi aramco

J

Aramco
Journal
of Technology

Liked this issue?
Sign up. It's free.

To begin receiving the *Aramco Journal of Technology*
please complete this form, scan and send by email to
william.bradshaw.1@aramco.com.

Got questions?

Just give us a call at +966-013-876-0498
and we'll be happy to help!

Scan the QR code to go straight
to your email and attach the form!

Subscription Form

Name

Title

Organization

Address

City

State/Province

Postal code

Country

Email address

Phone number

Number of copies